Universität Zürich[UZH]

Geographisches Institut

Dendrogeomorphic Analysis of Landslide Impacts on Norway Spruce on a Slope near Elm, Switzerland

GEO 511 Master's Thesis

Author: Maurin Karzig, 20-714-614

Supervised by: Dr. Holger Gärtner (holger.gaertner@wsl.ch), Prof. Dr. Markus Egli

Faculty representative: Prof. Dr. Markus Egli

24.10.2025

Acknowledgments

First, I would like to thank Dr. Holger Gärtner for his continuous guidance, invaluable advice, patient instruction in the field and the laboratory, and his immediate and friendly support whenever it was needed throughout the entire thesis.

I would also like to thank Anne Verstege, who equipped me for sampling and thoroughly checked my cross-dated samples. Furthermore, I thank the Swiss Federal Institute for Forest, Snow and Landscape Research WSL and the Dendrosciences Group for allowing me to use their laboratories and equipment. I am very grateful to Roman Thoma, the district forester from Elm, for his immediate support, accompanying me on the field visit, and allowing me to take samples in the Ramintal. A big thank you goes to Marianne Homberger for her spontaneous and generous hospitality in the vacation apartment in Elm, which saved me from having to travel home on several occasions. I would also like to thank Kai Frey for the good company and entertaining breaks at the WSL, whether in the student room, or during lunch or afternoon snack breaks. Finally, my gratitude goes to Antonia Hehli, Alexander Karzig, and Amelina Wernli for proofreading my work and for their motivational support.

Abstract

Landslides pose a major threat to people and infrastructure in mountain regions worldwide. Climate change is expected further to increase the intensity and frequency of mass movements. A detailed understanding of past events and the factors that influence slope dynamics is essential for improving hazard assessments. Dendrogeomorphology provides methods to reconstruct past landslide processes using tree-ring records and to combine them with field observations to assess slope activity. In this study, Norway spruce (*Picea abies* (L.) Karst) trees were sampled on a slope near Elm (Canton of Glarus, Switzerland). The extracted increment cores were processed and measured to evaluate growth responses in annual increment rings, such as eccentricity and reaction wood formation. During the analysis, it became evident that relying solely on eccentricity values did not provide reliable event frequencies. Only the inclusion of reaction wood occurrence improved the robustness of event detection. The identified event years were compared with precipitation data to test for statistical correlations, and the potential effect of drainage channels constructed in the 1990s on event frequency was analyzed. Precipitation did not appear to be a significant trigger for the events detected in the tree-ring chronologies, whereas the installation of drainage channels significantly reduced event frequency. Field inspections and tree-ring analyses suggest that the slope is likely to remain slowly active as long as the drainage channels continue to function. However, past landslide activity reconstructed from tree-ring analyses does not provide a reliable basis for predicting future slope behavior under changing climatic conditions. Further research is essential to better understand the interactions between slow-moving slopes and tree growth, thereby providing a sound basis for reliable predictions of future slope activity.

Content

List of Figures

List of Tables

1. Introduction

Landslides are among the most hazardous geomorphic processes. Depending on the size and exposure, these events can cause extensive damage to infrastructure, pose serious risks to human life, and cause enormous costs for the maintenance and reconstruction of infrastructure, particularly in densely settled alpine valleys (Šilhán, 2019, 2020). Even slow-moving landslides significantly influence hillslope evolution and hazard assessments (Malik et al., 2016). Landslide activity is closely related to climatic conditions. Thus, the climate-landslide relationship is of particular importance as increased climate changes are expected to occur in the future (Šilhán, 2021).

Climate change is widely recognized as a major driver of shifts in environmental processes and an increasing frequency of natural hazards worldwide (IPCC, 2021). Changes in average conditions already have serious consequences, with the most significant impacts of climate change being felt most strongly due to interannual climate variability and extreme weather events (Stoffel & Huggel, 2012). Globally, an increase in the frequency and intensity of extreme precipitation events has been identified, while a strong increase in the number of heat waves has been observed (Stoffel & Huggel, 2012). Mountain regions are particularly vulnerable to these impacts as rising temperatures and altered precipitation patterns strongly affect slope stability and geomorphic activity, making them key areas for observing early signals of climatic change (Beniston, 2006; Hock et al., 2019). Landslides typically develop on moderate to steep slopes and are, therefore, especially common in mountainous regions, where limited infrastructure redundancy as well as increased sensitivity to climate change strengthen their impacts (IPCC, 2022).

For the European Alps, conditions contributing to increased landslide potential are expected to intensify (IPCC, 2021). In the Alps, effects of global climate change manifest in more frequent and intense precipitation extremes, longer snow-free periods, and enhanced permafrost degradation, all of which contribute to a higher likelihood of mass movements (Beniston, 2006; Stoffel & Huggel, 2012). In Switzerland, recent climate scenarios confirm these trends. They further predict continued warming and a rising intensity of heavy precipitation, which is likely to further increase the occurrence of landslides and flooding, leading to widespread damage (NCCS, 2018). These developments highlight the urgent need for improved understanding of slope dynamics and local instability processes, particularly in alpine terrain where such hazards threaten infrastructure, forests, and mountain communities. Each mountain valley is affected differently by the increased natural hazards. To counter them, infrastructure such as flood protection and drainage networks must be properly designed (NCCS, 2018).

In the context of ongoing climate change, the influence of precipitation on slope stability deserves particular attention. Altered precipitation patterns and more frequent high-intensity rainfall events strongly affect hydrological conditions, often acting as primary triggers of landslide activity (Beniston, 2006; Hock et al., 2019; Lopez Saez et al., 2012; Macfarlane, 2009; Malik et al., 2016; Papciak et al., 2015; Šilhán, 2020). Quantifying the relationship between precipitation and slope movement is therefore essential for understanding slope dynamics and improving hazard assessment in alpine regions.

Since landslide activity is closely linked to hydroclimatic variability, a comprehensive understanding of climate-landslide interactions is crucial for predicting future hazards. To better assess and predict such hazards, both past and present slope movements must be measured. Due to global climate change and the effect of associated environmental changes on mass movements, new methods need to be developed to record and quantify past and recent processes (Gärtner et al., 2004). Recent advancements in monitoring techniques, such as laser-based geodesy, differential Global Positioning Systems, and radar, enable higher-resolution tracking of landslide movement

(Massey et al., 2013; Razak et al., 2011). Combined with analyses of causal factors, these techniques improve understanding, management, and prediction of slope behaviour (Massey et al., 2013). However, conventional monitoring and dating techniques remain limited in precision, cost, or applicability, particularly in steep, forested terrain (Curioni et al., 2024; Fabiánová et al., 2021). To make statements about prediction and mitigation, past processes and their spatial and temporal distribution should first be reconstructed through detailed chronologies (Stoffel et al., 2013; Wistuba et al., 2013). Radiometric techniques, such as radiocarbon, uranium-thorium dating, luminescence, and cosmogenic radionuclide dating, provide long-term records of past events. However, their precision is often limited, and they are costly, sample-intensive, and not suitable for all landslide types (Fabiánová et al., 2021; Šilhán, 2021). Additionally, historical data on past landslides is often scarce due to incomplete records, unreliable memories, as well as the remoteness of affected areas, highlighting the need for diverse absolute dating methods (Fabiánová et al., 2021; Lopez Saez et al., 2012). The resulting scarcity of reliable long-term records emphasizes the need for alternative approaches to reconstruct landslide chronologies.

Dendrogeomorphology provides such an alternative approach. By analyzing tree-ring growth anomalies to detect and date past slope movements (Alestalo, 1971; Stoffel & Bollschweiler, 2008; Stoffel & Corona, 2014). It combines geomorphology and dendrochronology: A precise geomorphological site assessment and process analysis must be carried out in advance to determine the geomorphological process that caused the disturbance (Gärtner et al., 2004). The dendrochronological part is based on the dating of a tree's reaction to external disturbances, which is recorded in tree rings (Šilhán, 2019). Trees respond to disturbances such as tilting, burial, or root damage with growth anomalies that can be dated with high precision, making this a cost-effective and reliable tool for reconstructing landslide chronologies, particularly in remote or otherwise inaccessible areas where other methods are limited (Alestalo, 1971; Gers et al., 2001; Šilhán, 2019, 2020; Wistuba et al., 2013). As a result, dendrogeomorphic techniques have become a powerful tool for understanding landslide dynamics, improving hazard assessments, and complementing other dating and monitoring methods.

Dendrogeomorphology has developed into a widely applied approach for reconstructing past slope processes since its beginnings in the 1970s with the pioneering work of Alestalo (1971). Early studies demonstrated the potential of reaction wood, eccentricity, and further growth disturbances to date geomorphic events (Braam et al., 1987; Shroder, 1978). Later studies incorporated detailed geomorphologic mapping and multi-indicator analyses, significantly improving accuracy and reliability (Gärtner et al., 2004; Stoffel et al., 2013; Stoffel & Bollschweiler, 2008). Recent advances have broadened dendrogeomorphic approaches by including more tree species, refining growth-disturbance indicators such as eccentricity and reaction wood, and integrating geomorphic mapping with modern monitoring and climate analyses across diverse landslide types (e.g., Fabiánová et al., 2021; Malik et al., 2016; Šilhán, 2017, 2020, 2021; Šilhán & Stoffel, 2015; Tichavský et al., 2019).

Despite these advances, challenges remain. In the study of slow-moving landslides, subtle and prolonged deformations complicate signal detection and dating accuracy (Handwerger et al., 2013; Malik et al., 2016; Malik & Wistuba, 2012). Furthermore, tree responses are age-dependent, disturbance signals differ in spatial extent, and equifinality complicates the attribution of growth anomalies to specific processes (Šilhán, 2019, 2020, 2021; Stoffel & Corona, 2014). These remaining challenges underline the need for further methodological refinement and provide the context for the present study.

The present study focuses on landslide movements of an alpine slope near Elm in Switzerland. Unstable geological layers have led to deep-seated slumping and recurrent mass movements (Grämiger, 2024). Loose surface material and erosion by valley stream further destabilize the slope, which remains active with estimated displacement rates exceeding 10 cm per year, occasionally even much higher (Grämiger, 2024). Even though clear geomorphic signatures of landslides are visible, no severe surface displacements have been reported yet. Of particular interest for the study is the fact that drainage channels were installed starting from the 1990s to drain the slope's surface water, stabilize the slope, and enable road construction for alpine farming further up the slope. Therefore, the still intact drainage channels could have an impact on the slope dynamics. However, long-term monitoring data on movement rates and depths are lacking, highlighting the need for alternative approaches such as dendrogeomorphic analysis.

Building on this framework, the present study aims to reconstruct landslide dynamics through the analysis of eccentric growth and reaction wood, while explicitly accounting for local geomorphological and climatic conditions. By applying dendrogeomorphic methods at this scarcely investigated, landslide-prone site, this study seeks to generate new insights into slope movement processes without the need for cost-intensive, long-term monitoring systems. The slope near Elm thus offers not only a representative case of ongoing mass movements, but also a unique opportunity to assess the effects of drainage systems on landslide activity and triggering factors such as precipitation. This knowledge contributes to improved hazard assessment and risk awareness for local communities.

1.1. Research question and objectives

To achieve the aims outlined above, the study is guided by the following research questions and hypotheses:

Overarching Research Question:

- *To what extent do landslides affect the tree growth of Norway spruce, and which factors influence landslide dynamics on a slope near Elm, Switzerland?*

Research Questions:

1. *To what extent does landslide activity cause growth disturbances in Norway spruce compared to a stable reference site?*
   - ➔ Hypothesis: Landslides in Elm trigger distinct growth reactions in Norway spruce, particularly the formation of reaction wood and eccentric growth.

2. *To what extent did the installation of drainage channels in the 1990s influence the frequency of landslides on the slope?*
   - ➔ Hypothesis: The installation of drainage channels in the 1990s reduced landslide activity and the associated mechanical disturbances recorded in tree rings.

3. *To what extent can reconstructed past landslide activity be used for predictions of future slope activities?*
   - ➔ Hypothesis: Tree-ring analysis can reconstruct past landslides with sufficient precision to identify patterns that support the prediction of future slope activity.

2. Study Area

2.1. Location

Through research and consultations with local authorities responsible for landscape management, an area with known large-scale slope movements on a south-east-facing hillside was identified. Although not widely known, the landslide poses significant local challenges for residents and infrastructure, giving the site high practical relevance. Consequently, this slope was selected as the study area. It is located near Elm, a small mountain village in the canton of Glarus, south-eastern Switzerland, at the Swiss CH1903+ coordinates 2'734'132, 1'198'356.

The slope (see Figure 1) is located in the Ramintal, an eastern side valley of the Sernftal, which branches off from the main Glarus valley. The Raminbach stream in the valley erodes the base of the slope. The slope is facing in a southeast direction with an inclination of approximately 25°, whereas the opposite slope is much steeper and dominated by rock outcrops. Due to its moderate gradient, the slope of the research has long been accessible for alpine farming and hiking. About 30 years ago, a road was constructed from Elm into the Gamperdun area to facilitate access for agriculture and forestry. This construction is of particular relevance to the study. According to eyewitnesses and historical aerial photographs, the slope had to be extensively drained with a network of channels prior to road building (see Chapter 2.4. *Drainage channels*). Today, the study site is best reached via this road and connecting hiking trails.

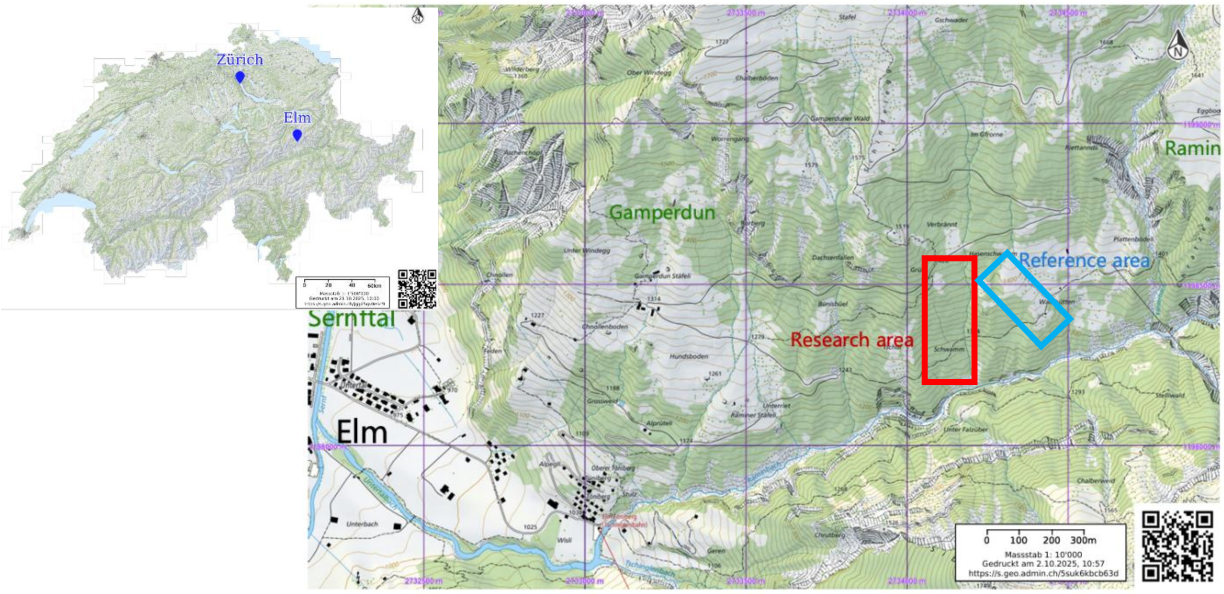

Figure 1: Map of Switzerland (left) showing the location of Zurich and Elm, and a map of the research area (red rectangle) and reference area (blue rectangle) on the slope near Elm, using the basemap of the Swiss Federal Office of Topography (Swisstopo, 2025a).

The slope is densely forested with deciduous trees in the lower parts of the area, *Picea abies* (L.) Karst, Norway spruce, as the dominant species. Accordingly, spruce was selected for the dendrogeomorphic study (see Chapter 2.5. *Tree species*). Forest management on this slope is limited to preventing forest overaging and processing the existing timber; however, there are no plans for protective forestry or high-value timber production.

The elevation of the research area is between 1260 and 1420 m a.s.l. Therefore, the altitude range of the slope is about 160 m, whereas the horizontal distance is about 300m. The uppermost soil horizon is very loose with varying thickness (Grämiger, 2024). The geological layers below are complexly stratified, causing a simple water infiltration, further destabilizing the slope (see Chapter

2.3. *Geology*). The small Schwammruus stream carries a large amount of water down to the valley floor into the Raminbach stream. The Raminbach stream carries all the collected water into the Sernftal valley, contributing significantly to the instability of the slope: Bank and toe erosion, particularly during flood events, remove the foundation at the slope foot and trigger shallow to deep-seated slides. Infiltrating surface water further accelerates these processes by saturating the debris cover. This combination of toe erosion, waterlogging, and unstable deposits creates predisposing conditions for recurrent slope movements and reactivation of older landslide bodies (Grämiger, 2024). Nevertheless, the slope is not widely known for active geomorphic hazards, as no major event has affected infrastructure or human life to date. Still, local residents are aware of its instability through frequent minor cracks as well as the extensive stabilization measures required along the road.

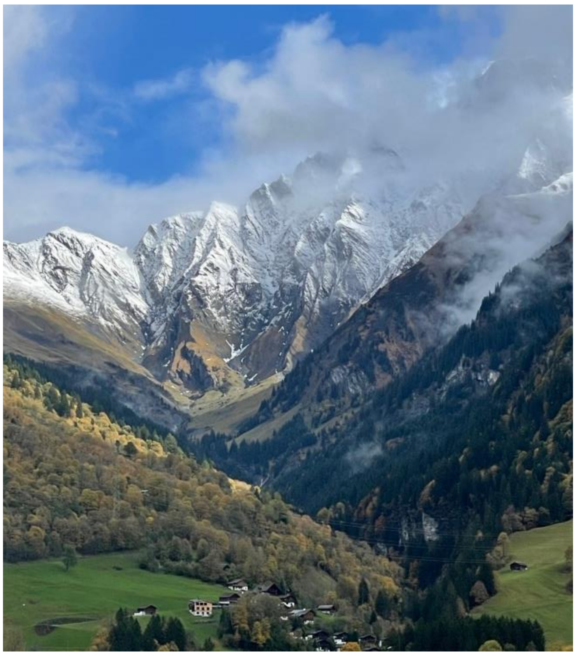

Figure 2: Photograph facing east taken from the opposite slope of the Sernftal above Elm, looking into the Ramintal. The study slope is visible on the left side.

According to the local district forester and a prior geological study by Dr. von Moos AG (Grämiger, 2024), the slope shows clear signs of instability. Cracks in the ground, subsiding areas, erosion at the slope foot by the Raminbach stream, and repeated deformations of the road illustrate ongoing movement. Field surveys by Grämiger (2024), which provided the geological information used in this thesis, were mainly conducted within a site perimeter located about 500 m west of the study area. Nevertheless, the characteristics of the subsurface, the composition of the soil, and other conditions, such as hydrology, erosion, and slope inclination, are comparable. The surveys documented both older and more recent scarps as well as shallow slides and fresh surface ruptures, all of which confirm ongoing slope instability. The affected area covers several tens of thousands of square meters and has required extensive stabilization measures along the road since the 1990s, including drainage channels to reduce water infiltration. The geological causes of these processes are outlined in Chapter 2.4. *Geology, soil, and slope conditions*.

Figure 3: Photographs of visual signs of slope movements: Cracks in the topmost soil layer and tilted trees (left), subsiding road (middle), and eroded foundation (right).

2.2. Reference area

In a geologically unstable and geomorphically active area, it is challenging to identify a reference site where landsliding can be completely excluded while still meeting comparable sampling criteria (species composition, solar exposure, slope aspect, nutrient availability, etc.). Therefore, a reference site (see Figure 1) was ultimately chosen that is somewhat flatter (20° inclination), situated at a similar elevation (1330-1410 m a.s.l.), and has the same exposure, but is located about 250 m further east and further towards the end of the valley. It is more open and contains a larger clearing used as pastureland, interspersed with tree groups and forest patches dominated by spruce of varying ages, which provided suitable material for sampling. Stable conditions, however, cannot be guaranteed, which is why the cores had to be sampled differently to minimize potential disturbances (see Methods, Chapter 4.2 *Sampling*). The substrate also appears somewhat loose, and the underlying layers may allow for easier water infiltration.

Additional characteristics of the reference site are important to note. While geomorphic activity is assumed to be lower than at the main study slope, minor processes such as shallow soil creep, snow pressure, or wind stress cannot be entirely excluded. The choice of this location was thus a compromise, balancing accessibility, comparability of tree growth conditions, and the need for a site with fewer slope disturbances. It is therefore assumed that trees on the reference slope form their annual rings primarily under the influence of non-geomorphological factors, with mass movements having only a minimal influence, meaning that the necessary conditions for reference sites formulated by Malik and Wistuba (2012) should be met. Though, as in all dendrogeomorphic studies, the reference chronology derived from this site must be interpreted with caution, acknowledging that disturbance-free conditions are relative rather than absolute.

2.3. Climate

The climatic conditions of the study area play a central role in tree growth and slope processes, as they determine both the ecological setting and the potential triggers of geomorphic activity. To characterize the regional climate, long-term meteorological records were consulted using data obtained from MeteoSchweiz (Federal Office of Meteorology and Climatology), which provides standardized climate sheets for individual stations across Switzerland. For this study, the dataset from the Elm station was used, covering the standard reference periods 1960-1990 and 1991-2020. The station is placed at an altitude of 958 m, at geographical coordinates 46.92 N / 9.18 E, corresponding to Swiss CH1903+ coordinates 2'732'266 / 1'198'424. The climate region is defined as an eastern Alpine northern slope (MeteoSchweiz, 2024b). The climate sheets of MeteoSchweiz summarize monthly and annual values for temperature, precipitation, and other climate parameters, based on homogenized measurements and consistent observation methods over the period. These records, thus, provide a reliable basis for describing the average climate of the study area, even though the weather station in Elm is located about 1.5 km further west and 300 m lower.

The mean monthly temperature in the study area follows a typical pattern of alpine valleys in moderate climate zones, with values below 0 °C from December to February, steadily rising above 0 °C in spring, reaching around 15 °C in July. Compared to the climate normal period 1961-1990, average monthly temperatures have increased by about 1-2 °C per month. Accordingly, the mean annual temperature has risen from 5.6 °C in 1961-1990 to 6.9 °C in 1991-2020 (MeteoSchweiz, 2024a, 2024b). Since the study site lies at least 300 m higher in elevation, temperatures can be expected to be about 3 °C lower.

During the 1991-2020 period, the total annual precipitation averaged at 1525 mm, with values of roughly 100 mm per month in winter and peaks exceeding 160 mm per month in summer (June-August). High summer precipitation is particularly important in a dendrogeomorphic context, as intense rainfall events during the growing season are a key trigger for landslide activity and strongly influence tree growth responses recorded in the ring structure (see Chapter 3.9. *Precipitation influence on slope activity*). Compared to the earlier climate normal period, summer precipitation increased by about 20 mm, while winter values decreased by 5-10 mm. Overall, the annual precipitation sum has risen by approximately 40 mm (MeteoSchweiz, 2024b, 2024a).

Additional climatic factors such as snow cover, wind, and sunlight also influence tree growth and slope processes. Since wind and sunlight are not recorded at the local weather station, only general assumptions can be made. As is common in many parts of Switzerland, westerly winds dominate and bring humidity and precipitation. Sunlight is abundant in summer, but from November onward, the lower parts of the slope receive little or no direct sunlight. During December and January, almost the entire study area lies in the shadow of the opposite mountain range, as observed during field visits. Reduced sunlight combined with snow cover, often exceeding 10 cm until March, delays the onset of earlywood formation and, thus, shapes growth conditions. However, little is known about specific snow deposition patterns at the site, although snow avalanches are not expected on this slope.

Figure 4: View towards the southwest from the reference area with some reference trees in the foreground. Only little sunlight reaches the study site in wintertime.

2.4. Geology, soil, and slope conditions

In the framework of this study, no detailed soil profile descriptions were carried out, although such an analysis would have been beneficial. However, recording the soil profile would have required a lot of additional material and effort and would have gone beyond the scope of a dendrogeomorphological study. Based on surface observations by Grämiger (2024), the soil is of varying thickness, consisting of deposited slope debris, with stones and blocks up to large boulders in a matrix of sandy-silty-clayey gravel. This soil is repeatedly disrupted and overlain by deposits from slope processes. The crumbly, loose texture of the substrate likely facilitates rapid water infiltration (Grämiger, 2024). Small rills often disappear into the ground and reappear further downslope, indicating heterogeneous subsurface drainage. In addition, the soils consist of unstable and reworked colluvial material with variable depth and local saturation after heavy rainfall. The continuous movement, infiltration processes, and fractured geological bedrock suggest that growing conditions for trees are challenging and provide little stability for root development.

The study area lies within the Helvetic nappes of eastern Switzerland and is part of a complexly deformed tectonic setting. The slope belongs to the Blattengrat nappe and other overlying or underlying nappes, which are composed mainly of alternating marls, shales, and sandstones of the Wang-/Amden Formation and the Elm Formation (northern Helvetic flysch group). These sequences often dip slope-parallel, creating unfavorable structural conditions for stability (see Figure 5). In addition, more competent units such as sandstones and limestones are interbedded with weaker marl horizons, further promoting large-scale deformation (Grämiger, 2024).

According to Grämiger (2024) and the Geological Atlas of Switzerland (Swisstopo, 2024a), the entire south-facing slope is interpreted as a deep-seated rock subsidence, with slumped masses of fractured rock several tens of meters thick. Above this, heterogeneous deposits of colluvium, slope debris, and alluvium form a permeable surface cover that promotes rapid infiltration. The looseness of this material, combined with continuous undercutting by the Raminbach at the slope foot, further accelerates instability. While no continuous geotechnical monitoring is available, landslide rates are estimated to exceed 10 cm per year in this active phase of thrust, with short-term accelerations of 40-60 cm annually. The landslide system is therefore still active, with potential for spontaneous reactivation, valley blockages with backwater, and the risk of debris-flow eruptions potentially endangering the settlements further down the valley. While the damage potential for roads and other infrastructure on the slope is lower, there nevertheless remains a risk of damage and costly repairs.

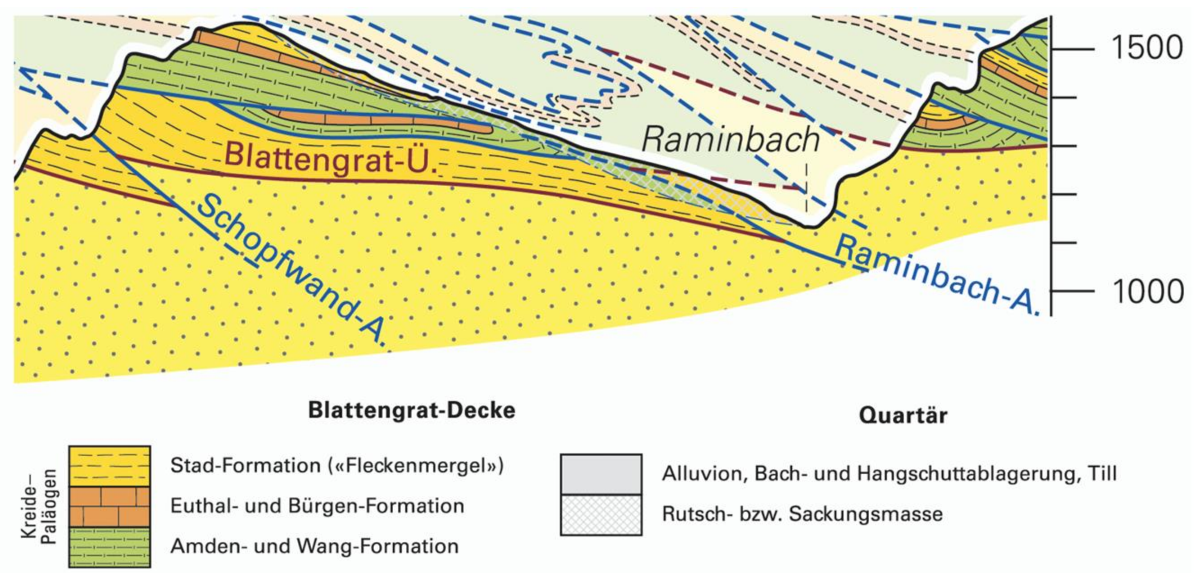

Figure 5: Geological profile from the Geological Atlas of Switzerland, showing the superimposed Helvetic nappes (yellow, orange, green) in the Ramintal west of Elm, with landslide and sagging masses and fluvial and slope debris deposits (gray areas with yellow/green stippling at the top of the profile in the center of the image) (Source: Grämiger, 2024, p. 6).

2.5. Drainage channels

The slope, with its numerous scarps and ruptures in soil and bedrock, is highly prone to rapid water infiltration. To reduce this effect, a system of drainage channels was constructed. Numerous drainage channels, particularly above the road, were dug and reinforced with cement. Some of these channels were inspected during field surveys and still appear intact and functional, draining water efficiently (see Figure 6) despite low maintenance. The extent of this construction effort in the 1990s is visible on historical aerial photographs in Figure 7 (Swisstopo, 2025b). The drainage channels were also mentioned by Grämiger (2024), who used these historical aerial photographs from Swisstopo to determine that large-scale surface drainage systems had been installed further up the slope from 1990 onwards.

Figure 6: Inspection of individual drainage channels with the Elm forest ranger.

The exact location and distribution of these channels can be seen using high-resolution relief maps (Swisstopo, 2024b). They reveal many drainage channels distinctly on the slope's relief (see Figure 8). However, it remains uncertain how effective these drainage channels have been since their construction in the 1990s, and whether they have contributed to an apparent increase in slope stability. This question will be further investigated using dendrogeomorphic methods.

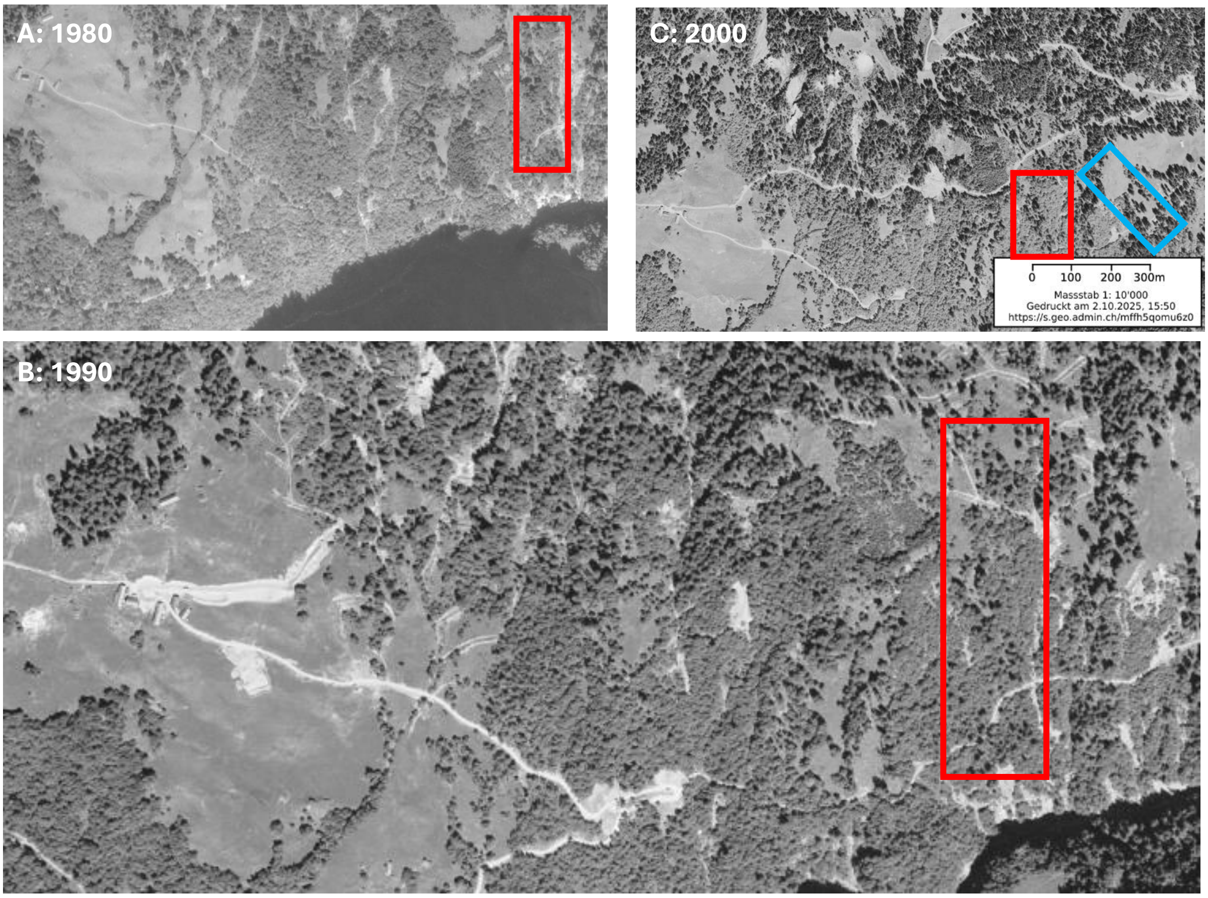

Figure 7: Three different aerial photographs showing: A: 1980 with small forest paths, B: 1990 with road construction and digging of drainage channels, and C: 2000 with a completed road. Research area in red and reference area in blue. Historical aerial photographs provided as Swissimage Zeitreise by Swisstopo (2025b).

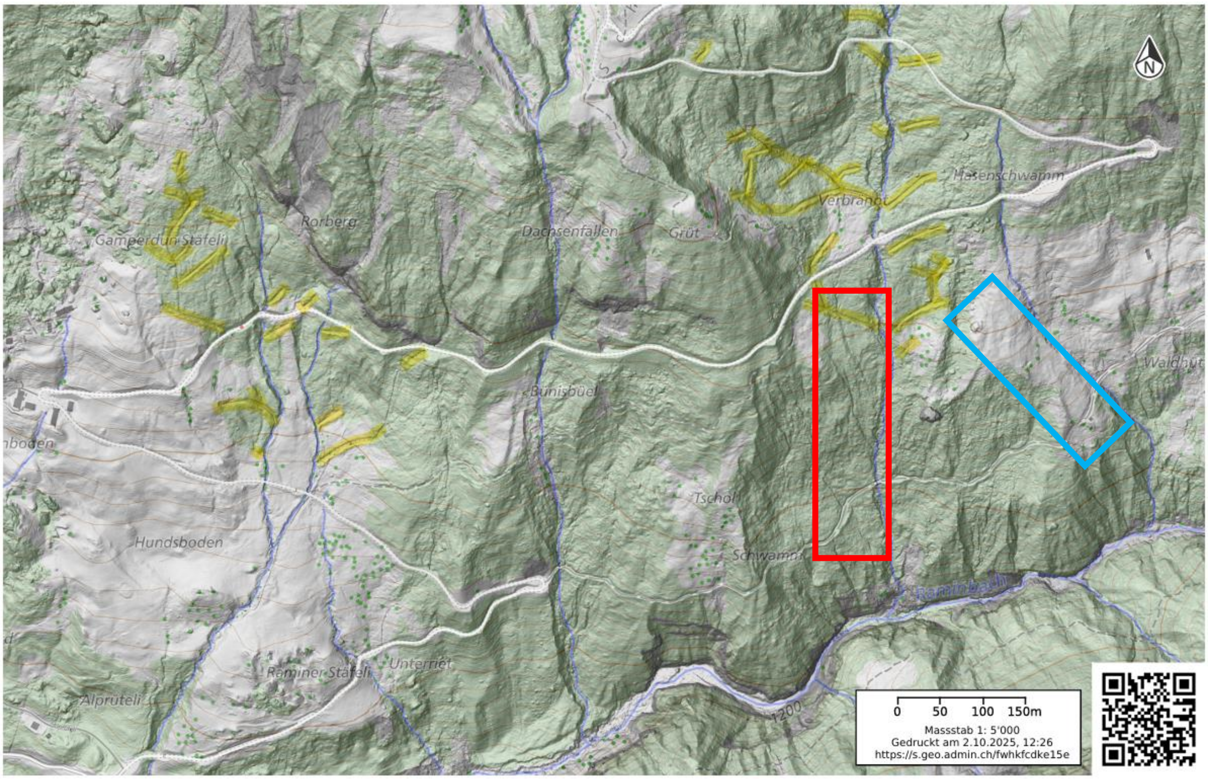

Figure 8: Relief map (swissALTI3D multidirectional) of the study slope with a topographic map in the background. Identified drainage channels are highlighted in yellow, research area in red and reference area in blue (Swisstopo, 2024b, 2025a).

2.6. Vegetation and sampling species selection

The vegetation in the study area is characterized by a mixed forest. While many maple, ash, and other deciduous trees grow in the lower parts of the slope, conifers become increasingly common above 1200 m a.s.l., with their frequency increasing with altitude. At the study site, Norway spruce (*Picea abies* (L.) Karst) occurs in high abundance, which is already evident in Figure 2. In addition to mixed forests covering the entire slope, there are also meadows with various types of grass, some of which are used for livestock farming.

Due to the abundant occurrence of spruce trees in the study area, they were chosen for sampling in this study. The altitudinal range of the slope (1260-1420 m a.s.l.) is typical for Norway spruce species. Norway spruce is widespread in montane and subalpine zones of Central Europe, where it commonly forms the dominant tree species at higher elevations (Šilhán, 2019). Due to its abundance in mountain forests and sensitivity to slope instability, spruce is one of the most frequently used species in dendrogeomorphic research (e.g., Fabiánová et al., 2021; Šilhán, 2017; Tichavský et al., 2019; Wistuba et al., 2013). For these reasons, it was logical to choose Norway spruce as the species for investigation.

Figure 9: Norway spruce in the research area, with visible stem tilting toward the left or the right side of the image, likely induced by geomorphic processes in the underlying slope.

Spruce is sensitive to both waterlogging and drought due to its shallow plate-root system. It is less resistant to geomorphic disturbances such as landslides or rockfalls compared to deep-rooted deciduous species (Tichavský et al., 2019). Disturbances often result in stem tilting and the formation of compression wood, which represents the most common growth anomaly in spruce on unstable slopes (Šilhán, 2019). From a methodological perspective, spruce offers clear advantages for dendrogeomorphic studies: its softer wood allows easier sampling, tree rings are well visible, and reaction wood formation tends to be distinct and consistent (Šilhán, 2020). These features make Norway spruce particularly well-suited for reconstructing landslide activity in the Central European mountain environment.

3. Theory

This chapter introduces the theoretical foundations of the study. Firstly, it explains the basics of tree growth and the principles of dendrochronology and geomorphology, as well as the principle of dendrogeomorphology. Secondly, the theoretical background of tree growth responses to slope processes is explained, and methods for detecting and interpreting these signals are introduced. In addition, this chapter outlines key challenges associated with tree-ring analysis and discusses the role of reference areas in minimizing uncertainties. Finally, the influence of external factors such as precipitation on landslide activity and the potential mitigating effects of drainage systems are addressed. Together, these elements form the conceptual framework for the applied methods and subsequent analysis.

3.1. Tree growth

Tree growth in diameter is caused by the activity of the cambium, a tissue that produces new wood cells beneath the bark. As a result, a ring forms over the course of a growing season, enlarging the trunk, branches, and roots. (Malik & Wistuba, 2012). In temperate regions with marked seasonality, trees produce distinct annual rings. The so-called increments consist of large, thin-walled cells (earlywood) that form in spring and early summer under favorable conditions, while smaller, thick-walled cells (latewood) develop later in the season as growth slows. The contrast between these tissues produces clear ring boundaries, particularly in conifers, where a light earlywood band is followed by a dark latewood band each year (Malik & Wistuba, 2012). Regarding the whole tree's growth, typically, a tree not influenced by geomorphic or other external forces develops a straight, vertical trunk due to its natural, upward growth response to gravity.

The width of annual rings reflects environmental conditions and developmental stage. Growth is affected by site conditions such as altitude, exposure, hydrological conditions in the subsoil, nutrient availability, temperature, and precipitation (Gärtner et al., 2004). Narrow rings typically reflect stress conditions, such as those caused by drought, whereas wider rings indicate beneficial conditions, such as sufficient water availability (Malik & Wistuba, 2012). Because tree-ring width integrates a broad spectrum of ecological factors, this parameter is the most analyzed in dendrochronology (Esper & Gärtner, 2001). Moreover, ring width changes systematically with tree age: juvenile wood usually shows wider and more variable rings due to rapid early growth, while ring width gradually declines as trees mature and biomass is distributed around a larger stem circumference. This biological trend is known as the age trend (Esper & Gärtner, 2001).

Beyond climatic and ecological influences, trees respond sensitively to geomorphic disturbances caused by slope instability. These impacts trigger mechanical responses, which will be further discussed in Chapter 3.3. *Dendrogeomorphology.* The type and intensity of such growth disturbances often reflect the characteristics of the geomorphic process, making trees valuable indicators of past slope dynamics and providing the basis for dendrogeomorphic reconstructions (Šilhán, 2020). A noticeable tilt or curvature of a tree trunk is due to external influences such as geomorphic processes (Gärtner et al., 2004). The morphology and anatomy of disturbed trees provide valuable information on slope processes. Continuous slow movements often result in curved, saber-shaped stems as roots anchor in deeper soil layers while upper layers creep downslope. In contrast, a greater variety of tree forms is found on slopes that move in sudden, episodic events (Schmid & Schweingruber, 1995). The spatial extent of these features reflects the scale of the process, with widespread events leaving a signal in many trees (Stoffel et al., 2013). The strength and nature of growth responses depend on factors such as tree origin, root depth, and the depth of the landslide, with deeper slides typically inducing more pronounced effects. Sensitivity of trees to landslide activity further varies with species, age, size, and local geological conditions (Šilhán, 2020). Thanks to the sensitivity of trees to respond to disturbances and reflect them in their growth, the time of the disturbance can be dated, which forms the basis for dendrogeomorphology.

3.2. Dendrochronology and geomorphology

Dendrogeomorphology (Alestalo, 1971) builds on two complementary disciplines: dendrochronology, which focuses on the analysis of annual growth rings as archives of environmental variability, and geomorphology, which examines landform development and slope processes. Understanding their individual principles is essential before considering how they intersect in dendrogeomorphic research. Therefore, the following section first introduces the fundamentals of dendrochronology.

3.2.1. Dendrochronology

Dendrochronology is the science of dating and interpreting annual growth rings of trees, providing a precise and high-resolution archive of past environmental variability. Dendrochronology differs from other absolute dating methods since ring counts alone are insufficient. Instead, tree-ring series are cross-dated across multiple samples to verify their annual nature and avoid errors from missing or false rings.

In temperate regions, distinct seasonal contrasts produce annual growth rings through cambial activity, with earlywood forming at the start of the growing season and denser latewood later in the year (Guibal & Guiot, 2021). The dendrochronological analysis of growth rings offers annual resolution with high accuracy, as tree growth is strongly structured by seasonal cycles (Malik et al., 2016). By aligning ring sequences from different samples by matching patterns of narrow and wide rings, the correct placement of each annual ring in time is ensured (Guibal & Guiot, 2021). Climatic variation directly influences tree growth by affecting metabolism and cambial activity, which shapes ring width and wood anatomy. This dependency leads to synchronous growth reactions among trees within a site and, under certain conditions, across larger regions, providing the basis for dendroclimatological research and supporting the reliability of cross-dating (Esper & Gärtner, 2001). Additionally, ring characteristics are limited by environmental factors and additional influences such as soil, topography, tree age, or competition (Guibal & Guiot, 2021).

Tree-ring records are therefore crucial for understanding past climate variability, particularly across mid- to high-latitude landmasses where trees with seasonal cycles are most abundant. They allow comparison of modern warming trends with earlier periods not influenced by anthropogenic activities (Esper & Gärtner, 2001). Beyond climatic signals, trees also record geomorphic disturbances such as impact, loading, burial, or erosion to the exact year and, under favorable circumstances, even to the season (Stoffel et al., 2013). Individual trees also record mechanical disturbances from external processes, making them valuable archives for reconstructing geomorphic activity such as landslides (Stoffel & Corona, 2014). However, while such disturbances are accurately dated, tree rings usually cannot reveal the specific nature of the triggering process (Stoffel et al., 2013). Therefore, a precise geomorphological site assessment and process analysis must be carried out before tree selection and sampling (Esper & Gärtner, 2001).

3.2.2. Geomorphology

Geomorphology provides the theoretical and methodological basis for site assessments. It focuses on the study of landforms, surface processes, and their interactions on slope stability. The documentation of these geomorphic processes and related natural disasters is a major key to the assessment of ongoing hazards and risks (Stoffel & Corona, 2014). For an appropriate hazard assessment, detailed landslide chronologies are necessary, yet records of past activity are often incomplete (Lopez Saez et al., 2012) and biased toward large events, particularly in remote areas (Šilhán & Stoffel, 2015). Therefore, the reconstruction of past geomorphic processes is essential, with precise field-based landform analysis providing the foundation for such reconstructions (Gärtner et al., 2004). Through these site assessments, researchers can identify landforms, detect surface processes, and infer implications for slope stability.

A detailed understanding of the climate-landslide relationship is of particular importance, as landslide activity is closely related to hydroclimatic conditions, and climate changes are expected to occur in the future (Šilhán, 2021). Mass movements can have catastrophic effects, for instance, large-scale and rapid events such as landslides, rockslides, and rock avalanches triggered by long-term or heavy precipitation events (Malik & Wistuba, 2012). In some cases, landslides can dam streams, leading to pronounced changes in channel profiles and enhanced erosion. Overall, a wide range of landslide types exists, differing in morphology, internal structure, velocity, and movement mechanisms (Šilhán, 2021). Mass movements occur in various forms, including lateral spreading, toppling, rockfall, landslides (focus in this study, a movement of material along a recognizable shear surface), debris flows, and soil flows, each defined by distinct movement mechanisms and material behavior (Malik & Wistuba, 2012). Recognizing this diversity is essential for understanding slope processes and forms the basis for applying dendrogeomorphic methods to investigate how mass movements are recorded in tree growth.

3.3. Dendrogeomorphology

Dendrogeomorphology combines methods from dendrochronology and geomorphology to reconstruct past mass-movement activity through tree-ring analysis. Trees growing in climates with distinct seasonality produce an annual ring, allowing reconstruction with annual and sometimes even seasonal resolution. Therefore, they provide one of the most accurate natural archives for studying slope processes (Malik & Wistuba, 2012). Sensitive tree species, whose ring-width variability responds strongly to environmental factors such as temperature and precipitation, are particularly valuable for dendrochronological analyses (Fantucci, 1999). Disturbances caused by slope movements are also recorded in the annual growth rings. Even small transformation processes of the slope's morphology are recorded (Malik et al., 2016). By dating past events preserved in tree rings, the dynamics of slope processes over the period covered by the dendrochronological record can be assessed (Gärtner et al., 2004).

Trees growing on unstable slopes are subject to a variety of apparent disturbances, including tilting, burial, root and stem damage, scars, and bark removal (Fantucci, 1999). Among these responses, tilting is particularly common on active landslides. Destabilized trees deflected from their upright position react by forming reaction wood (Braam et al., 1987; Šilhán & Stoffel, 2015). Reaction wood and other growth responses such as ring eccentricity, abrupt growth suppression (e.g., due to severe root damage (Gers et al., 2001)) or release, as well as sprouting or tree mortality, are recorded in the annual rings (Fantucci, 1999; Shroder, 1978). Different types of mass movements (e.g., lateral spreading, landsliding, debris flow) typically tilt trees in a single direction, and the resulting growth response depends on whether the inclination is upslope or downslope (Malik

& Wistuba, 2012). An overview of the different reactions of a tree with eccentricity to a landslide is illustrated in Figure 10. The direction of tilting reflects slope kinematics: in rotational sliding stems often tilt upslope near the head scarp, whereas in planar sliding they may remain upright but show growth suppression from root damage, or tilt downslope; under slow deformation, trees can gradually regain an upright position, producing a characteristic J-shaped stem base (Curioni et al., 2024).

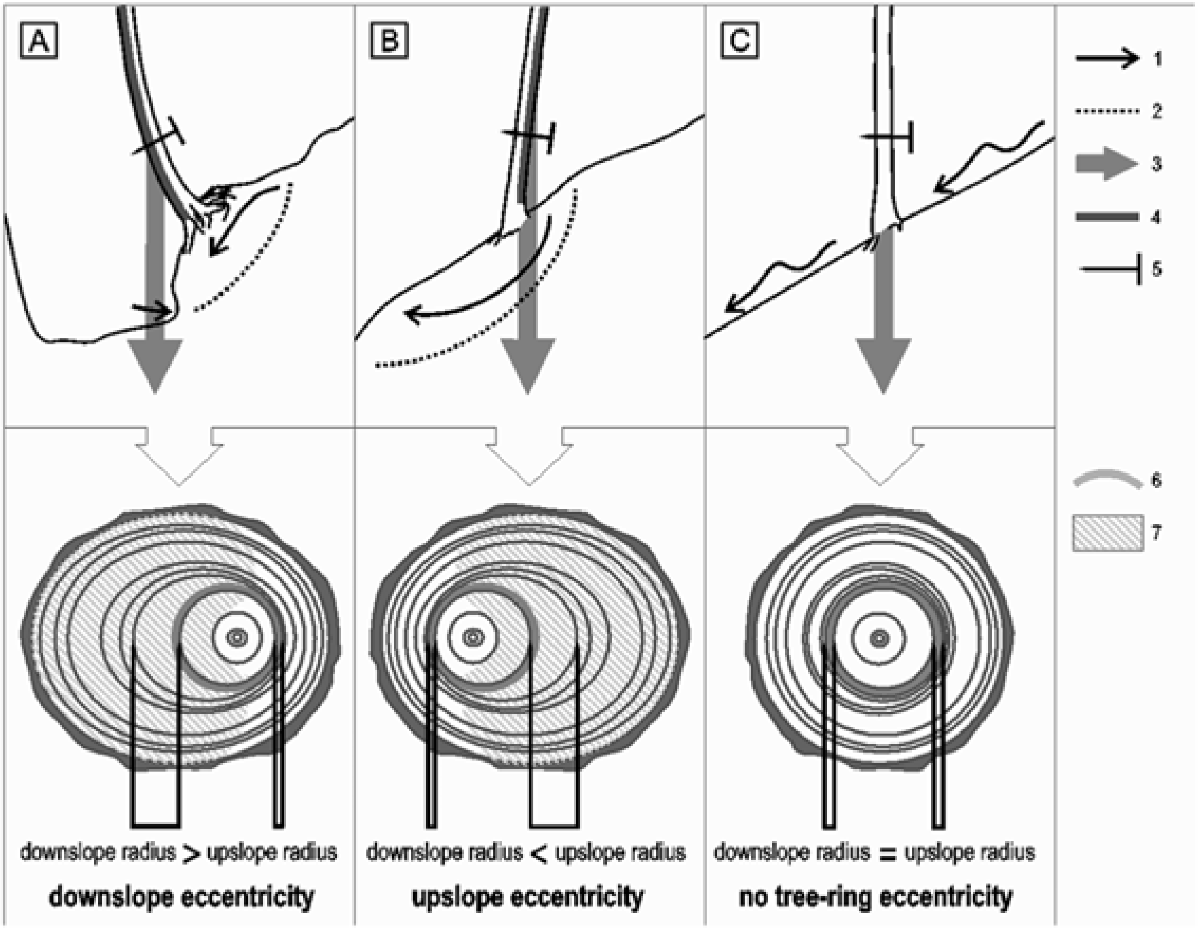

Figure 10: Development of eccentricity of tree rings: A - downslope eccentricity of a tilted tree, B - upslope eccentricity, C - lack of eccentricity in a straight stem (example of Picea abies). Numbers: 1 - direction of impact of geomorphic processes, 2 - sliding surfaces, 3 - gravity force, 4 - stem zones with wider rings and reaction wood, 5 - stem cross-sections, 6 - ideally concentric ring, 7 - zone of reaction wood development (Source: Malik & Wistuba, 2012, p. 184).

For a complete assessment of the trees on a sliding slope and a reconstruction of geomorphic processes, individuality needs to be maximized when trees are sampled. Visibly damaged or deformed trees with scars, eccentricity, or reaction wood are of particular interest to date geomorphic events (Esper & Gärtner, 2001). Detailed knowledge of site parameters is of great importance to conclude system behavior (e.g., threshold values for process initiation). Therefore, the researcher should specify the key parameters, such as geology, substrate, vegetation cover, temperature, precipitation, exposure, elevation, and slope, for the entire study area (Gärtner et al., 2004).

Growth anomalies like width changes, anatomical features, and eccentricity can now be analyzed and interpreted as evidence of slope instability in comparison to a reference chronology of trees with supposedly undisturbed growth. As some tree species like spruce stands can reach ages of 200-300 years in Central Europe, this allows dendrochronological reconstructions of landslide activity spanning several decades to centuries (Malik et al., 2016). Thus, dendrogeomorphic methods cover a longer period than any instrumental methods and can capture recurrence intervals, thresholds, and long-term slope behavior (Malik et al., 2016). The obtained results using dendrogeomorphic methods can be of great value, providing useful information on hazard zoning, urban planning, insurance assessment, and risk awareness (Šilhán, 2021).

3.4. Reaction wood

As already stated, reaction wood is a valuable indicator of past mass movement related to the tree's ability to regain a vertical position after tilting (Stoffel et al., 2013). Inclination of the stem results from the sudden pressure induced by geomorphic processes directly, by the associated deposition of material, or by the slow but ongoing destabilization of a tree through landslide activity or erosion (Lundström et al., 2007; Stoffel & Corona, 2014). Therefore, the degree of tilting strongly depends on the local morphological, geological, and soil conditions (Lundström et al., 2007; Šilhán, 2017). When a tree is tilted, subsequent trunk growth seeks to restore verticality, with the strongest reaction occurring on the side where the stem's inclination has shifted the center of gravity (Stoffel & Corona, 2014). Earthflows and rotational slides often disrupt and remodel topographic surfaces, causing survivor trees to exhibit tilting and root-plate damage, which in turn initiates the formation of reaction wood and may lead to abrupt growth reductions (Astrade et al., 1998; Stoffel & Corona, 2014).

Two types of reaction wood are distinguished: compression wood produced by coniferous trees and tension wood formed by deciduous trees (Malik & Wistuba, 2012; Šilhán & Stoffel, 2015; Timell, 1986). In conifers, reaction wood forms as compression wood on the lower side of leaning stems, characterized by eccentric growth rings that reflect geomorphic disturbances such as landslides (Gärtner et al., 2004; Šilhán, 2020; Timell, 1986; Wistuba et al., 2013). Compression wood is distinguished by wider and darker rings with thicker, rounded tracheid walls, higher latewood proportion, increased lignin content, and therefore greater density and hardness, visible as a dark brown ring (see Figure 11) composed of thick-walled cells (Malik & Wistuba, 2012; Šilhán & Stoffel, 2015; Stoffel & Corona, 2014; Timell, 1986). While compression wood in conifers is clearly identifiable, tension wood in deciduous trees is difficult to recognize macroscopically and requires microscopic analysis (Šilhán, 2021). Accordingly, most dendrogeomorphic studies rely on conifer species (Stoffel & Corona, 2014).

The analysis of reaction wood provides valuable insights into the timing and intensity of landslide disturbances. Reduced proportions of reaction wood compared to post-disturbance rings can often be attributed to the seasonal timing of landslide activity, demonstrating that dendrogeomorphic dating may, under favorable conditions, achieve even seasonal precision (Lopez Saez et al., 2012; Šilhán, 2017). However, the intensity of the growth response depends more on the disturbance experienced by individual trees than on the overall magnitude of the geomorphic process (Šilhán, 2017). Although reaction wood is a key indicator of the year of disturbance, its formation may be delayed, particularly after severe or repeated tilting. Such events can be identified by variations in the amount, color, or orientation of reaction wood within the tree-ring record (Braam et al., 1987; Fantucci, 1999; Shroder, 1978; Stoffel & Corona, 2014). This highlights the importance of careful cross-dating and the use of additional growth disturbance signals beyond reaction wood, such as eccentricity, abrupt growth suppression, or release, for reliable dendrogeomorphic reconstructions (Šilhán, 2017).

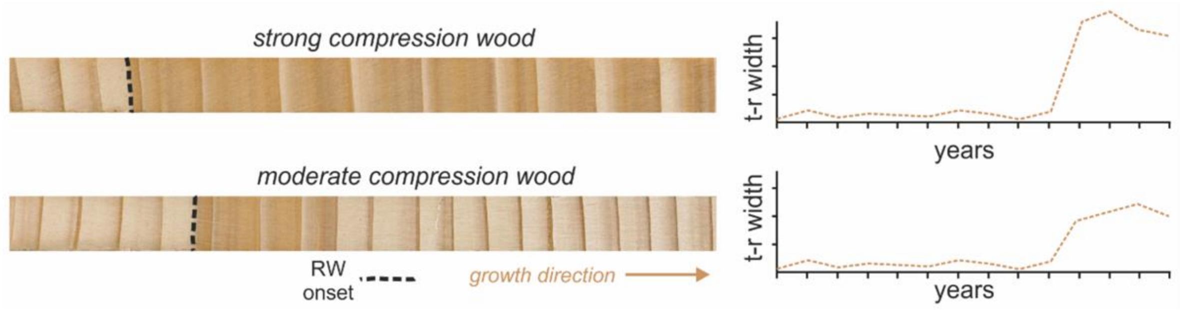

Figure 11: Example of compression wood in the tree-ring series of coniferous trees, shown together with increment curves that illustrate the associated growth release. Abbreviations: RW = ring width, t-r width = tree-ring width (Source: Šilhán, 2021, p. 7).

3.5. Eccentricity

Another important and already introduced signal of growth disturbance is eccentricity. Landslide-induced tilting commonly produces reaction wood, but this response is often accompanied by asymmetric ring formation. Thus, several authors regard eccentricity as a particularly sensitive indicator of past slope movements (Šilhán, 2021; Šilhán & Stoffel, 2015; Wistuba et al., 2013). While both types of reaction wood, compression and tension, are frequently associated with eccentric growth, the relationship between the two remains only partially understood (Šilhán, 2020).

Eccentric growth occurs when a tree produces wider rings on one side of the stem and narrower rings on the other, displacing the pith from the geometric center of the cross-section (Malik & Wistuba, 2012). Therefore, eccentricity is identified in ring-width graphs by the long-term divergence of upslope and downslope curves, reflecting asymmetric growth between stem sides (Malik & Wistuba, 2012). It is most caused by the unilateral formation of reaction wood in response to mechanical stress (Braam et al., 1987; Gärtner et al., 2004; Šilhán, 2017). Eccentricity may also result from non-geomorphic factors such as uneven nutrient availability, moisture availability, asymmetric crown and root development, yet typically without concurrent reaction wood. Therefore, the presence of reaction wood specifically indicates external mechanical influences, such as those from geomorphic processes (Gärtner et al., 2004; Gers et al., 2001).

Even minor mechanical stress from slight or short-lasting stem tilting can cause growth eccentricity. In tilted conifer stems, gravity triggers increased growth on the compressed, lower side (Wistuba et al., 2013). This means that coniferous trees, and among them Norway spruce, produce wider rings on the lower part of the inclined stem, usually accompanied by compression wood (Malik & Wistuba, 2012). The onset of eccentricity or reaction wood indicates when a tree first responded to a mass-movement event (Braam et al., 1987). Determining its end is more difficult, as these growth changes may persist for several years (Malik & Wistuba, 2012).

Interestingly, older coniferous trees typically respond to stem tilting by developing eccentric growth rather than reaction wood, as their stems are less elastic than those of younger trees (Šilhán, 2017; Šilhán & Stoffel, 2015; Stoffel & Bollschweiler, 2008). However, when annual rings get narrower due to limited conditions, tree-ring eccentricity becomes less significant. In such cases, reaction wood can still form even without visible eccentricity (Šilhán & Stoffel, 2015). Where measurable, eccentric growth provides a clear and quantifiable record of past mechanical disturbance. The eccentricity index is therefore applied to objectively describe the extent and direction of growth asymmetry in tilted stems.

3.5.1. Eccentricity index

For many years, researchers have used eccentricity indices to quantify tree-ring asymmetry as a sensitive indicator for geomorphic disturbances (Malik & Wistuba, 2012; Wistuba et al., 2013). Because eccentricity responds to external mechanical forcing, such as slope movement, it provides a useful signal for identifying landslide activity (Papciak et al., 2015; Wistuba et al., 2013). The principle is not new: Based on Alestalo's (1971) principle of the direction of sampling, eccentricity indices can be calculated using differences in ring width between opposite sides of a trunk to reveal both the timing and intensity of disturbance events, including landslides (Gärtner et al., 2004). While the basic idea has remained consistent, subsequent work has sought to refine how eccentricity is calculated and interpreted.

Some of the early indices were limited in their ability to distinguish between different disturbance types, to provide standardized comparisons across sites, or to be explicitly appropriate for other types of geomorphic disturbances. Braam et al. (1987) established their index for studies on mud flows. An index by Casteller et al. (2008) was calculated for snow avalanches (adapted from an index by Schweingruber (1996) on the impact of snow creep) but could not provide a comprehensive solution for the analysis of landslides (Wistuba et al., 2013). Over time, the calculation methods have been adapted and improved. Malik and Wistuba (2012) emphasized the need for indices that are not only sensitive to abrupt changes in a landslide slope but also robust enough to be compared with stable reference sites. Building on this line of work, Wistuba et al. (2013) presented an improved formulation that directly compares upslope and downslope ring widths. This version of the eccentricity index provides a clear measure of both the direction and magnitude of stem tilt or deformation, reduces ambiguity in identifying disturbance types, and simplifies application by avoiding the need for complex statistical treatment.

A further refinement of eccentricity analysis is the use of thresholds based on mean values plus standard deviations of the index to identify distinct and abrupt changes. By focusing on marked increases toward positive values or decreases toward negative values, such thresholds help to date the most likely periods of landslide activation and enable consistent comparison across research and reference sites (Malik & Wistuba, 2012). As these thresholds are derived from stable reference slopes, only events strong enough to exceed the natural variability are included, while weaker signals likely caused by ordinary growth disturbances (e.g., wind stress, snow creep) are excluded (Wistuba et al., 2013). The dimensionless index of Wistuba et al. (2013) thus enables more detailed and comparable reconstructions of landslide characteristics, allowing spatial as well as temporal analysis beyond the dating of single events. Šilhán (2019) highlighted several advantages of this approach. It offers a clear statistical procedure for detecting abrupt eccentricity changes, applies thresholds that help eliminate eccentricity inertia, explicitly considers tilting direction, and reliably identifies events consistent with expert-based interpretations. Nevertheless, some limitations remain. The method relies on reference chronologies, although tree eccentricity is also individually driven instead of being influenced only by regional growth factors, and reference trees themselves may yield false signals. Moreover, the index does not account for delayed growth responses, which can result in artificial sequences of consecutive event years (Šilhán, 2019).

The eccentricity indices used in this thesis follow Wistuba et al. (2013) as they have been tested in several studies on avalanche and landslide slopes and shown to be suitable for capturing slope movements through tree rings (Burkhalter et al., 2019; Malik & Wistuba, 2012; Papciak et al., 2015; Šilhán, 2019; Sitko et al., 2022; Słowik-Opoka, 2020). Further indices, such as that by Šilhán & Stoffel (2015), built on Braam et al. (1987), extract signals without reference chronologies (applied by e.g., Bovi et al., 2019; Oven et al., 2019; Tichavský et al., 2019). This allowed delayed responses and signal intensity to be considered, although they are limited by their categorical grouping and potential for noise (Šilhán, 2019). As each approach has specific weaknesses, the choice of method should be matched with the sampling strategy, particularly with respect to tree age (Šilhán, 2019).

3.6. Additional growth indicators

Beyond reaction wood and eccentricity, trees exhibit a range of growth disturbances reflecting geomorphic activity. Abrupt growth reductions may result from branch loss, root damage, apex decapitation, or trunk burial (Stoffel et al., 2013). Debris burial suppresses growth through reduced root activity and the mechanical weight of overlying material (Stoffel & Corona, 2014). Tilting can induce strong suppression on the upslope side or even missing rings (Braam et al., 1987; Shroder, 1978; Šilhán, 2017). Growth releases may occur in surviving trees benefiting from increased access to light and nutrients after neighboring vegetation is removed (Lopez Saez et al., 2012; Stoffel & Bollschweiler, 2008; Stoffel & Corona, 2014). The decrease (suppression) or increase (release) of growth is reflected by changes in overall ring width around the entire stem, whereas eccentricity is represented by asymmetric growth, with wider rings forming on one side.

Anatomical indicators such as callus tissue, traumatic resin ducts, and tracheid or vessel anomalies also serve as valuable evidence of past disturbances (Stoffel & Corona, 2014). However, their detection typically requires microscopic analysis and extensive sampling, which makes them less practical for broader dendrogeomorphic surveys. Consequently, this study focuses on macroscopic growth indicators that allow reliable dating of geomorphic activity while maintaining a feasible analytical effort. Still, these additional growth indicators were kept in mind during eccentricity and reaction wood analysis to face delays in growth reactions, unreliable event timing, and other challenges in tree-ring analysis.

3.7. Challenges of tree-ring analysis

There is broad agreement in the literature that dendrogeomorphic studies face challenges related to tree-ring formation and analysis. One major issue in dating ecological events (whether climatic, geomorphic, etc.) is the occurrence of missing and false rings (Malik & Wistuba, 2012), which researchers seek to minimize by using reference trees unaffected by geomorphic processes (see Chapter 3.8.). Another important source of error is delays in reaction wood formation, which earlier studies found to be relatively common (Braam et al., 1987; Shroder, 1978). Otherwise, tree-ring analysis alone may be unreliable as well, as delayed or microscopically subtle compression wood can obscure event timing (Heinrich et al., 2006). This underlines the importance of careful cross-dating and the use of multiple growth disturbance signals for reliable dendrogeomorphic analysis (Heinrich et al., 2006; Šilhán, 2017).

Tree-ring disturbance signals differ in spatial extent. Some signals, such as scars, resin ducts, or reaction wood, remain confined to parts of the stem, while others, like growth releases, suppressions, or vessel anomalies, are expressed more widely within or across trees (Stoffel & Corona, 2014; Timell, 1986). The tree's sensitivity to react to disturbances is also age-dependent, further complicating the dating of geomorphic events (Šilhán, 2019). Younger trees generally react more strongly to geomorphic processes, whereas older trees may respond more weakly or with a delay (Šilhán, 2019).

These variations in growth response and the potential for analytical errors highlight the need for comparative references. To distinguish geomorphically induced growth disturbances from those caused by climatic or ecological factors, reference sites containing undisturbed trees are indispensable. The following section outlines the purpose and selection criteria for such reference sites.

3.8. Reference site

To reliably identify geomorphic disturbances in tree rings, growth patterns from landslide-affected trees must be compared with reference chronologies developed from undisturbed sites (Malik & Wistuba, 2012; Tumajer & Treml, 2013). Disturbances at the study site must be distinguished from normal growth variability, which is reflected in reference curves. For each tree species, a local reference chronology is therefore essential, representing undisturbed growth under the same environmental conditions but without the influence of slope processes (Gärtner et al., 2004).

The reference slope should be located as close as possible to the landslide site, with similar inclination, exposure, elevation, bedrock, and species composition, while showing no evidence of past or present mass-movement activity (Malik & Wistuba, 2012; Tumajer & Treml, 2013). Under these conditions, it can be assumed that tree growth at the reference site is primarily shaped by non-geomorphic factors, and the influence of mass movement on tree-ring width is minimal (Malik & Wistuba, 2012). The oldest trees growing near, but outside, the landslide area are often used to develop such chronologies, as they help detect missing, false, or wedging rings and account for non-geomorphic influences like climate variability or insect outbreaks (Šilhán, 2020).

Accurate dating of disturbed samples depends on precisely matching their ring patterns with those of undisturbed trees, allowing reliable identification of deviations and abrupt growth changes (Gärtner et al., 2004; Tumajer & Treml, 2013). This makes reference chronologies indispensable in dendrogeomorphic research, particularly for identifying common disturbances induced by landslides, such as stem tilting (Šilhán, 2021).

3.9. Precipitation influences on slope activity

On the slope near Elm, where unstable geology and surface water are known to drive slope activity, precipitation is a particularly relevant factor. Environmental conditions strongly control both tree growth and slope processes (Gärtner et al., 2004). Among them, precipitation and the resulting hydrological changes are consistently identified as dominant triggers of landslide activity, particularly for slow-moving slides (Macfarlane, 2009; Malik et al., 2016). Therefore, quantifying the interaction between precipitation and landslide mobility is decisive for characterizing the role of landslides in landscape evolution and hazard mitigation (Handwerger et al., 2013)

Periods of accelerated displacement are typically associated with prolonged rainfall, snowmelt, or reduced evapotranspiration, leading to long-term ground saturation that lowers the threshold for slope failure (Massey et al., 2013; Papciak et al., 2015). High-intensity rainfall events, in particular, have been identified as direct triggers of landslide reactivation (Lopez Saez et al., 2012; Papciak et al., 2015; Šilhán, 2020). Sequences of wet summer-winter-summer conditions may further destabilize slopes, while snow accumulation and thaw enhance water input to the subsurface (Papciak et al., 2015). Other scientists discovered that seasonal velocity changes are commonly linked to increases in pore-water pressure, which reduces effective stress along basal shear zones and keeps slopes close to failure thresholds (Handwerger et al., 2013; Macfarlane, 2009; Malik et al., 2016).

At the same time, precipitation-landslide relationships are not always straightforward. Some studies have found that strong precipitation years do not consistently correspond with more intense growth reactions in trees (Schmid & Schweingruber, 1995). Detailed monitoring shows that displacement patterns often reflect complex seasonal cycles rather than simple rainfall totals (Handwerger et al., 2013). Although findings on precipitation-landslide relationships are sometimes inconsistent, it remains important to test whether rainfall variations are reflected in tree growth disturbances of the study site. Even without monthly precision, dendrogeomorphic data can reveal correlations between precipitation and slope activity. Within this assessment, there is special interest in discovering the influence of artificial drainage channels on mitigating these processes, since both precipitation and subsurface drainage control the hydrological regime of unstable slopes. Therefore, the following sections deal with the channel's contribution to slope stability.

3.10. Drainage channels for slope stability

As mentioned in Chapter 2.5. *Drainage Channels* (within the study site description), drainage channels were constructed on the investigated slope to remove excess water and increase slope stability. Efficient drainage pathways, whether natural or artificial, are essential in regulating porewater pressures within slopes, thereby reducing the risk of catastrophic landslide failure while allowing slow, seasonal movements to persist (Handwerger et al., 2013; Jones et al., 2023). In the literature, however, the efficiency and effectiveness of drainage systems on slow-moving landslides remain only partially understood. While deep drainage solutions have been implemented and described at several monitored sites worldwide, their specific responses to rainfall remain poorly documented (Macfarlane, 2009). According to Jones et al. (2023), the effectiveness of drainage channels depends on design quality, hydrogeological conditions, and maintenance. They require a setup period before they start to stabilize groundwater levels, and their function can decline due to clogging or limited drainage capacity. Long-term stability is best achieved when drainage systems also reduce short-term groundwater spikes, are regularly maintained, and are used alongside other stabilization measures (Jones et al., 2023). Overall, while drainage clearly influences slope stability, its long-term efficiency and interaction with precipitation remain insufficiently quantified, which represents a key knowledge gap in landslide hazard mitigation. Therefore, this study aims to investigate possible relationships between drainage channels and slope activity reduction.

4. Materials and Methods

This chapter outlines the methodological approaches used to reconstruct slope movements by applying dendrogeomorphic techniques. Dendrogeomorphology combines geomorphological field analysis with dendrochronological dating to identify and date growth disturbances in trees affected by slope processes. This method provides a cost-efficient and precise means of reconstructing past landslide activity, particularly in forested terrain where conventional monitoring is limited. In this study, Norway spruce (*Picea abies* (L.) Karst) was selected as the species for sampling due to its abundance in the area and its high sensitivity to slope instability.

The methodological procedure included detailed field inspection and mapping of geomorphic features (Chapter 4.1.), selection and sampling of suitable trees (Chapters 4.2. and 4.3.), and subsequent laboratory processing (Chapters 4.4., 4.5. and 4.6.). The obtained ring-width data and high-resolution images were then analyzed to measure eccentricity and reaction wood (Chapters 4.7. and 4.8.). Finally, the reconstructed disturbance events of all sampled trees were compared with regional precipitation data (Chapter 4.9.).

4.1. Field inspection and mapping

The methodological framework began with a detailed geomorphological field inspection to delineate landslide features, select representative sampling sites, and identify trees showing visible signs of deformation or disturbance. Guidelines for this step were based on the field procedures described by Gärtner et al. (2004). Contrary to the description by Malik & Wistuba (2012), dendrogeomorphic studies do not begin directly with tree sampling in areas presumed to be affected by geomorphic processes. Instead, they first require a geomorphological analysis to identify and delineate the landforms that record past events. Only after this geomorphic assessment are trees chosen from the affected population for sampling.

The slope of interest was recommended by the district forester of Elm, who identified several active sliding areas but emphasized the suitability of the slope in the Ramintal. This site is densely forested, easily accessible, and largely unexplored by researchers. Before the first field visit, available maps, geological studies, and historical aerial photographs of the area were examined. Based on his long-term observations, the forester provided insights into the slope's activity, visible deformation patterns, and their effects on vegetation, terrain, and infrastructure. Searches through available archives confirmed that little prior research had been conducted on this slope, which is likely due to its low immediate hazard potential for the population. Despite the currently low immediate hazard potential, ongoing slow movements continue to destabilize the slope surface, posing a risk of damage to the road and, in the event of larger failures, potential blockage of the Raminbach stream, which could trigger flooding or debris-flow hazards affecting the village of Elm.

The forester also highlighted the extensive drainage-channel construction carried out in the 1990s to stabilize the slope, visible in historical aerial imagery from Swisstopo (2025b) and described in Chapter 2.5. *Drainage channels*. Geological information from Grämiger (2024) was further consulted to support the later field inspection. An initial site visit was conducted together with the district forester to inspect terrain conditions and tree deformation at several accessible sites. The information gathered from map and archive research was verified in the field, and potential sampling areas were assessed following the procedure outlined by Gärtner et al. (2004). This step placed the study area in its broader geological, climatic, and anthropogenic context at the mesoscale, as described in Chapter 2 (*Study Site*). The forester indicated active sliding zones, visible surface deformation, and tree conditions, and granted permission to extract increment cores for dendrogeomorphic analysis.

Figure 12: Two tilted research trees with a considerable amount of material accumulated upslope, while the terrain behind them descends more steeply. The trunks are not oriented vertically, suggesting possible slope movement processes. An example of analyzing the morphology and composition of erosional features in relation to the tree growth.

A second visit was conducted, and sampling equipment was brought to initiate data collection after the geomorphological assessment. Within the main landslide area, a section dominated by Norway spruce (*Picea abies* (L.) Karst) was selected, as conifers offer clear dendrochronological signals and easier sampling and analysis (see Section 2.6. *Tree species*). At the microscale, the morphology and composition of erosional and depositional features were analyzed to infer the processes responsible for their formation (as for the trees in Figure 12), following the approach of Gärtner et al. (2004). A nearby area with stable terrain and spruce trees unaffected by slope processes was also identified as a reference site. There, the terrain is less steep and shows fewer signs of geomorphic activity. Despite extensive meadow sections, sufficient forest patches with comparable growth conditions to the study area were present.

Subsequently, additional time was devoted to mapping and classifying terrain features upslope and downslope, documenting geomorphological processes, and recording observations on a Swisstopo (2025a) base map. However, complete geomorphological mapping and detailed soil profiling were beyond the scope of this study, though such analyses would have been valuable. One major problem appeared during the field inspection: There was also large-scale deforestation of old trees, primarily spruce, in the area (see Figure 43 in the Chapter 9 *Appendix*). Unfortunately, this coincidence limited the selection of trees to be sampled. The felled trees had not yet been removed, but were still lying on the ground, making it more difficult to move around the site and map the geomorphic conditions. Still, there were enough trees suitable for collecting samples in the area. A detailed sketched map is presented in Chapter 5.1. and illustrates the identified geomorphic features, allowing for interpretations of the slope movement events detected in individual trees.

4.2. Selection of trees

After gathering information about the slope's dynamics and associating landforms with specific processes, spruce trees were selected in the research area. Therefore, suitable trees were selected for sampling (see Figure 15 for their locations). Trees were excluded if they showed complex branching, division into multiple trunks, mold or fungal infestation, or any other disturbances unrelated to geomorphic processes, as these factors could affect sample quality. Based on the theoretical considerations regarding the different growth responses of younger and older trees to disturbances, trees were selected in a balanced way across the entire slope. Trees from all ages were sampled without prioritizing individuals that already showed visible growth disturbances (Stoffel et al., 2013). Such an even and systematic selection is essential to ensure reliable and unbiased reconstructions of past mass-movement activity (Stoffel & Corona, 2014).

At each tree site, the location was marked on the map. Following the approach of Wistuba et al. (2013), the shape of tree stems, including the tilting angle and curvature of the stem, was recorded in a digital list. Further, the morphology of the slope in both the immediate and wider surroundings was documented. As part of that, the inclination of the slope was recorded, and if necessary, further comments on special features were noted. This helped to identify the involved geomorphic processes. The inclination of the slope surface and of individual tree stems relative to the horizontal was estimated using a smartphone-based clinometer application. Measurements were taken from approximately 10 m by aligning the phone with the slope or tree axis. The application provided a simple yet sufficiently accurate inclination angle at each sampling location. Each tree's inclination was measured from two perpendicular directions (90° apart) to account for both upslope-downslope and lateral leaning angles. All field observations are documented in different lists provided in Chapter 9 *Appendix* (Tables 6-8).

The reference area is located close to the landslide zone and shares similar environmental conditions. The sampling was widely distributed across the defined reference area. However, extensive meadow sections on the slope reduced the forest cover, so certain parts could not be included in the sampling. In particularly suitable locations, several appropriate trees located close to each other were sampled simultaneously (see Figure 14). To ensure that reference tree growth primarily reflects non-geomorphic influences, only trees with upright stems and no visible signs of disturbance were selected. Despite this careful selection and the lower slope inclination of approximately 15-20° compared to the main study area, slight ground movement cannot be fully excluded. Therefore, an additional sampling measure was applied (see Chapter 4.2.), assisting in creating a more reliable reference for identifying missing or false rings and accounting for external factors such as climate.

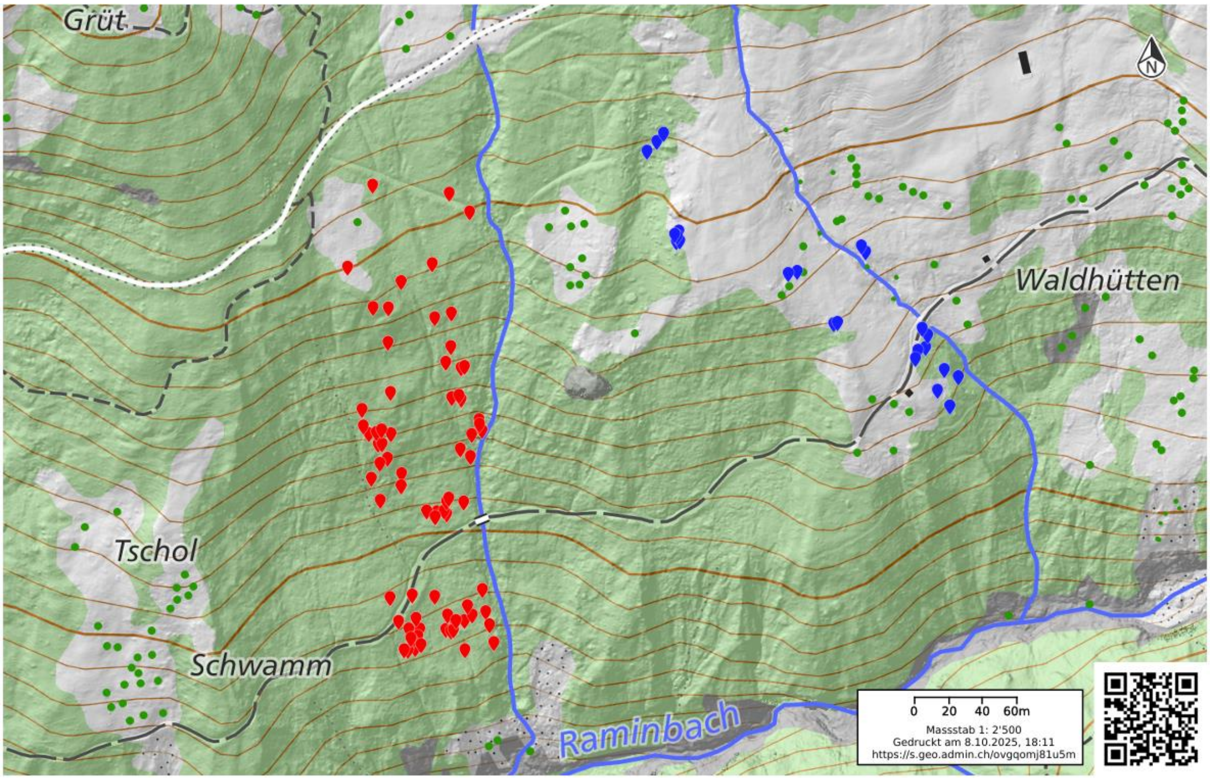

Figure 13: Selected trees of the study site (red points) and the reference site (blue points) without sample description for a general overview (Swisstopo, 2025c).

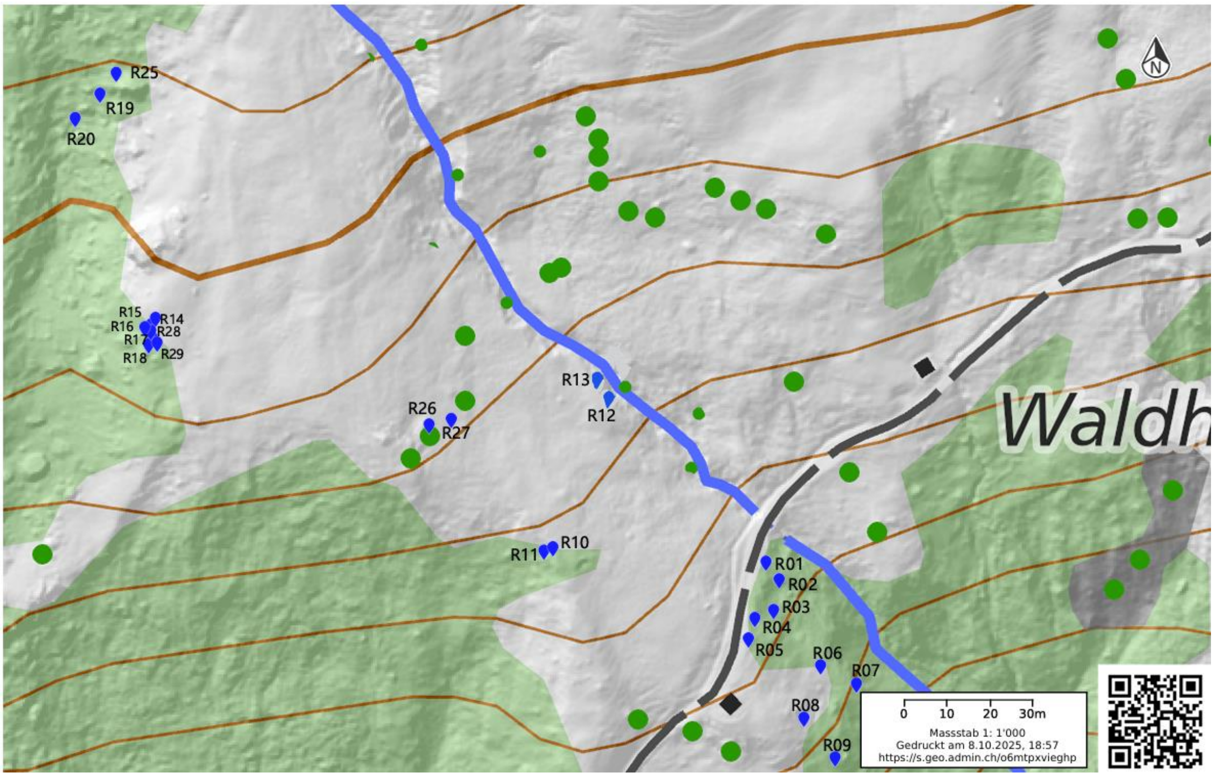

Figure 14: Map with the reference tree locations ElmR01-ElmR19 and ElmR25-ElmR29 (Swisstopo, 2025c).

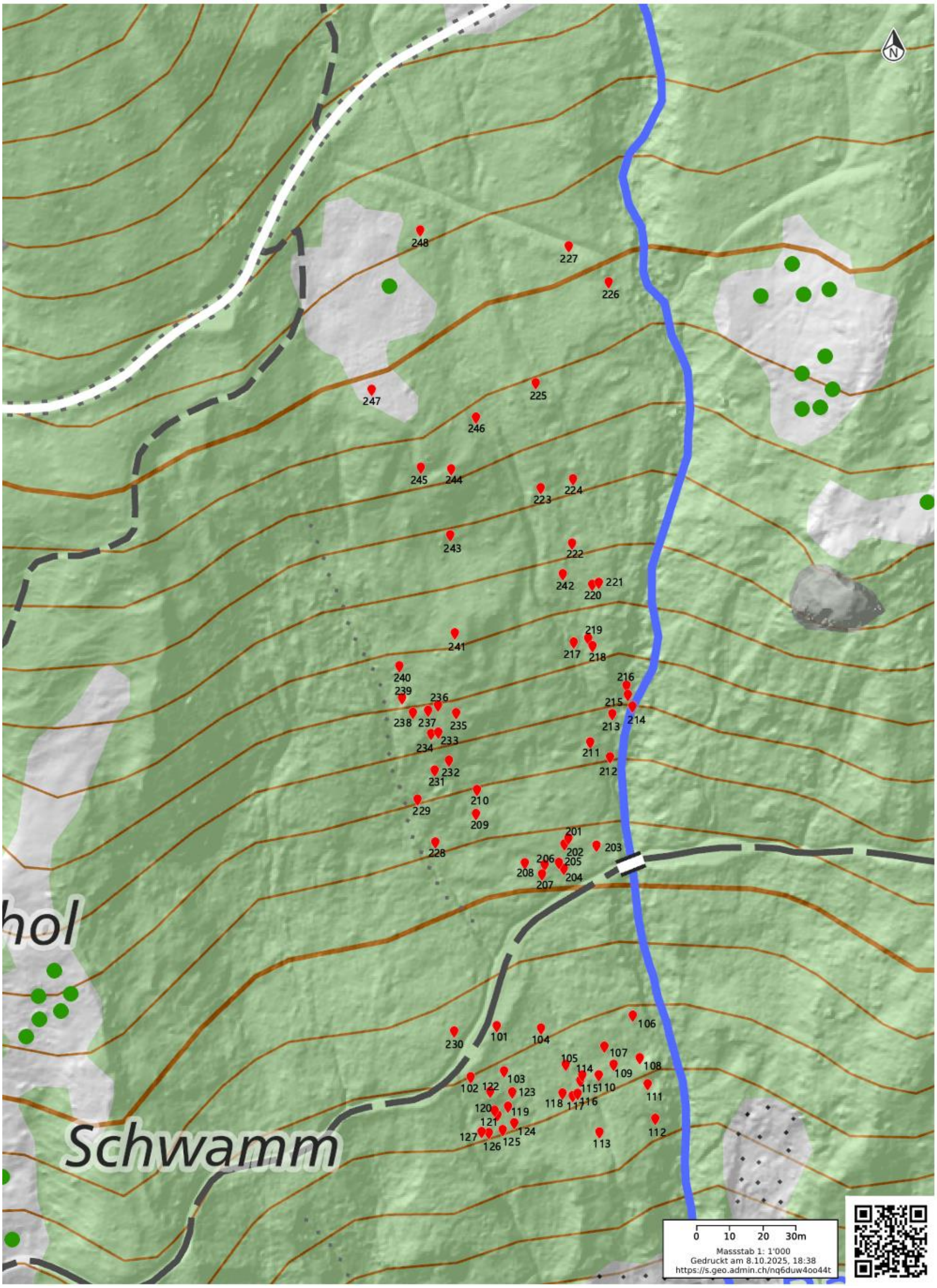

Figure 15: Map with the research tree locations Elm101-Elm127 and Elm201-Elm248 (Swisstopo, 2025c). The path that cuts through the study area divides it into a southern research area 1, located downhill, and a northern research area 2, located uphill.

4.3. Sampling

Figure 16: Photograph of sample Elm105 and sampling equipment (Pressler Bohrer, extractor, and power drill).

After the observation of slope morphology and finding the ideal trees to be sampled, the extraction of increment cores from the trees could be started, following the guidance given by the study by Gärtner et al. (2004).

Fieldwork was carried out over a period of seven days, with most of the time dedicated to extracting, labeling, and wrapping increment cores. The method of extraction causes only minimal damage to the trees compared to cutting them down for full cross-sections, which, although providing the most complete record of growth disturbances, is highly destructive. For this reason, non-destructive increment coring is the standard approach in dendrogeomorphic studies (Šilhán, 2020). The cores were extracted using a Pressler increment borer (see Figure 16) with a maximum length of 40 cm and a diameter of 0.5 cm. To increase efficiency during sampling, a Metabo power drill was used to assist the coring process. The drilled core could then be extracted from the tree using an extractor. All materials were provided by the Swiss Federal Institute for Forest, Snow and Landscape Research WSL. Although no absolute dating of the tree age (as in climate-related dendrochronological analyses) was intended, the tree's pith was targeted in each case in order to obtain the longest possible chronology of the tree.

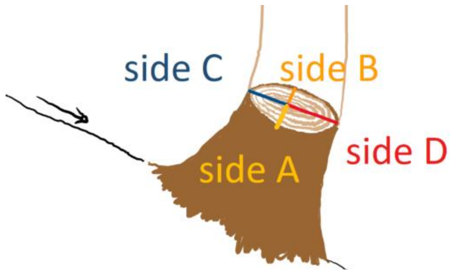

Figure 17: Schematic cross-section of an inclined tree in a landslide area showing potential reaction wood formation. It visualizes the coring directions for research samples (sides C and D) at the point of greatest curvature and for reference samples (sides A and B).

Two cores were extracted from each tree, with a decisive difference between research and reference samples. For research samples, two cores were taken: one in upslope stem direction (labelled as side C) and one in downslope stem direction (side D). The height of coring needed to be carefully chosen according to established procedures. For studies reconstructing site-specific environmental conditions, the two cores are taken from a uniform height at the standard breast height of 1.3 m above the ground. In dendrogeomorphic sampling, however, targeted sampling based on tree morphology and influence type is essential, as growth reactions are unevenly distributed along the trunk (Gärtner et al., 2004). As learned, trunk tilting represents the most visible indicator of geomorphic influence on trees and results from ground movement or material accumulation. The strongest growth reactions are expected near the most curved part of the trunk. In conifers, such growth reaction forms on the lower, compressed side. Therefore, sampling should ideally be done close to this point of maximum curvature (see Figure 17). If this is unclear, the samples should be taken from the lower trunk region at about 0.6 m above ground, where the reaction is usually most pronounced (Gärtner et al., 2004). This procedure was not considered by (Wistuba et al., 2013) who took their cores at the standard height, even though growth reactions were in their interest of the dendrogeomorphic study.

For reference trees, two increment cores were taken from the side, i.e., at a right angle to the direction of inclination on opposite sides of the trunk, to minimize compensatory growth responses to slope inclination that could distort ring-width patterns. Although most reference trees grew relatively straight, this sampling direction helped reduce the occurrence of growth responses, which are more likely present on the downslope, compressed side, especially on steeper slopes. (Gärtner et al., 2004). Seen from the uphill side of a tree, samples taken from the right side were labeled as A, and those from the left side as B for the same tree, as shown in Figure 17.

Figure 18: Overview over all 200 research and reference samples on a core holder in the laboratory.

Samples from the research area were labeled "Elm101" to "Elm127" for trees located below the pathway in *research area 1* and "Elm201" to "Elm248" for those above the path in *research area 2*. Together, these two areas constitute what is generally referred to as the overall research area throughout this thesis. Thus, both groups belong to the same dataset. Each sample was additionally marked with the letters C or D to indicate the direction of coring on the respective tree (see Figure 17). Reference trees were labeled "ElmR01" to "ElmR29" ("ElmR20" to "ElmR24" were replaced by new reference samples) following selection, with letters A or B denoting the right or left sides of the trunk (as seen from above) from which the cores were extracted. To ensure enough samples, 25 reference trees and 75 research trees were sampled (see Figure 18). With this high number, any samples that cannot be cross-dated can be excluded.

As soon as an increment core was extracted, it was carefully placed into a core holder (printed at the institute) and labeled with its corresponding identification code, while notes on the morphology of the slope and the tree were recorded digitally. The finished, labeled increment cores were placed in a waterproof transport box and were not adjusted again until further processing in the laboratory.

4.4. Sample processing

4.4.1. Sample preparation with a core-microtome

At the WSL laboratory, the samples were unpacked and sorted. Afterwards, a plain surface of all cores needed to be obtained for later digital recording. This could be achieved by sanding the cores, which would improve the visibility of ring boundaries and reveal individual cell structures. However, this process could damage thin cell walls and fill the cells with dust, which would impair clarity in narrow or light-colored rings. Therefore, selected core sections were cut with a core-microtome (see Figure 19) developed by Gärtner and Nievergelt (2010). Each sample was fixed in the sample holder of the microtome. Then, the core was lightly moistened with water and a brush to soften the surface. Using a microtome blade at an angle of approximately 45° to the sample, thin shavings of 20 µm were successively removed until a smooth, horizontal surface with a width of 2 mm was obtained. This method ensured that the cell structures and annual rings remained intact and clearly visible, providing a sufficiently wide surface for subsequent microscopic analysis and high-resolution imaging.

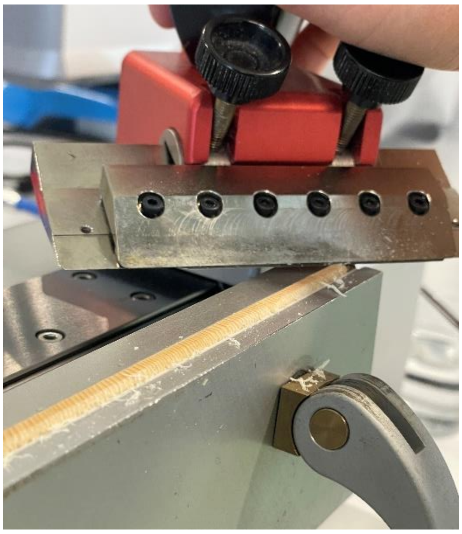

Figure 19: Photograph of the core-microtome during sample preparation. A core mounted on the holder is moistened and cut with the microtome blade in 0.02 mm increments to produce a smooth, cell-level visible surface for analysis.

4.4.2. High-resolution imaging using Skippy

Following sample preparation, all cores were digitally recorded in high resolution for subsequent ring-width measurement. Recording was carried out using a newly developed imaging device specifically designed for high-resolution photography of tree-ring samples. The system, Skippy, is equipped with a Sony Alpha 7R IV full-frame camera (see Figure 20) that automatically captures images while the core is advanced by approximately 5 mm between shots. This automated process ensures continuous overlap between consecutive images, producing a complete, high-resolution digital record of each core. At the end of each core, a piece of millimeter paper was placed to allow later calibration of pixel size with the correct length scale.

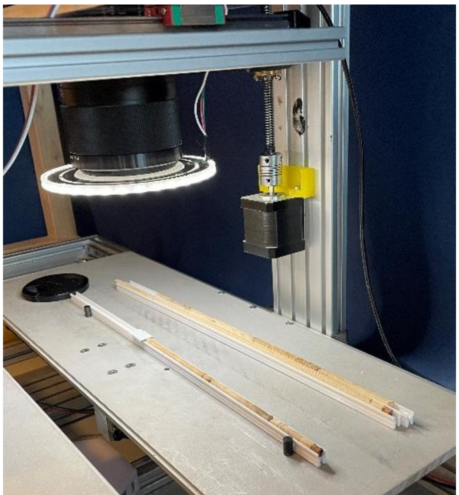

Figure 20: High-resolution imaging of a sample and a millimeter paper using Skippy in the laboratory.

4.4.3. Image stitching and panorama creation

The individual photo sections were combined to create a continuous panoramic image of each increment core. This stitching process was carried out using the software PTGui Pro (by PTGui), which assembles all high-resolution photographs into a single, seamless image (see Figure 21). The resulting panorama was subsequently cropped and correctly labeled for the following step of annual ring-width measurement. Difficulties only arose when the focus was automatically set incorrectly for individual photos during shooting. The blurry photos had to be excluded from the panorama, as they might otherwise have been stitched together at the wrong anchor points. If there were many blurry photos in a row, the corresponding sample had to be retaken with Skippy in high resolution.

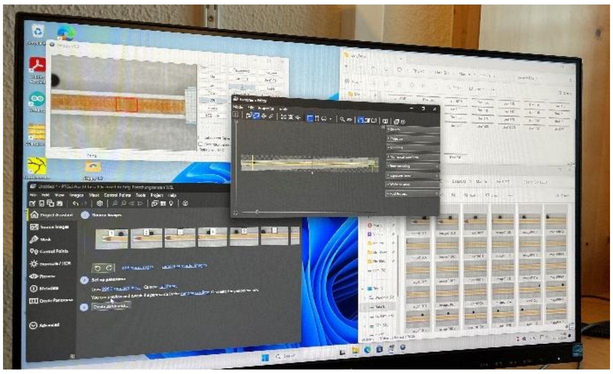

Figure 21: Using PTGui to stitch images together to create a panorama for later ring width analysis.

4.5. Measurement of ring width using CooRecorder

The final panoramic images were used as input for tree-ring width measurement, which was performed using CooRecorder 9.5 (Cybis Elektronik & Data AB). Each panoramic image was uploaded individually, the sequence start year was set to 2024, and ring boundaries were marked one by one. To ensure comparability among all samples, ring widths were recorded as consistently as possible, maintaining a perpendicular measurement direction between ring boundaries across all cores. An important step after marking the annual rings was the calibration of the pixel size with the correct length scale using the millimeter paper at the end of each core. The resulting ring width data served as the basis for cross-dating to establish a consistent site chronology.

This work-intensive process could occasionally result in minor inaccuracies, which were subsequently corrected during cross-dating using TSAPWin (see Chapter 4.6.). Before cross-dating, the completed measurements had to be converted into a compatible file format. This was achieved using CDendro (Cybis Elektronik & Data AB), which transformed the raw position data files from the ring-width measurement (.pos) into format header files (.fh). These .fh files contained the processed ring-width data together with metadata such as sample name, measurement direction, and units, enabling their import and further analysis in TSAPWin.

4.6. Cross-dating

Cross-dating was carried out to ensure the correct alignment of annual rings across all samples. The software TSAPWin Scientific 4.81 (RINNTECH) was used for visual comparison, as it allows curves to be shifted and overlaid in multiple directions. This facilitated the detection of discrepancies, missing or false rings, as well as recognition of similar ring width patterns. The similarity of year-to-year growth trends between two tree-ring series, known as *Gleichläufigkeit* (parallel variation), is an important parameter for assessing cross-dating accuracy. As a common procedure, curve comparison was carried out visually by checking growth curves for years with parallel (*gleichläufig*) or opposing (*gegenläufig*) trends to verify the consistency of cross-dating and to identify potential errors.

In dendrogeomorphic studies, reference samples are used to establish the background level of variability in tree-ring eccentricity. They capture the natural range of asymmetry caused by ordinary growth processes such as climate, sun exposure, tree shape, competition, or minor disturbances, but without the local influence of landslide activity in the research area. Reference trees are therefore ideally collected outside the active landslide zone. Such samples are never entirely disturbance-free but still provide a dataset that reflects the normal noise level against which event signals can be identified. Comparing eccentricity from landslide-affected slopes with that from stable reference slopes makes it possible to distinguish unusual eccentricity events that are specifically linked to landslide activity (Wistuba et al., 2013).

4.6.1. Creating a reference chronology

The procedure began with the reference trees. First, the two cores of each reference tree (A and B samples) were compared visually. By aligning their growth curves in TSAP, years with strong and weak growth were identified and verified against the ring boundaries marked in Coorecorder. Any inconsistencies between the two cores were carefully inspected and corrected directly on the core panoramas using Coorecorder. For example, missing rings were detected, and errors in the marking of the years were corrected. Once both cores of a tree were matched, an average curve for this tree was created, forming a within-tree chronology that represents the individual growth history of the tree. Several such tree-level mean curves (approximately five trees) were then compared to establish a first site-level mean reference curve, which served as the basis for cross-dating all further samples. Using this procedure, all reference curves were compared against each other. Trees with significant divergences, growth deformities, or irregularities were classified as unsuitable trees for reference and were excluded from the overall mean. Excluding such biased series from further analysis is a common practice to avoid distortion of the site chronology (Esper & Gärtner, 2001).

Some trees were excluded during sample preparation, and new samples were gathered instead, as these trees were too young to be meaningful. The reason is that the tree-ring width naturally declines with age due to the tree's expanding size (see Chapter 3.1. *Tree growth*). This creates large differences between juvenile and adult wood and causes bias when averaging series from trees of different ages (Esper & Gärtner, 2001). Still, a comparability between trees with varying growth rates can be ensured by standardizing raw tree-ring width data into dimensionless indices like an eccentricity index (see Chapter 4.7.), removing age-related disturbances (Esper & Gärtner, 2001). Thus, for this thesis, no age-detrending of ring widths was applied. However, juvenile growth and very narrow rings were cautiously interpreted, as these may increase noise or lead to false positives. Therefore, instead of very young trees that were less than 20 years old, older trees were selected.

The reference samples that were successfully cross-dated with each other served as the basis for comparison with the research samples and were exported as text files using the CDendro program. These files were subsequently processed in Microsoft Excel (Microsoft Corporation, version 2509), where tree-ring width curves were visualized and calculations for eccentricity, threshold values, and event counts were carried out.

The gray-coloured lines in Figure 22 represent the individual cross-dated reference samples, while the red curve shows their mean chronology. Although individual variations occur due to differences in growth patterns, age, and site-specific conditions, all series follow the same general trend, indicating a high degree of *Gleichläufigkeit*. These minor differences were minimized by averaging the series into a mean reference curve, which enhanced comparability and provided a clear signal. This reference chronology, therefore, serves as a robust baseline against which growth anomalies in the research samples can be identified and interpreted.

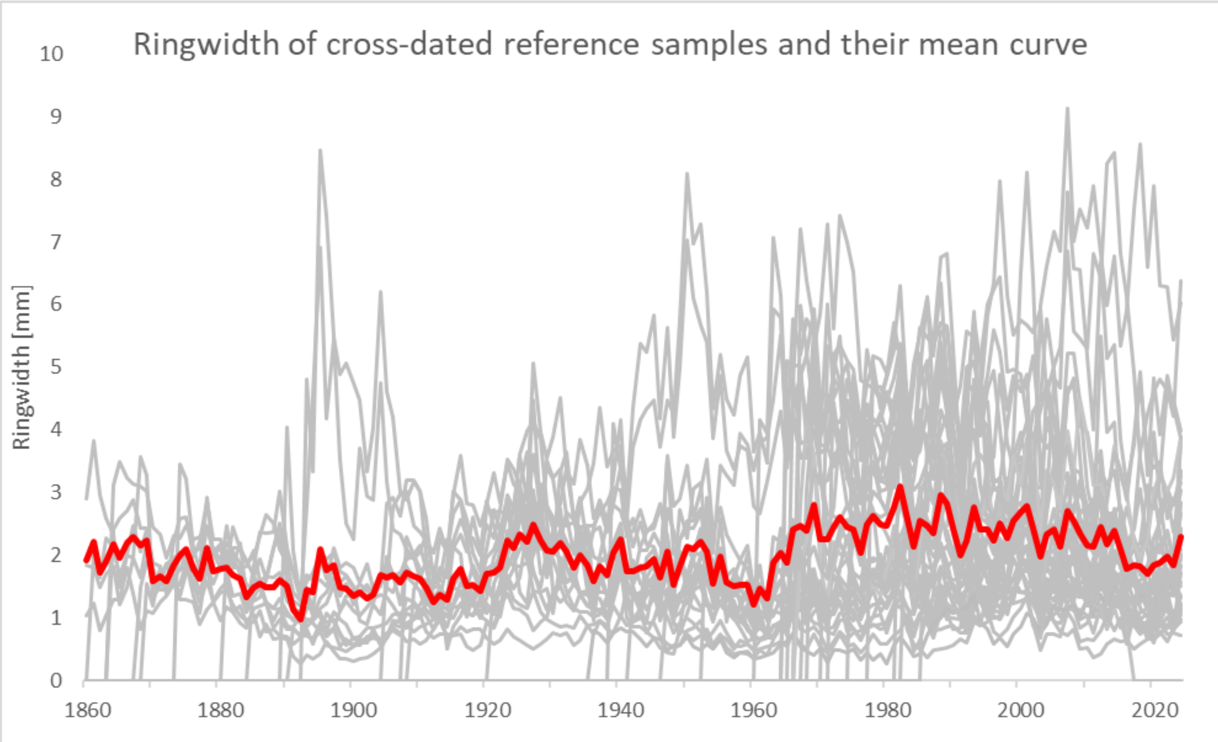

Figure 22: Ringwidth curves of all cross-dated reference samples (gray) and the mean reference curve (red).

4.6.2. Cross-dating research samples

For the disturbed trees, the cores in the direction of the tree's inclination (C and D samples) were first cross-dated against each other to establish the within-tree chronology. Again, caution was taken when interpreting the early parts of the chronologies, as juvenile wood typically shows wider and more variable rings than mature wood. Unlike in the reference area, no mean curves were calculated for the research trees, as averaging would suppress the individual disturbance signals that are central to the analysis. In this case, variability among trees is desirable and will later be examined in combination with ring-width changes and the occurrence of reaction wood. Afterwards, the cross-dated research curves were compared with the established reference chronology to distinguish geomorphological disturbance signals from variations related to climate and site conditions. This comparison was crucial for identifying anomalies in the research samples, as abrupt growth changes may result from geomorphic events or from climatic fluctuations.

Pointer years identified in the reference chronology (e.g., very narrow rings in drought years) were used as fixed anchors for shifting curves when necessary. Particular attention was given to the number of samples, as the reference chronology shows a decline in sample depth toward earlier periods, since fewer long-lived trees were available for cross-dating. No fixed threshold for the minimum number of trees was applied to define the usable part of the reference chronology. However, the early sections of the chronology, where sample depth was low, were used with caution when cross-dating the research samples. Samples showing weak or inconsistent correlations with the reference chronology were excluded from the dataset, following the quality-control approach of Šilhán (2021). The remaining samples provided a robust basis for further investigation.

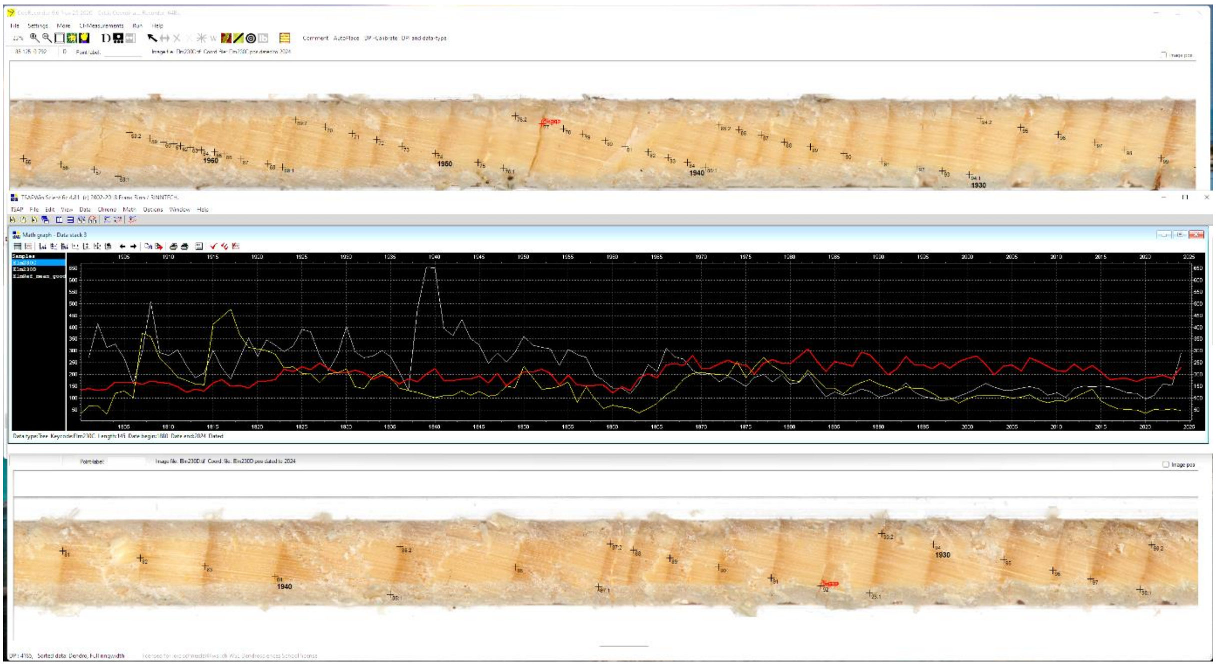

Figure 23: Workflow of cross-dating research samples (here Elm230) with the reference chronology using the TSAP program for ring-width curves and Coorecorder for verification.

Although Figure 23 is too small to recognize details, it illustrates in the central window how the curves of two samples of the same tree (yellow and white lines) are compared with the averaged reference chronology (red line) using TSAP. By simultaneously reviewing the annual ring markings in Coorecorder, errors could be easily identified, missing rings could be determined, and the samples could be aligned with the reference chronology. Despite good alignment with the reference chronology and overall agreement in ring-width patterns, cross-dated samples from the same tree can still differ markedly in their absolute widths. This phenomenon, known as eccentricity, is visible in ring width graphs (as in Figure 23) as a long-term divergence between the upslope and downslope curves. It occurs when the ring width on one side of the stem changes strongly relative to the opposite side (Wistuba et al., 2013). Building on these observations, the next step involves quantifying this asymmetric growth by calculating the eccentricity index and defining thresholds that help distinguish geomorphically induced growth anomalies from natural variability (see Chapter 4.7.).

4.7. Eccentricity and threshold calculation

To evaluate slope movements recorded in tree growth, eccentricity indices were calculated and subsequently compared against thresholds derived from reference trees. This procedure provides the basis for distinguishing ordinary growth variability from disturbance signals that can be attributed to landslide activity. The following section outlines the calculation of the eccentricity index, which quantifies asymmetry in annual ring growth between upslope and downslope directions. It is subsequently described how annual changes and reference-based thresholds were applied to detect event years.

4.7.1. Calculation of the eccentricity index

The eccentricity index was calculated following the procedure of Wistuba et al. (2013), which has been widely used in dendrogeomorphic studies. The method compares upslope and downslope ring widths of individual trees, transforming their differences into index values in percentage. Disturbance years were identified when index values exceeded thresholds defined by the mean and standard deviation of the reference samples. The eccentricity index thus expresses the relative difference between ring widths on the upslope and downslope sides of the stem. The formulas and calculation steps applied in this study are outlined below, with all computations performed in Microsoft Excel.

In the first step of the procedure (1), downslope ring widths (D_X) were subtracted from the corresponding upslope values (U_X) to obtain tree-ring eccentricity (E_X) expressed in millimeters:

$$E_X[mm] = U_X - D_X \tag{1}$$

Each equation X stands for an annual tree ring of each sample. If the downslope radius is larger than the upslope radius, downslope eccentricity is assumed, whereas if the upslope radius exceeds the downslope radius, upslope eccentricity is inferred. When ring widths are greater on the upslope side, the resulting eccentricity values are positive ($E_X > 0$), and when they are greater on the downslope side, the values are negative (E_X< 0). This difference indicates the direction of tree tilting and was therefore maintained for all subsequent calculations. In the second step, eccentricity values were divided by the narrower radius on the respective side and transformed into percentages by multiplying them by a factor of 100, using separate formulas for positive (2), non-existing (3), and negative (4) eccentricities:

when $E_X[mm] > 0$: upslope eccentricity; $Ei_X[\%] = (E_X/D_X) * 100 > 0$ (2)

when $E_X[mm] = 0$: lack of eccentricity; $Ei_X[\%] = E_X[mm] = 0$ (3)

when $E_X[mm] < 0$: downslope eccentricity; $Ei_X[\%] = (E_X/U_X) * 100 < 0$ (4)

In this approach, the narrower radius of each tree ring is set as the baseline (±100%), and the wider radius is expressed relative to it using the eccentricity index in percentage; higher positive upslope or lower negative downslope values indicate stronger tilting responses in the respective year (Wistuba et al., 2013). To determine annual changes for dating landslides, the difference between the eccentricity index values (Ei_X) of a given annual ring and the respective preceding year was calculated as follows (5):

$$vEi_X[\%] = Ei_X - Ei_{X-1} \tag{5}$$

The yearly variation of eccentricity index in percentage vEi_X [%] was calculated for each tree ring in all taken increment cores. The most probable landslide activations were identified by abrupt changes in eccentricity index values, particularly sudden increases upslope or sudden decreases downslope. Other shifts, like decreases within the positive or increases within the negative range, may reflect subsequent recovery and were therefore excluded, as was also performed by Wistuba et al. (2013).

4.7.2. Threshold calculation

To separate true landslide signals from ordinary growth disturbances, eccentricity patterns from study trees were compared with those from stable reference slopes. Reference chronologies provide a baseline of variability caused by non-geomorphic factors such as wind stress, snow creep, or crown asymmetry, and thus allow growth changes induced by landsliding to be distinguished more reliably (Wistuba et al., 2013). In this study, thresholds were calculated using the year-to-year variation of the eccentricity index (vEi) rather than the index level itself. This approach isolated abrupt changes associated with disturbance while avoiding the influence of persistent, long-term asymmetry (e.g., stem form or baseline tilt). This reduced false alarms and improved comparability between trees and years. Event years were then identified when positive or negative vEi values exceeded the thresholds derived from the reference samples.

To determine these thresholds for the reference slope, annual variations in tree-ring eccentricity were analyzed across all years and samples, i.e., average levels of eccentricity recorded on stable slopes, unaffected by mass movement processes (Malik et al., 2016). Arithmetic means and standard deviations were calculated separately for increases and decreases in the year-to-year variation of reference eccentricities. Adding the means to the standard deviations produced two threshold values, positive for upslope and negative for downslope. These reference thresholds were then used to identify and date the most probable times of mass-movement activation on corresponding landslide slopes. In the final step, year-to-year variations in the eccentricity index were compared with these thresholds, taking into account the direction of change. Years showing increases into positive values or decreases into negative values that also exceeded the respective thresholds were considered to indicate landslide events. This analysis followed the approach of (Wistuba et al., 2013) and was applied to eccentricity patterns of individual trees across the research and reference sites. That way, the impact of non-geomorphic factors such as strong wind or snow creep could be eliminated from further analysis of tree rings produced on landslide-affected slopes (Malik et al., 2016). In summary, possible landslide activity was identified in the tree-ring record as sharp increases or decreases in the variation of eccentricity index values. Only those exceeding the reference thresholds in the expected direction were interpreted as probable dates of mass-movement activation.

4.7.3. Filtering secondary and non-geomorphic signals

Many apparent event years occurred during prolonged recovery phases following strong tilting events. In such cases, trees often continued to produce eccentric growth for several years as they gradually regained vertical balance. This continued adjustment led to persistently high eccentricity values that could be mistaken for new event years. However, they represented post-disturbance recovery rather than renewed geomorphic activity (see Figure 24). To exclude these secondary responses, only those years in which the eccentricity index changed sign (from positive to negative or vice versa) and exceeded the calculated threshold were classified as potential new events. Years showing high eccentricity values but no change in sign (e.g., remaining positive from one year to the next) were excluded during the filtering process.

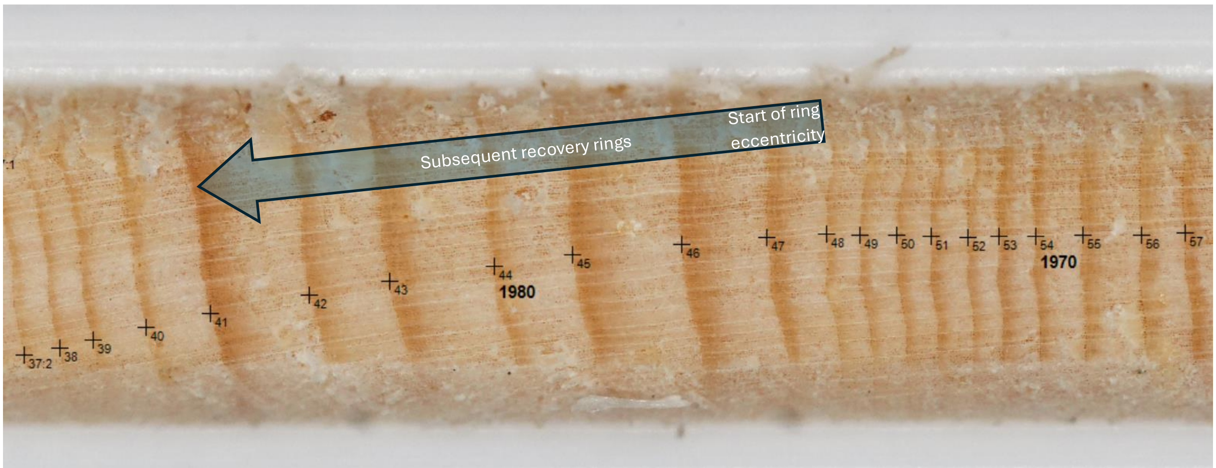

Figure 24: Research sample Elm124D shows clear eccentricity beginning with ring 47 (year 1977), followed by an additional increase in ring width in subsequent years (further to the left of the Figure), which is most likely a secondary growth response aimed at restoring stability after the same landslide event.

This filtering process was implemented in Microsoft Excel by combining logical conditions that checked for both sign changes and threshold exceedance in the eccentricity index. Only values meeting these criteria were retained, while all others were assigned a value of zero and excluded from the event list.

Despite this filtering, not all remaining anomalies necessarily indicated geomorphic processes. Some may have reflected non-geomorphic influences such as wind stress, snow creep, or climatic variability. To further minimize such false detections, all candidate events identified by the index were subsequently checked through visual inspection of ring-width curves and reaction wood patterns (see Chapter 4.8.).

4.8. Visual analysis

Visual analysis was used to verify potential event years identified by the eccentricity index. Each suspected year was examined in the ring-width curves, including the preceding ring, since compression wood may have already appeared in the latewood. Only the first year of disturbance was classified as an event year. Subsequent eccentric rings were considered follow-up years of the same disturbance, unless a further strong increase in eccentricity was accompanied by a recurrence of reaction wood. In such cases, the year was interpreted as an additional event that triggered an even stronger growth response. This procedure helped to separate true landslide events from recovery growth or external, non-geomorphic influences.

Many previous studies have relied primarily on eccentricity analysis as an indicator of disturbance (Malik & Wistuba, 2012; Šilhán, 2019; Wistuba et al., 2013). However, combining both growth responses, eccentricity analysis, and wood-anatomical inspection for reaction wood provides a more accurate and reliable timing of disturbance events. In this study, the occurrence of reaction wood was therefore used as an additional criterion to confirm or reject potential events. Remaining uncertainty concerns the end of the growing season: if a tree was tilted very late in the year, no reaction wood could form, and the response would only appear in the following ring. Although some uncertainties remain, visual analysis enables more reliable detection of disturbance signals, highlighting the importance of subsequent analytical steps.

4.8.1. Visual comparison with ring width curves

Ring-width curves of each core were visually compared with one another and with the mean reference curve. This allowed divergences to be identified and distinguished as either broad external influences (e.g., climate variability, snow creep, wind stress) or local slope movement. Strong divergences between the two curves of the same stem were analyzed in detail. Years where such divergences were clearly visible, while the reference curve showed no comparable reaction, were marked as event years in the eccentricity index table. Not all years identified by the index were confirmed. Some were identified as follow-up years of earlier disturbances, while others were responses to external factors already captured by the reference, and were therefore excluded.

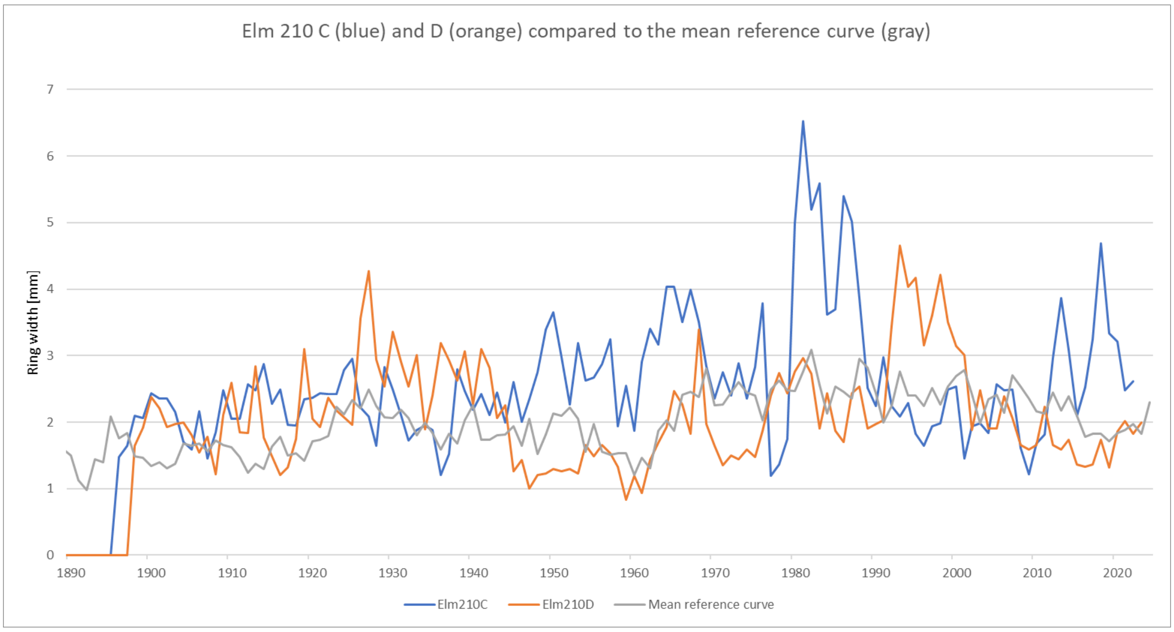

Figure 25: Ring-width curves of sample Elm210 showing recurring positive (downslope core 210D, orange) and negative (upslope core 210C, blue) eccentricity compared with the mean reference curve (gray).

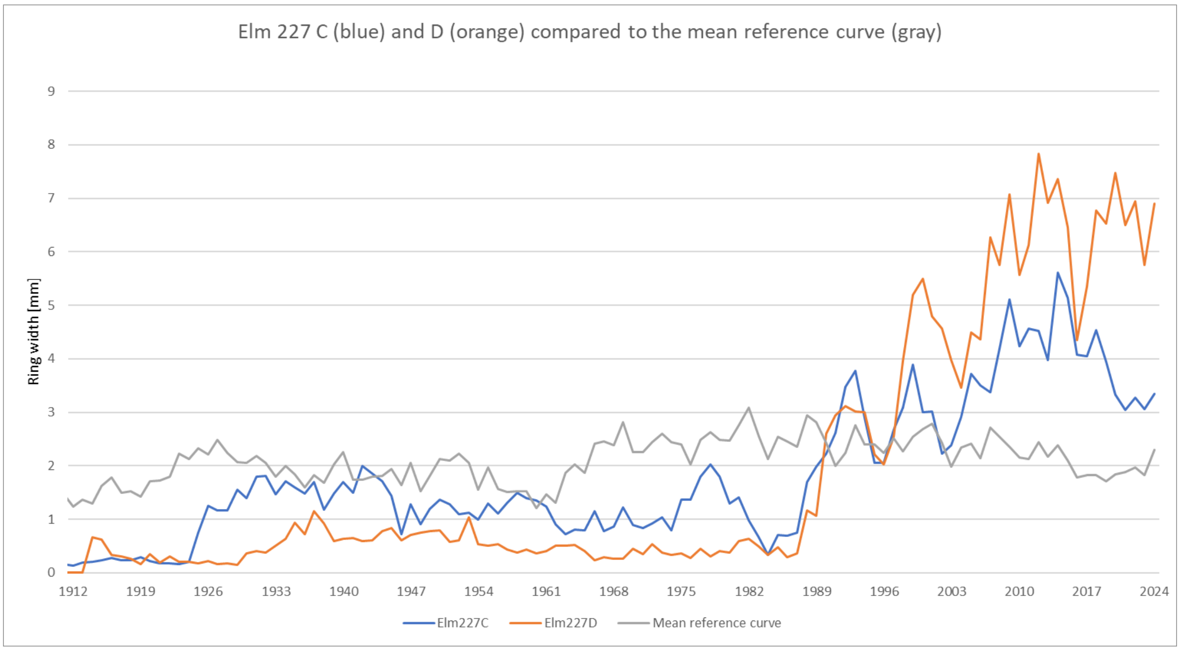

Figure 26: Ring-width curves of sample Elm227 showing more consistent ring widths and only a single shift in eccentricity, compared with the mean reference curve (gray).

Figures 25 and 26 show ring-width curves with recurring positive and negative eccentricity as well as partly prolonged periods of subsequent eccentric growth. These curves were compared with the events listed in the table, which was derived from eccentricity values and threshold values, thereby ruling out several false events. The remaining potential events could then be verified visually in combination with reaction wood, which is essential for accurate interpretation.

4.8.2. Visual compression wood analysis

As a final step, possible events were examined for the presence of reaction wood, providing an additional criterion for confirmation. This anatomical check was applied to both reference and research samples to minimize the major limitation of the used eccentricity index noted by Šilhán (2019). In particular, this approach does not account for possible delays in the tree-growth response, and eccentricity can vary considerably among individual trees within the same landslide area. In reference trees, the occurrence of reaction wood helped identify potential signs of landslides that would otherwise have been overlooked, whereas in research trees, it served to verify whether events that exceeded the thresholds of the eccentricity index were accompanied by structural changes in the wood.

The analysis also addressed the possibility of delayed responses: in some cases, growth eccentricity persisted for several years after an event or appeared with a lag. To account for this, reaction wood was assessed not only in the identified candidate year but also within a window of one or two years. This procedure reduced the risk of misinterpreting the first eccentric year as the event year by default, and of treating consecutive index years as independent events.

Reaction wood was identified primarily on high-resolution images of the increment cores, which allowed for visual inspection of the ring structure along the core length (see Figure 27). In cases where identification remained uncertain, additional checks were performed directly on the cores under the microscope. Clean cross-sections were obtained using a microtome, whereas the visibility of structural differences was enhanced by light sanding. This combination of approaches made it possible to detect the characteristic darker coloration and altered cell structure that indicate compression wood in conifers.

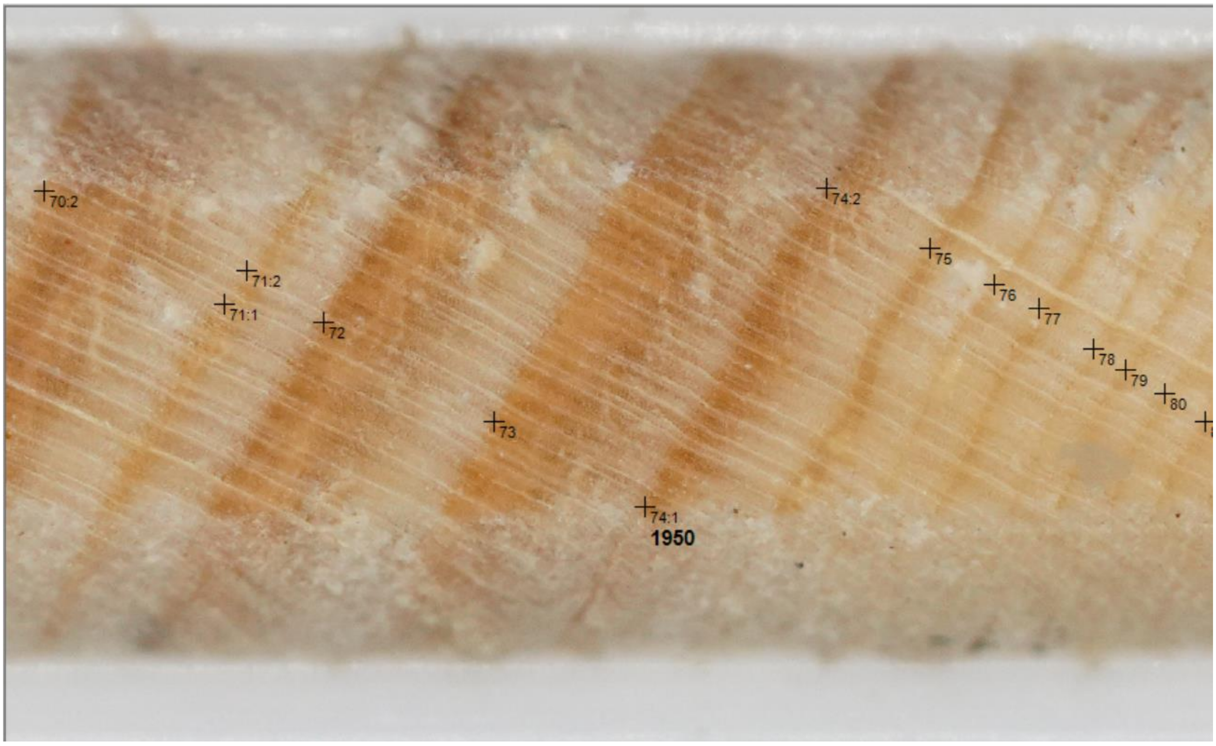

Figure 27: Sample Elm127C with reaction wood in ring 74 (1950) and in subsequent rings on the left side. However, ring 75 (1949) may also contain reaction wood in the latewood, as indicated by its darker color despite little increase in eccentricity compared to the rings before.

4.9. Comparison with precipitation data

As precipitation is one of the main triggers of landslides, it is of particular interest to examine whether variations in precipitation intensity are reflected in the tree-ring records. Therefore, the results of dendrogeomorphic dating, the detected events, based on eccentricity and reaction wood, were compared with precipitation records from weather stations covering more than a century, as also performed by other researchers (Handwerger et al., 2013; Leonelli et al., 2021; Malik et al., 2016; Papciak et al., 2015; Wistuba et al., 2013). Both visual and statistical approaches were applied to assess potential relationships.

4.9.1. Precipitation data origin and data processing

To assess the relationship between precipitation and slope movement activity, two precipitation datasets were consulted and compared to determine which was more suitable for the subsequent analysis. The first data source was the MeteoSchweiz station data: Monthly precipitation sums were obtained from the MeteoSchweiz database (Climap 8.6.4) for the Elm weather station (station ID 3180; WMO 06682; altitude 958 m; parameter *rre150m0*, corresponding to monthly total precipitation in mm) from 1900 to present. This dataset provided locally measured, high-resolution precipitation data close to the study site. Secondly, gridded climate data from the KNMI Climate Explorer were found: Regional precipitation time series (1901-2023) were extracted from the CRU TS 4.08 dataset by averaging them over the grid cells 9.0-9.5° E and 46.5-47.0° N. These

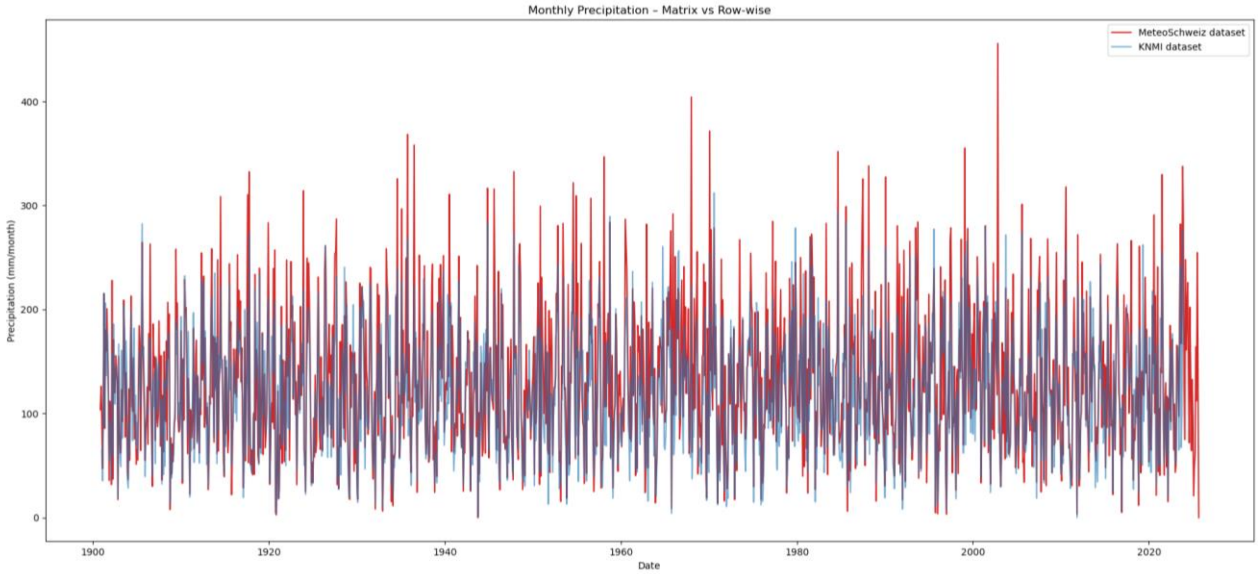

Figure 28: Monthly precipitation sums from MeteoSchweiz from the Elm station (red) and CRU TS4.08 from KNMI Climate Explorer, both shown from 1900 to 2025. The two datasets show close agreement, which supports using the Elm station record for further analyses.

gridded data provide a homogenized, spatially averaged record for the study area and the surrounding area. After comparing both datasets, their curves showed strong agreement over the overlapping time period (see Figure 28). Therefore, the Elm station record was chosen for further statistical comparisons with the event chronology, as it directly represents the local precipitation conditions of the investigated slope.

During this process, it became clear that not only monthly precipitation amounts but also daily data had to be taken into account, as a single short-term but intense precipitation event could significantly impair slope stability. Relying solely on monthly or annual sums risked obscuring such short-term extremes, as days with little or no rainfall could average out the totals and make a critical event appear less significant. Therefore, a daily precipitation dataset was used, obtained from the MeteoSchweiz database from the Elm weather station (station ID 3180; WMO 06682; altitude 958 m; parameter *rre150d0*, corresponding to daily total precipitation in mm), covering the period from 1900 to the present.

The precipitation data was processed in Python using the “pandas” library. For the Elm dataset, daily/hourly entries were aggregated to monthly sums, while annual sums were calculated as totals of the twelve months. For the matrix dataset, the wide format was reshaped into long format and converted into a monthly time series. The tree-ring event data were stored in a separate table containing the year and the number of events, and then merged with the precipitation data based on the year. Initial comparisons between precipitation and event frequencies were conducted visually using Excel (dual-axis line/pile charts) and Python (time series plots with “matplotlib”). These visualizations served to identify potential patterns, coincidences, or trends before applying formal statistical tests. Afterwards, statistical tests were conducted in Python with the “scipy.stats” package.

As is common in dendrogeomorphic datasets, the number of available tree samples varied considerably over time. In earlier periods, fewer trees were present, which reduced the probability of detecting slope movement signals regardless of the actual activity on the slope. A direct comparison of the raw event numbers across the entire chronology would therefore introduce a sampling bias. Thus, the number of detected events was normalized by the number of trees available each year, which resulted in a relative event frequency. This normalized metric was used for all statistical analyses, while raw event counts were retained for descriptive illustration.

4.9.2. Annual and monthly precipitation sums and extremes

First, yearly precipitation totals were calculated by summing all monthly values. They were compared with the percentage of trees where events were detected to test for general relationships between wetter or drier years or sequences of years and event frequencies. In addition to annual totals, two different measures of monthly precipitation intensity were tested: the maximum monthly precipitation value within each year and the sum of precipitation values of the three wettest months per year. These shorter metrics were selected to account for the possibility that short-term extremes rather than annual totals may act as relevant triggers for slope activity.

4.9.3. Daily precipitation sums and extremes

Additionally, daily precipitation totals were considered by extracting the highest daily precipitation value of each month. These extreme events were then statistically compared with the detected growth disturbance events to examine whether a correlation existed between the precipitation metric and the events of slope activity.

4.9.4. Statistical tests

For each of the precipitation metrics described above, correlations with the annual number of events were calculated using Python. Pearson's correlation was applied to assess potential linear relationships, while Spearman's rank correlation was used to test for monotonic but non-linear associations. Both approaches provided complementary information that enabled robust testing regardless of data distribution.

4.9.5. Period comparison due to drainage channels

To investigate possible changes in the event frequency after the installation of drainage channels in the 1990s, the dataset was split into pre- and post-1990 periods. A Mann-Whitney U test was applied to evaluate whether event rates differed significantly between the two periods. Effect sizes were additionally quantified using Cliff's delta.

4.9.6. Statistical test for lagged relationship

To account for potential delayed slope responses to precipitation, an additional analysis was carried out to test for possible lagged relationships. For this purpose, precipitation metrics from each year (annual totals, maximum monthly sums, sum of the three wettest months, and the highest daily precipitation per year) were compared with the event rate of the following year. This approach addresses the possibility that slope movements may have occurred with a delay relative to peak precipitation, for instance, due to cumulative hydrological effects, delayed slope saturation, or the timing of tree-ring formation. Pearson's correlation coefficient and Spearman's rank correlation were again applied to look for potential linear or monotonic relationships with the same events one year later.

4.10. Further Considerations

A spatial representation of the disturbed trees in a Geographic Information System (GIS) had originally been considered. However, the sparse spatial clustering that got visible in the event table indicated that such a representation would display only a few events per year, scattered across the site. The detected events were not temporally concentrated or spatially clustered in specific landslide areas but instead occurred irregularly across the slope. For this reason, and due to time constraints, the GIS analysis was not pursued further.

5. Results

This chapter presents the results obtained through the methodological approaches described in the previous chapter. These findings form the basis for the subsequent discussion and interpretation of slope dynamics, tree-growth responses, and their relationship to external factors such as precipitation.

5.1. Geomorphic field observations and site characteristics

Fieldwork contributed to the results by providing detailed geomorphological observations and site characteristics, as well as a mapped overview of key features (see Figure 29). In the research area, steep scarps alternating with gentler terraces and sections of about 30° inclination were common, while the steepest slopes exceeded 50° and caused notable downslope material transport. Deposited material often accumulated in slopes above trees or in flatter sections, forming bulges and mounds that likely influenced tree growth. Clear indicators of recent mass movements, such as ground cracks or detachment scarps, were absent, suggesting predominantly slow, long-term slope displacement rather than abrupt events. Only small rills, fissures, and surface cavities up to 40 cm in size were observed. These were too small-scaled to map and more indicative of water infiltration processes than of landslide activity. Other features of hydrologic processes, such as dry stream channels, were common and are likely active during periods of high precipitation. During fieldwork in late 2024, however, only the Schwammruus stream, drainage channels, and the Raminbach carried water. The anthropogenic drainage channels were easily recognized by their straight course and concrete structure.

The investigated trees displayed strong variability in age (30-240 years), growth form, and site conditions. Many showed tilted or curved stems: some leaned downslope or upslope, while other trees grew laterally. Trees with tilted lower trunks often straightened upward in their upper sections of the stem. The substrate around the trees ranged from steep slopes to flatter areas and varied between 5° and 50° angles of inclination. Notes on the morphology of the slope and the individual trees on it were recorded and attached to Chapter 9 *Appendix*. For certain trees, the steepness of the slope or the descent of the terrain corresponded to the expected tilt. However, some trees experienced a tilt in their trunks even though the ground had a slight slope. Others, on the other hand, were straight even in steep scarps. Thus, no clear relationship between tree tilting angle and slope inclination could be identified.

The reference area exhibited fewer geomorphological features and a lower average slope of 20°. Most trees exhibited vertical growth with minimal signs of geomorphic disturbance. On the meadow, trampled paths were visible. There were fewer bulges, depressions, or dry gullies, and no signs of recent geomorphological activity were found, indicating a stable slope.

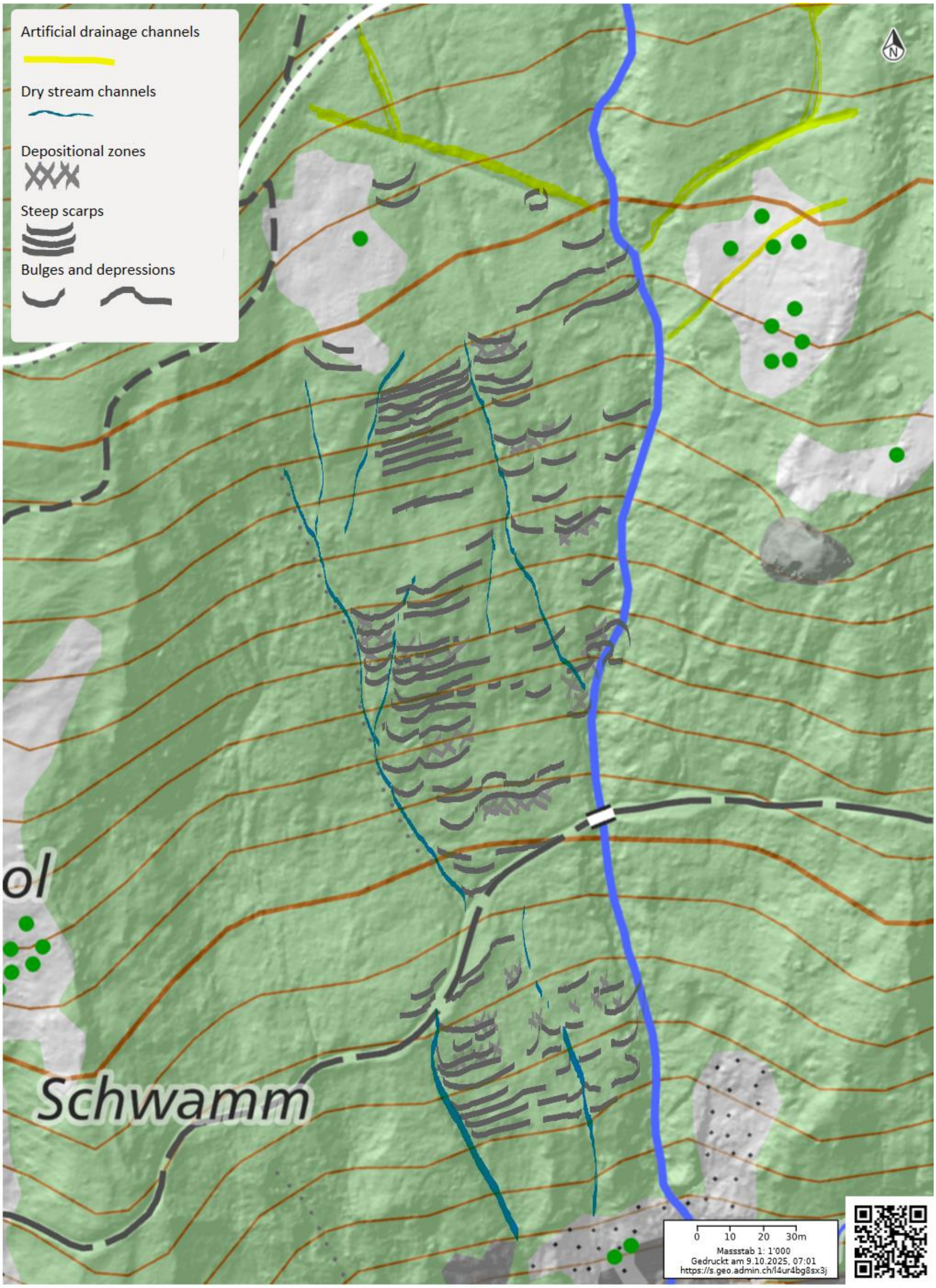

Figure 29: Hand-drawn geomorphological map of the research area, illustrating observed slope features such as scarps, terraces, bulges, material accumulations, dry stream channels, and artificial drainage channels. Tree locations and other relevant observations are included. The accompanying legend explains the mapped symbols and geomorphic units. The basemap is a SwissTLM map from Swisstopo (2025c).

5.2. Tree-ring data overview

Of all reference samples, trees ElmR08, ElmR09, ElmR10, ElmR11, and ElmR13 showed poor correlation or deviated markedly from the others due to external influences. Consequently, they were classified as unsuitable for inclusion in the reference chronology and were excluded from the overall mean. Trees ElmR21-ElmR24 were omitted during the preparation of the samples step, and new samples were gathered instead, as these trees were too young to be meaningful. In total, 20 out of 25 sampled reference trees were successfully cross-dated. These trees had an estimated average age of 117 years, with a mean chronology length of 105 rings, ranging from a minimum of 46 years to a maximum of 202 years.

Most research samples were successfully cross-dated with the reference chronology, showing strong correlations and consistent growth patterns. However, some samples could not be matched to the site chronology without inserting an unrealistically high number of missing rings or showed weak and inconsistent correlations. Therefore, the following samples were excluded from further analysis: Elm102, Elm104, Elm106, Elm117, Elm121, Elm122, Elm125, Elm126, Elm204, Elm206, Elm208, Elm209, Elm217, Elm223, Elm224, and Elm225.

In total, 59 trees from the 75 research trees were successfully cross-dated and included in the ring-width analysis. The age of these trees varied considerably, with the youngest being at least 25 years old. The other trees were over 30 years old and reached an age of up to about 240 years. The trees examined had an average age of 112 years. Since the distance to the pith and the number of missing rings not captured in the cores had to be estimated from the two samples taken per tree, some uncertainty remains regarding the exact age. As the pith was not always reached, the mean length of the usable chronology available for ring width, reaction wood, and subsequent analyses was approximately 99 years.

The reference curves and the mean reference chronology were already presented as intermediate results in Chapter 4.6. *Cross-dating* (Figure 22). The ring-width curves from the research area are now shown separately for the two sub-areas represented by the Elm100 and Elm200 samples. The mean reference curve served as a benchmark for identifying natural, non-geomorphic fluctuations.

Figures 30 and 31 reveal a pronounced variability in the ring-width curves of the research trees. The many overlapping grey lines largely merge into a shaded area, highlighting the high degree of ring eccentricity, even though the samples were classified as gleichläufig (showing parallel growth trends) during cross-dating. Since these eccentricities significantly exceed the variability represented by the reference chronology, additional factors beyond slope movement have likely influenced tree growth. These aspects are discussed in more detail in the discussion chapter.

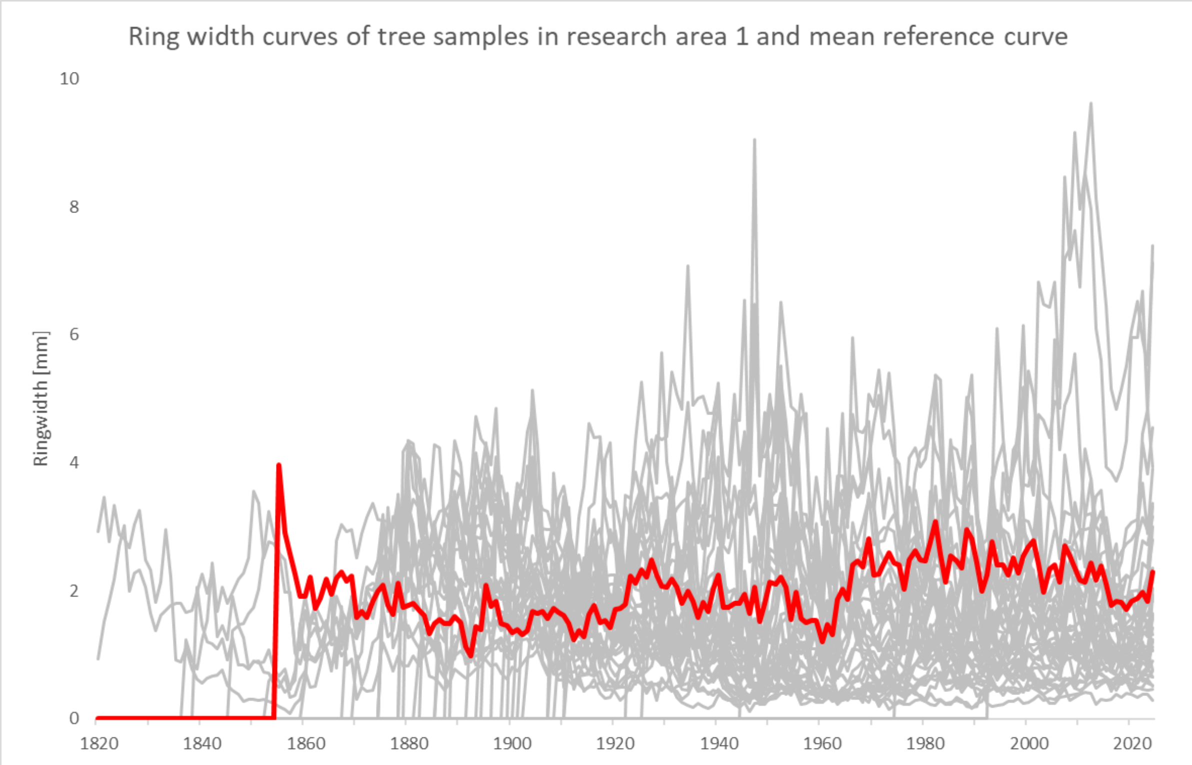

Figure 30: Ringwidth curves of trees sampled in research area 1 (Elm100 trees, gray) and mean reference curve (red). The gray curves represent the ring width of the research cores, both in the upslope and downslope directions. The red curve represents the mean reference curve.

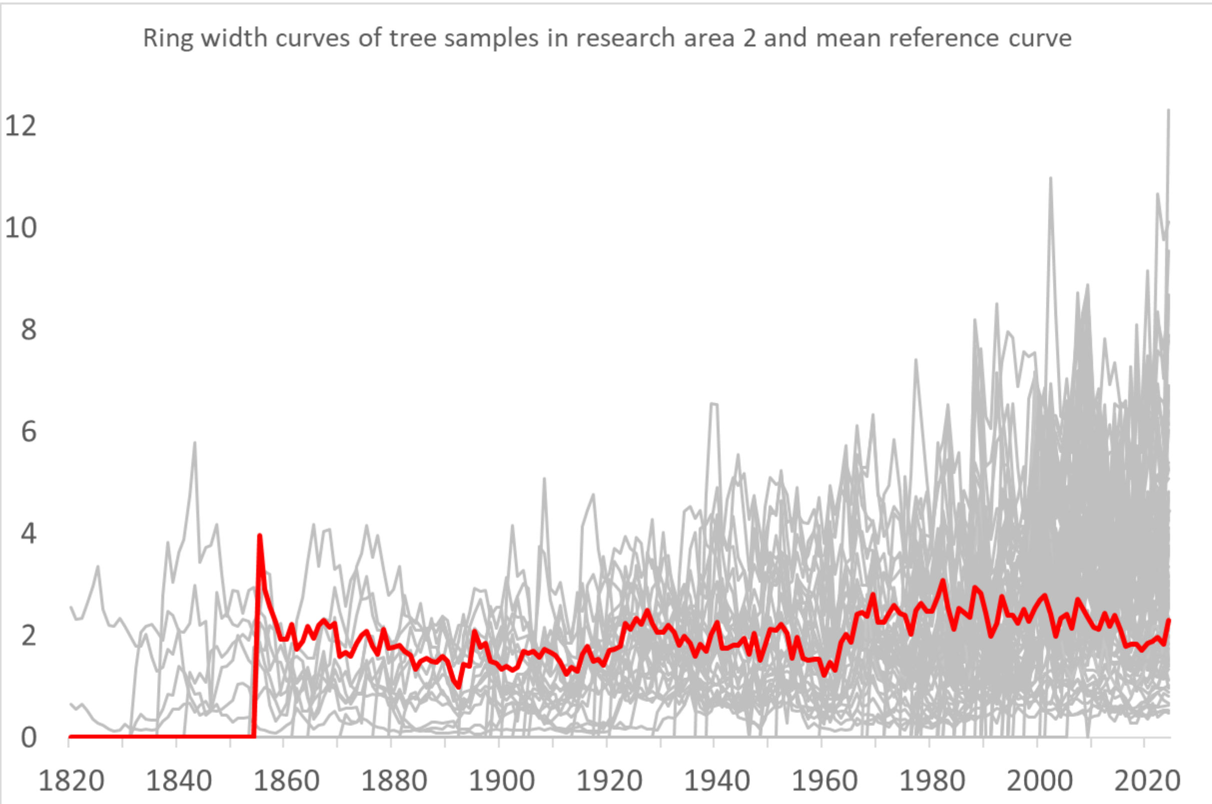

Figure 31: Ringwidth curves of trees sampled in research area 2 (Elm200 trees, gray) and mean reference curve (red). The gray curves represent the ring width of the research cores, both in the upslope and downslope directions. The red curve represents the mean reference curve.

Figure 30 shows that research samples from area 1 often differed considerably in ring width from the mean reference curve, but their overall trends remained largely parallel. Noticeable growth increases in research area 1 occurred around 1935 and 1945, which were not visible in the reference chronology. After these periods, most curves realigned more closely with the reference trend. A clear decrease in ring width was visible across almost all samples in 1991, followed by a return to previous levels or greater variability around 1993. Many samples showed another decrease in ring width during the years 2004 and 2015. From 2018 onwards, most ring widths displayed more variations. Due to the large number of samples in research area 1 (19 trees, 38 cores), detailed patterns were difficult to identify in this figure.

Figure 31 shows that samples from area 2 followed the reference trend more closely for most of the chronology. Again, an increase in ring width around 1935 stood out without being reflected in the reference curve. Some rings showed peaks between 1943 and 1948, followed by closer alignment with the reference curve. The decline in 1991 was visible in some, but not all, samples. Ring widths tended to increase again or showed more variability around 1999, 2005, and 2015, a pattern only minimally reflected in the reference curve. Again, due to the large number of samples in research area 2 (40 trees, 80 cores), it is difficult to identify detailed patterns within the figure. While these figures illustrate overall growth patterns and deviations, the significance of these variations became clearer when analyzed using eccentricity indices. These allowed growth asymmetries and potential disturbance events to be identified more precisely.

5.3. Eccentricity patterns and event detection

Using the tree-ring width data, the total number of eccentricity events was calculated in Microsoft Excel and refined through additional filtering criteria. The aim was to reconstruct the most realistic number of slope-related events within the whole chronology. The initial events identified by comparing variations in the eccentricity index with the calculated thresholds from Table 1 provided a first indication of potential disturbance years. However, the very high number of over a thousand detected events quickly suggested that many of them were false positives, fulfilling the mathematical criteria but not representing geomorphically induced disturbances.

Table 1: Calculation and rounded values for positive and negative thresholds.

Category	Mean [%]	Standard deviation [%]	Threshold [%]
Positive:	0.27	0.28	**0.55**
Negative:	-0.27	0.29	**-0.57**

Table 2 shows a marked reduction in the number of detected events across successive filtering steps. The steep decline after the first stage demonstrates that many of the initially identified anomalies were related to secondary growth responses or non-geomorphic influences. An excerpt from the Excel table was included in the Chapter 9 *Appendix* (Table 4) showing the recorded events in the years 2000-2024 after the first filtering step, in which only years with a change in the eccentricity index sign were classified as potential new events. The further decline revealed by the visual inspection underscores the importance of integrating multiple lines of evidence for reliable event detection.

Table 2: Number of upslope and downslope eccentricity events before and after three filtering steps.

Eccentricity type	Based on index and threshold	After filtering secondary events	After curve comparison	After reaction wood verification
Upslope events	514	236	90	49
Downslope events	512	363	144	95
Total events	**1026**	**599**	**234**	**144**

After applying all filtering steps, a more realistic number of 144 events remained. These events were distributed over the chronology and form the basis for further calculations and comparison with precipitation data. Figure 32 illustrates the distribution of all events after filtering over the chronology. The total number of trees included in the chronology was initially low but gradually increased as more trees became available over time. The total number of trees generally behaved similarly to the maximum number of events over the chronology. This underscored that as the number of trees involved increased, so did the probability of detecting an event. No distinct temporal pattern or pronounced peaks in event frequency are visible. The maximum number of events per year was four events, which occurred in 1963 and 1999. As fewer trees were involved in the earlier event (1963), this year represented a relatively stronger impact.

Nevertheless, several periods of increased activity could be identified, even though these periods were not that strong, as they include just two to three events per year in average: 1913-1916, 1927-1929, 1935-1938, 1947-1952, 1963-1964, 1974-1977, 1979-1983, 1987-1988, 1995-2001, 2003-2005, 2011-2015, and 2017-2022. Whether these main periods of higher event frequency correspond to slope processes or precipitation patterns remain to be clarified. Further insights are provided in Chapter 5.4. *Results from precipitation modelling*.

The spatial distribution of detected events showed no notable patterns. In most years, only a few trees recorded events, and neighboring trees were rarely affected simultaneously. Therefore, no spatial visualization of annual events was produced. Such a map would have displayed only a few spatially independent trees each year, and even over longer periods, no meaningful spatial patterns would have emerged.

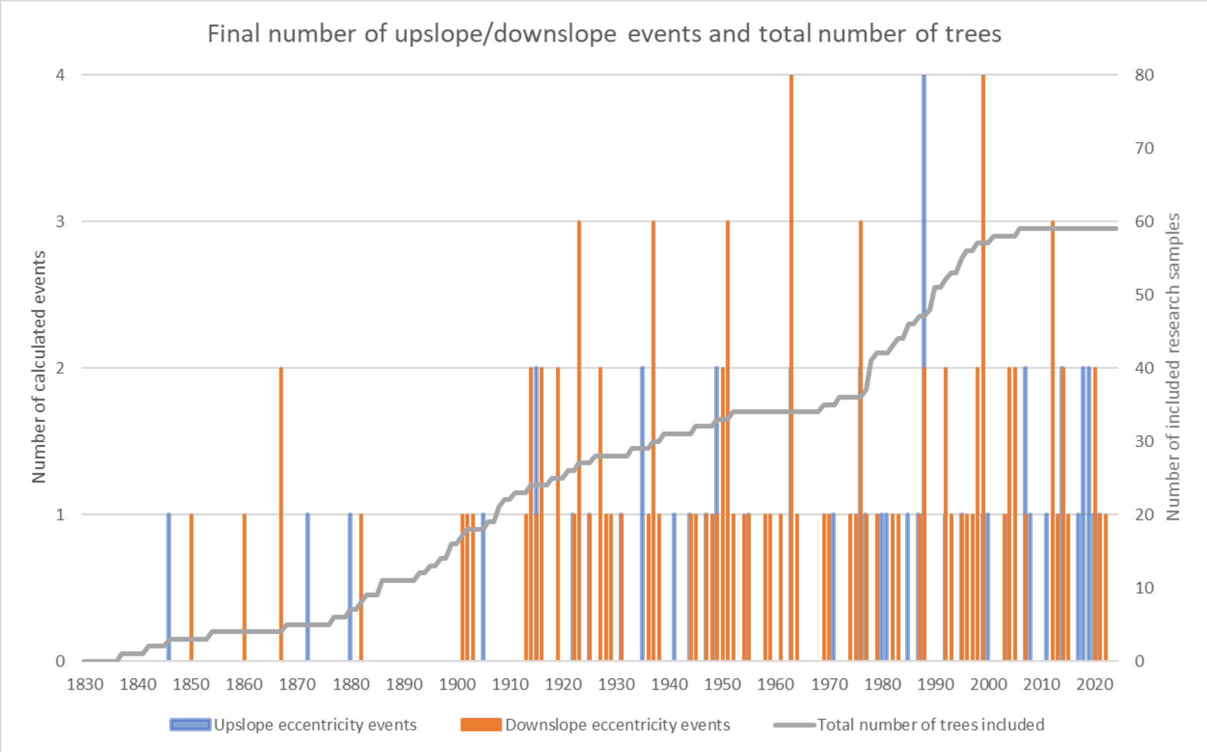

Figure 32: Number of upslope (blue) and downslope (orange) events per year after all filtering steps. The gray line shows the total number of trees that were included in the chronology in the respective year.

Two years stood out from the rest. In 1988 and 1999, many samples showed an increase in ring width compared to the reference chronology. However, this increase occurred on both sides of the trunk, thus, no clear eccentricity could be detected. In addition, these rings often showed signs of reaction wood. These observed changes in tree growth indicated a distinct response to external influences not detected in the reference area. In the case of sample Elm236 in the year 1988, there was increased ring width on the upslope side and, additionally, reaction wood on the downslope side visible, even without clear eccentricity (see Figure 33).

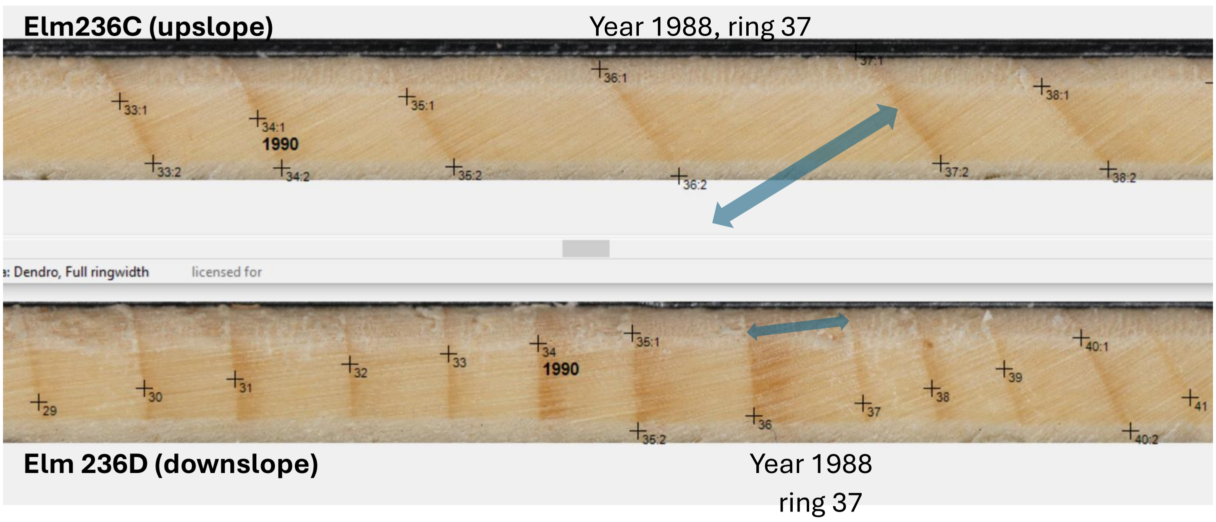

Figure 33: Sample Elm236 showing a distinctive reaction on both sides of the stem, with growth increase in ring width on sides C and D, as well as reaction wood on side D.

Consequently, such reactions were also counted and added to the total number of events with an eccentric upslope or downslope direction. Therefore, instead of 144 events, 164 events were counted for the following calculations. Excerpt from the Excel table showing the recorded events after the final filtering step based on reaction wood and the integration of samples with increased growth but without eccentricity. An excerpt of the final Excel table was included in the Chapter 9 *Appendix* (Table 5). The table shows the recorded events after the final filtering step based on reaction wood and after the integration of samples with increased growth but without eccentricity. Figure 34 shows the total number of events per year, including all detected events, providing an overview of the full spectrum of the detected disturbance signals across the chronology.

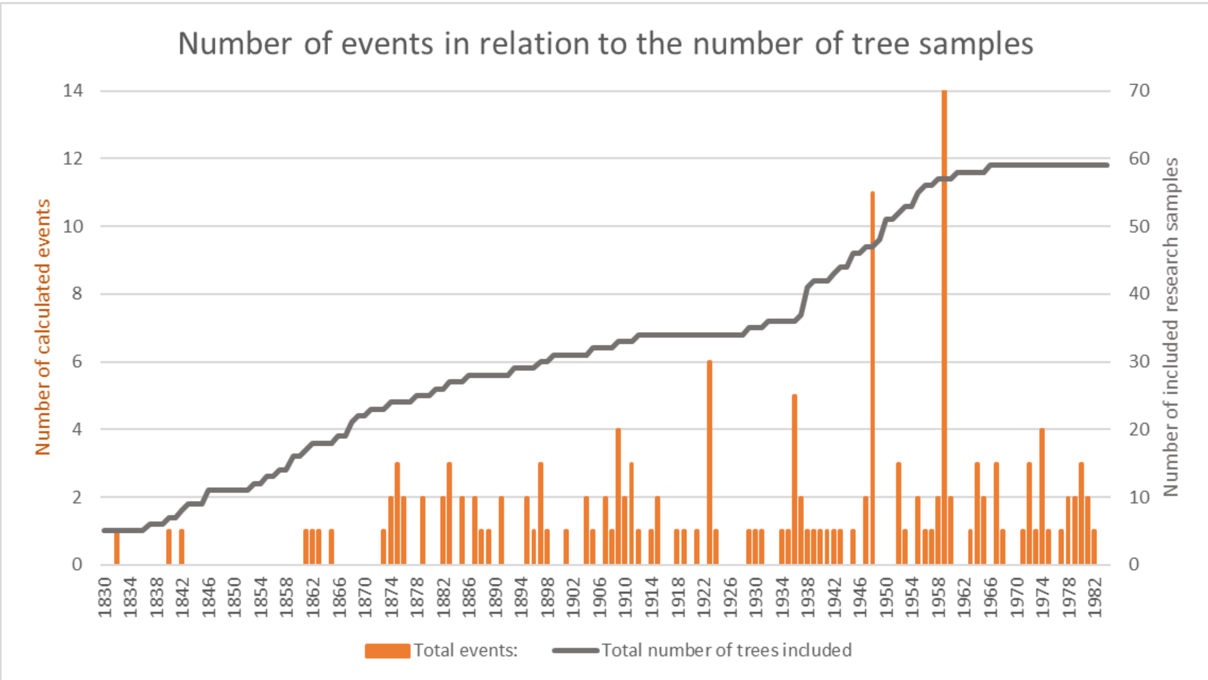

Figure 34: Number of events (orange) in relation to the number of tree samples involved for the respective year (gray).

5.4. Results from precipitation modelling

To assess whether precipitation influenced slope movement activity, the event chronology was compared with precipitation records from the MeteoSchweiz Elm station. Results are presented first through visual comparisons of time series and subsequently through statistical tests. Figure 35 illustrates the number of available samples per year, the absolute number of detected events, and the relative percentage of trees indicating an event. In the early part of the chronology (1840-1880), the number of samples was still low. Consequently, even individual events accounted for a disproportionately high relative percentage of the total record. With an increasing number of samples, the proportion of reacting trees rarely exceeds 10%.

The marked increase in the number of samples around 1975 made a higher absolute number of events more likely. Between 1950 and 1990, apart from three outlier years, the rate of events appears to be relatively low, with maximally 2.5% of trees showing an event. After 1995, rates of 5% were regularly reached again. However, there are hardly any more outlier years with more than four events. The high relative shares observed in 1988 and 1999 reflected the large number of samples that were included due to increased ring width and reaction wood. Similar to before, several multi-year periods stood out in which events were recorded across consecutive years, indicating phases of higher activity. Such periods include 1901-1905, 1913-1916, 1922-1931, 1935-1939, 1947-1952, 1974-1983, 1995-2001, 2011-2015, and 2017-2022.

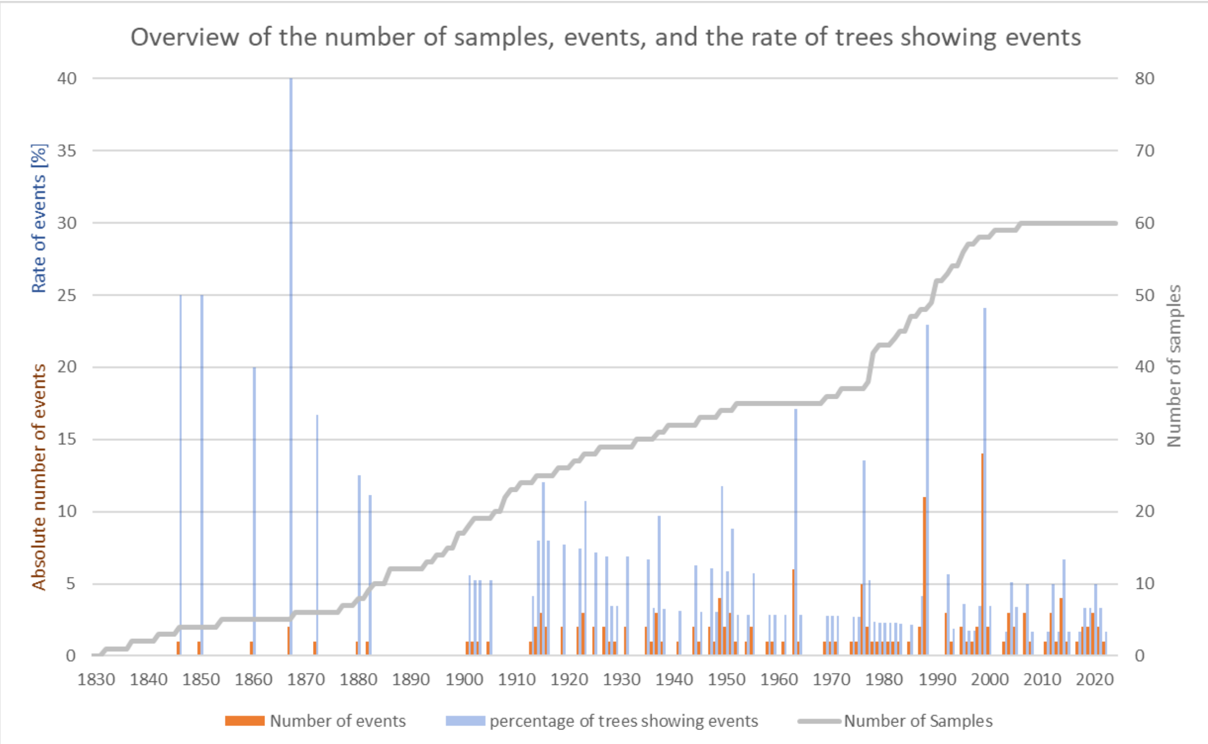

Figure 35: Overview of the number of samples (gray), the absolute number of events (orange), and the relative rate of trees showing events (blue) from 1830 to present.

5.4.1. Visual comparison of precipitation and event rates

As a next step, the temporal evolution of precipitation was visually compared with the rate of detected events. Graphs that display monthly accumulated precipitation (blue) alongside the normalized event rate, expressed as the number of events relative to the number of available tree samples (orange), were produced. It is important to note that precipitation records are available only from 1900 onward, which is why earlier events were excluded from this analysis. This comparison allows for an initial, qualitative assessment of whether peaks in precipitation correspond to an increase in the detected slope movements, and whether any broader temporal trends, such as long-term increases or decreases, can be observed.

The annual precipitation totals at the Elm station (see Figure 36) appeared relatively constant over the measured period. The values fluctuated between approximately 1300 and 1900 mm per year. Every 10-20 years, a notably drier year could be observed, for example, in 1921, 1934, 1943, 1973, 1984, 1991, 1998, 2005, and 2015, followed by a period of several years with higher precipitation. When comparing these patterns with years of higher event rates, especially the clusters of several consecutive event years, many events occurred between such drier years. Around the turn of the millennium (e.g., 1998 and 2005), however, this relationship was no longer visible. In the years when more than 20% of the trees responded to a potential event (1988 and 1999), the precipitation curves displayed no distinct pattern. Precipitation totals were relatively high in these years, but no consistent tendency could be identified in the preceding or following years. Additional insights could emerge from a closer inspection of monthly precipitation data.

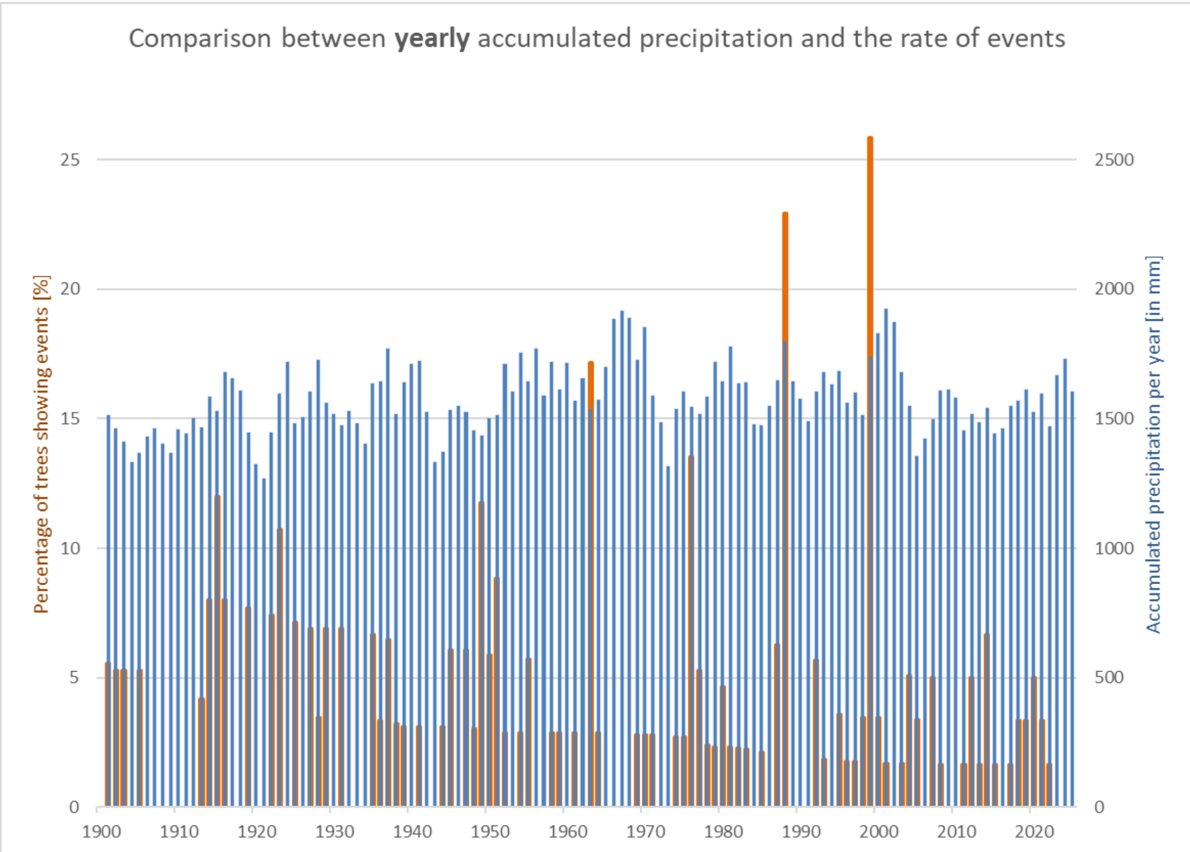

Figure 36: Comparison between yearly accumulated precipitation (blue) and the percentage of trees showing events (orange) from 1900 to present.

Figure 37 shows monthly precipitation values combined with the percentage of trees that indicated an event in the corresponding year. However, it is difficult to read because the monthly bars are very narrow. Accordingly, the figure is not well-suited for detailed visual observations. The seasonal cycles of precipitation in Elm (higher precipitation in June-August, lower in December-February) cannot be recognized at all. Nevertheless, it can be observed that the years with a high event proportion above 15% (1963, 1988, and 1999) all coincided with at least one month of increased precipitation early in the year. Conversely, other years with even higher monthly precipitation did not show similarly high event proportions.

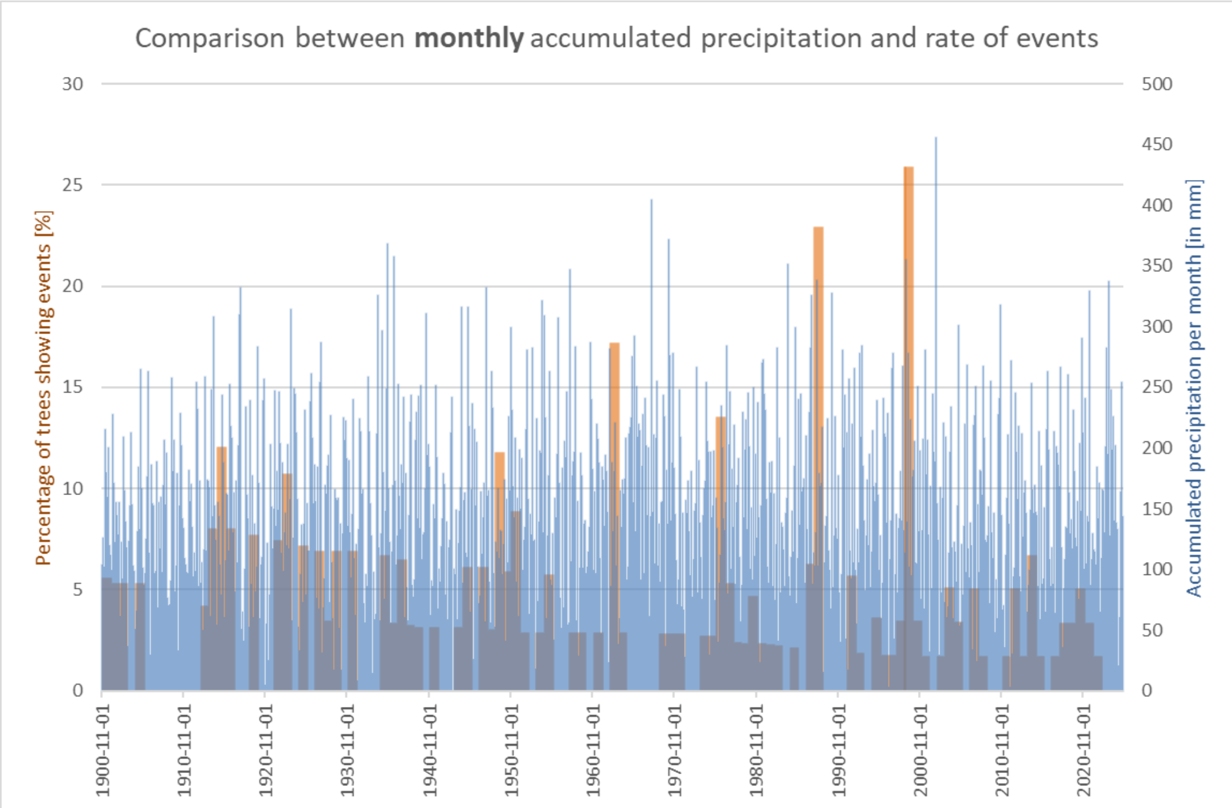

Figure 37: Comparison between monthly accumulated precipitation (blue) and the percentage of trees showing events (orange).

To complement the annual and monthly values, a cumulative sum of the normalized event rate was calculated. This representation smooths out short-term variability and highlights long-term shifts in event frequency, making potential trend breaks more visible. Figure 38 displays this relative event contribution over time, together with the drainage intervention year as an anchor point for later analysis. The cumulative curve shows an overall steady increase in the normalized event rate. Between about 1880 and 1915, the curve was nearly flat, indicating a stagnation in detected events. From roughly 1920 to 1980, the increase was nearly linear, reflecting a constant proportion of annual events. Before 1990 and again before 2000, the curve showed a noticeable steepening, indicating an increased rate of detected events. This pattern corresponds to the event peaks observed in 1988 and 1999. After these periods, the cumulative curve flattened again, reflecting a slower accumulation of events.

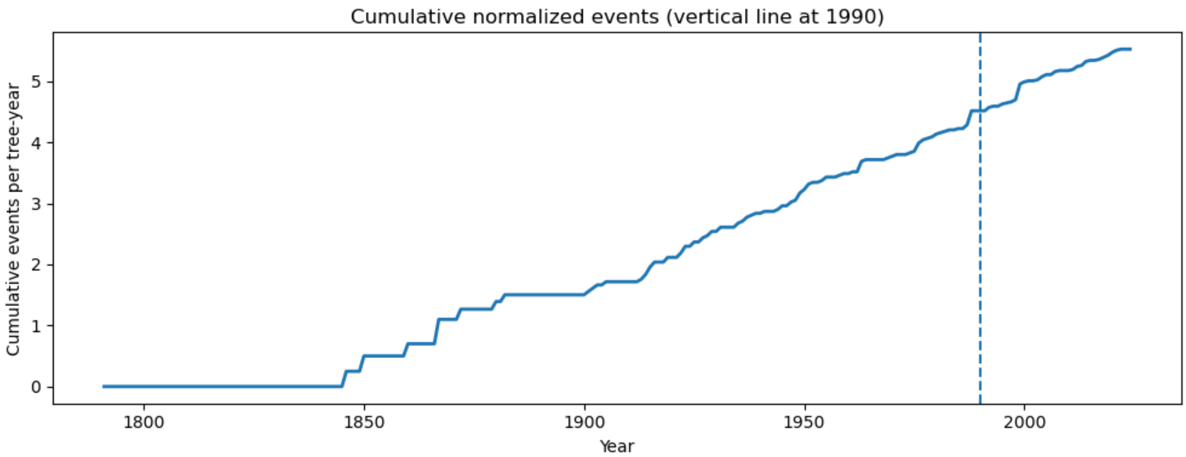

Figure 38: Cumulative normalized event curve over the study period, expressed as cumulative events per tree-year. This dimensionless metric accounts for varying sample depth and shows the total number of events relative to the number of tree-years, revealing a steady accumulation of growth disturbances through time.

While these graphs provide a first impression of potential relationships between precipitation and event rates, formal statistical analyses are required to evaluate the strength and significance of these patterns using different precipitation metrics.

5.4.2. Statistical analysis of precipitation-event relationships

To test whether the visually observed patterns represent significant relationships, correlation and group comparison analyses were carried out between precipitation metrics and event rates. For the statistical analyses, event rates were expressed as values between 0 and 1 rather than as percentages. This corresponds to the same information (e.g., 0.2 = 20%) but was chosen to simplify calculations.

5.4.2.1. Annual precipitation sums

The correlation between annual precipitation totals and the event rate was weak but reached statistical significance for the Pearson test (r = 0.181, p = 0.0428, n = 125). The Spearman correlation was similar in magnitude (r = 0.169) but did not reach the significance threshold (p = 0.0588). All statistical test results are summarized in Table 3 for a better overview. The scatterplot in Figure 39 shows the associations between the normalized event frequency and annual precipitation sums, each with a fitted regression line. The points are widespread without a clear clustering along the fitted trendline. A slight positive slope is visible, indicating that higher precipitation totals tend to correspond with somewhat higher event rates. However, the cloud of points remains broad, and the low R^2 value reflects that precipitation explains only a very small portion of the variance in event occurrence. In other words, while the trendline points upward, the relationship is weak and far from deterministic.

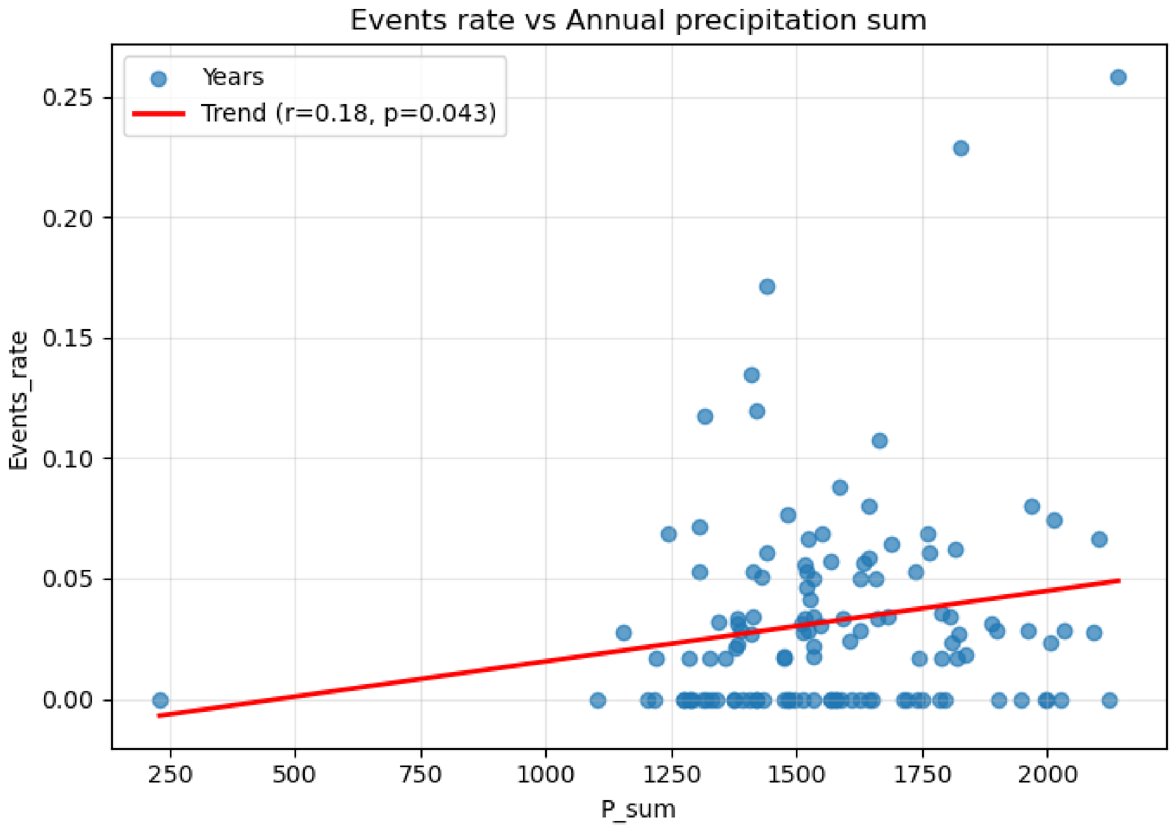

Figure 39: Scatterplot showing the relationship between annual precipitation sums and event rate, with individual years plotted as blue points and a fitted trendline in red.

5.4.2.2. Maximum monthly precipitation

When testing the maximum monthly precipitation of each year, correlations with the event rate were weaker and not statistically significant (Pearson r = 0.109, p = 0.227; Spearman r = 0.070, p = 0.439; n = 125). The same scatterplot (Figure 40) as before was used for depicting maximum monthly precipitation. The fitted trendline is nearly flat, and the points are broadly scattered across the diagram, with no visible concentration along the line. This visual impression reflects the low correlation coefficients and indicates that the maximum monthly precipitation alone did not account for variation in event rates.

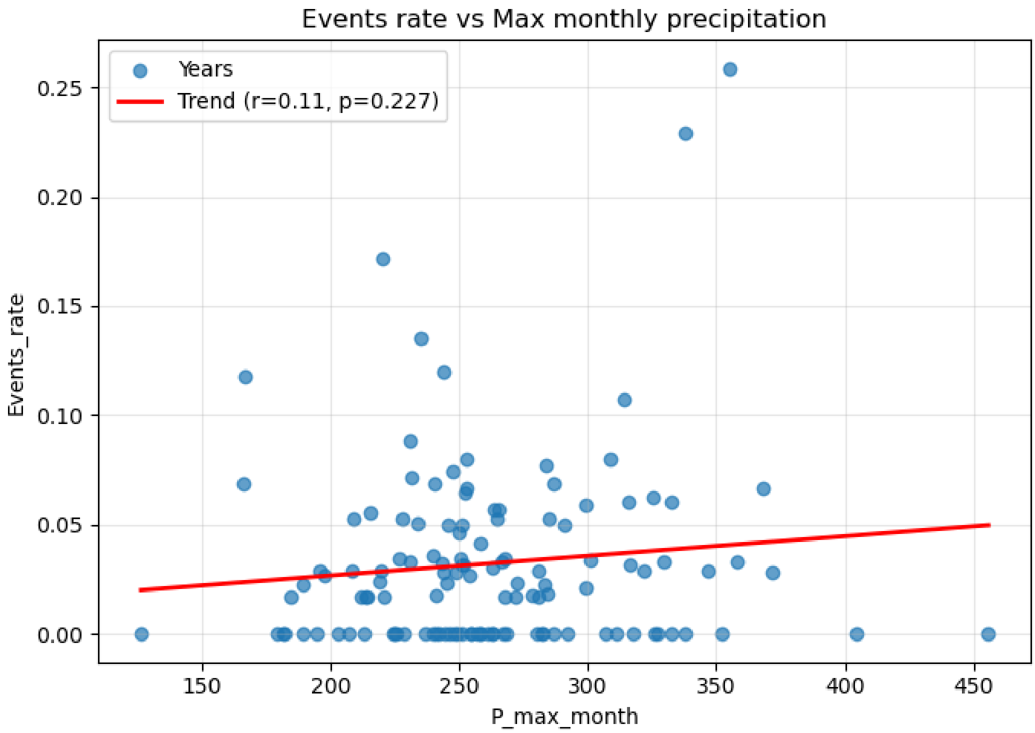

Figure 40: Scatterplot showing the relationship between maximal monthly precipitation totals and event rate, with individual years plotted as blue points and a fitted trendline in red.

5.4.2.3. Sum of the three wettest months

The aggregated precipitation of the three wettest months per year showed no significant relationship with the event rate (Pearson r = 0.086, p = 0.343; Spearman r = 0.051, p = 0.575; n = 125). Again, a scatterplot (Figure 41) was produced to visualize tendencies using the sum of the three wettest months per year. The points are widely dispersed without any visible clustering, and the fitted trendline is essentially flat, which underlines the absence of a detectable association.

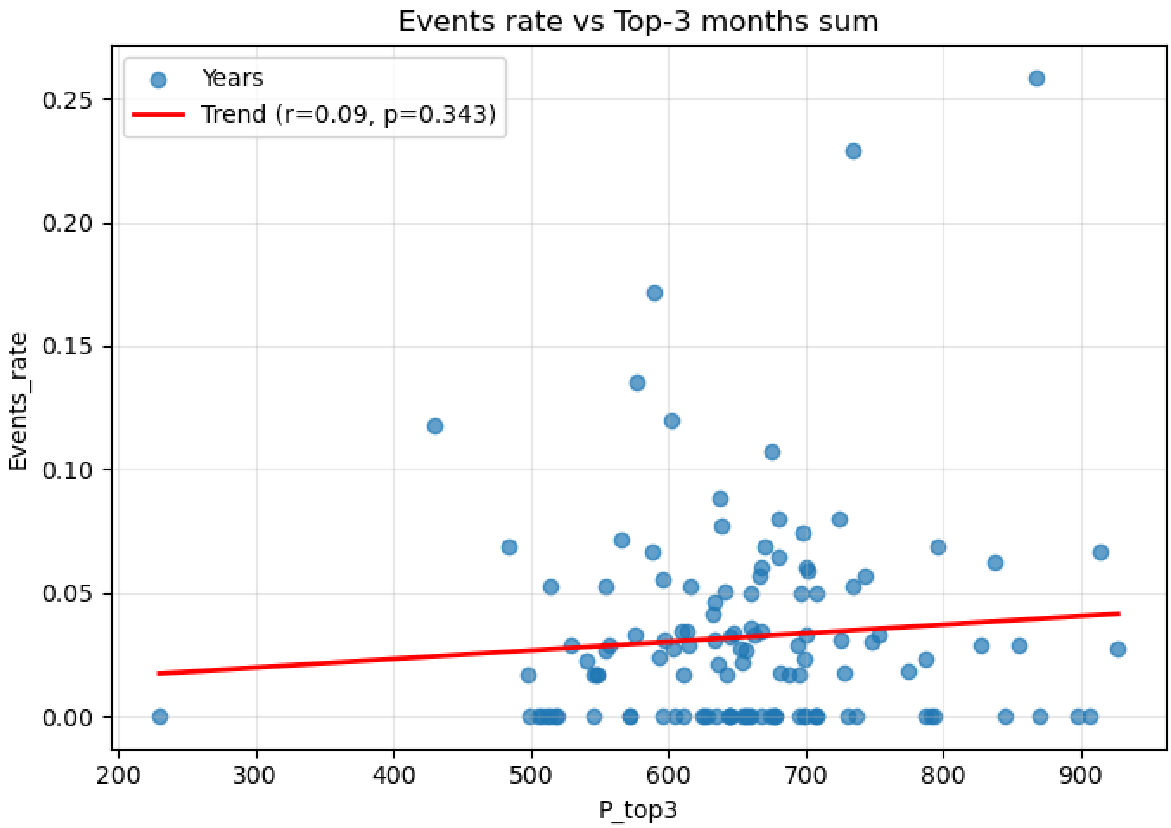

Figure 41: Scatterplot showing the relationship between the three wettest months' precipitation totals and event rate, with individual years plotted as blue points and a fitted trendline in red.

5.4.2.4. Highest daily maximum per year

To assess whether single-day precipitation extremes are associated with increased slope activity, the relationship between the annual event rate and the maximum daily precipitation per year was examined. The resulting correlations were weak and statistically non-significant (Pearson r = -0.050, p = 0.578; Spearman r = -0.059, p = 0.512; n = 125). The scatterplot (Figure 42) shows a wide spread of points without a discernible trend, and the fitted regression line is almost horizontal, indicating no clear association between the variables.

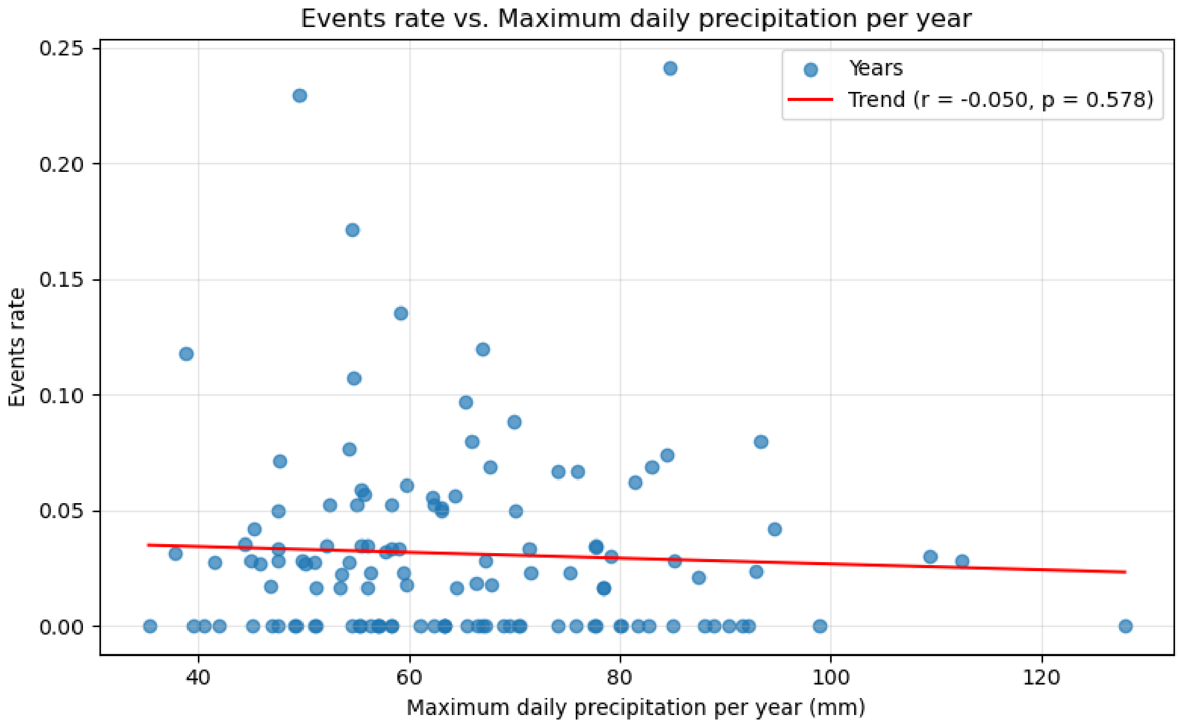

Figure 42: Scatterplot showing the relationship between the maximum daily precipitation total per year and event rate, with individual years plotted as blue points and a fitted trendline in red.

5.4.2.5. Period comparison

To assess potential changes in event frequency following the installation of drainage channels in the 1990s, normalized event rates were compared between the pre-1990 (n = 199) and post-1990 (n = 35) periods. The Mann-Whitney U test showed a statistically significant difference between the two groups (U = 2402.00, p = 0.000685), with a medium effect size (Cliff's delta = -0.310). The negative delta value indicates that event rates were generally lower in the period after 1990 compared to before.

5.4.2.6. Lagged correlation analysis

Considering a one-year lag between precipitation and the event rate did not improve the strength of correlations. Across all four tested precipitation metrics, coefficients remained weak and statistically insignificant. Annual precipitation totals showed virtually no relationship with the following year's event rate (Pearson r = -0.015, p = 0.871; Spearman r = 0.007, p = 0.938). Similar results were obtained for maximum monthly precipitation (r = 0.056, p = 0.537), the sum of the three wettest months (r = 0.044, p = 0.628), and the daily maximum of precipitation per year (r = 0.132, p = 0.145). These findings suggest that delayed slope reactions to precipitation on an annual time-scale are unlikely to be the reason for the absence of strong correlations observed in this dataset.

5.4.2.7. Overview of the main statistical results

Table 3 summarizes the results of the correlation analyses between event rates and different precipitation metrics (without the 1-year lag tests). Only the annual precipitation sum showed a weak but statistically significant correlation with the event rate in the Pearson test, while all other metrics (maximum monthly precipitation, the sum of the three wettest months, and the highest daily maximum per year) were not significantly correlated in all other tests.

Table 3: Results of correlation analyses between event rate and precipitation metrics. Pearson correlation tests reflect linear relationships, while Spearman rank correlations capture monotonic associations. n indicates the number of years included in each test.

Precipitation metric	Test	r / U statistic	p-value	n	Result
Annual sum	Pearson	r = 0.181	0.0428	125	significant (weak)
	Spearman	r = 0.169	0.0588	125	not significant
Max monthly	Pearson	r = 0.109	0.227	125	not significant
	Spearman	r = 0.070	0.439	125	not significant
Sum of top-3 months	Pearson	r = 0.086	0.343	125	not significant
	Spearman	r = 0.051	0.575	125	not significant
Highest daily maximum per year	Pearson	r = -0.050	0.578	125	not significant
	Spearman	r = -0.059	0.5117	125	not significant
Pre vs Post 1990 of event rate	Mann-Whitney U	U = 2402.00	0.000685	pre = 199 post = 35	significant (medium effect, d = -0.310)

In summary, the analyses showed hardly any statistically significant correlations between reconstructed event rates and the tested precipitation metrics, regardless of whether annual totals, seasonal sums, or extreme daily precipitation values were considered. Although some years with increased event frequencies coincided with months of high precipitation, such overlaps were inconsistent across the chronology. These results form the basis for the subsequent discussion, where potential explanations, uncertainties, and broader implications of the findings are examined.

6. Discussion

In this chapter, the results of the thesis are discussed, and relevant influencing factors and processes are considered. In addition, the findings are placed in the context of the consulted literature, followed by a discussion of the strengths and weaknesses of different approaches. This discussion aims to position the significance of this study within the broader context of research on natural hazards in the face of climate change.

6.1. Overview and interpretation of key findings

Geomorphological field observations provided important insights into the slope dynamics in the Ramintal. Overall, they confirmed the findings of Grämiger (2024), who described predominantly slow and long-term mass movement processes rather than abrupt landslide events. In other parts of the slope, cracks, subsided areas, and detachment scarps were visible. In the research area, no clear indicators of rapid slope failure were apparent. However, the geological investigations by Grämiger (2024) suggested much evidence of landslides and the underlying rock subsidence. Material is clearly in motion, being eroded more quickly on steep sections and deposited on flatter terraces and around trees, forming mounds. Besides, small rills and the loose texture of the substrate were observed, supporting the findings of Grämiger (2024) that water easily infiltrates and further destabilizes the slope. The investigated trees showed a wide range of ages, forms, and site conditions, often displaying tilted or curved stems without a consistent relationship to slope inclination. In contrast, the reference area had gentler slopes, vertical tree growth, and minimal geomorphic disturbance, indicating overall slope stability. These findings are an important part of answering the first research question, confirming that landslide activity caused growth disturbances in research trees.

To account for the extent of disturbances, growth responses were measured. Tree-ring curves revealed high synchrony within the reference chronology but high variability among the research trees, explaining high eccentricity values and suggesting influences beyond natural growth trends. High growth anomalies occurred around 1935 and 1945, as well as a pronounced decline around 1991, followed by periods of increased variability, particularly around 1999, 2005, and 2015 to 2018, although not all trees were affected the same way. These complex disturbance dynamics required further analysis, and the variation of the eccentricity index was calculated to quantify the years of higher eccentricity. However, the calculated number of detected events was beyond realistic numbers. So, additional filtering criteria were used, allowing true landslide events to be distinguished from recovery growth or non-geomorphic influences. Afterwards, a total of 144 events remained, with several periods with increased activity (2-3 events per year): 1913-1916, 1927-1929, 1935-1938, 1947-1952, 1963-1964, 1974-1977, 1979-1983, 1987-1988, 1995-2001, 2003-2005, 2011-2015, and 2017-2022. The decrease in detected events following visual verification underlines the importance of integrating multiple lines of evidence for reliable event detection. In two years, 1988 and 1999, many trees formed rings of increased width and reaction wood, despite the absence of clear eccentricity. Such events were additionally interpreted as indications of external disturbances and added to the final number of events (now 164 events). The growth disturbances caused by landslide events appeared in periods of higher activity. However, no clear temporal clustering could be observed.

To account for the change of geomorphic activity on the slope after the installation of drainage channels in the 1990s, the normalized event rate before and after 1990 was tested. It revealed a statistically significant decrease in activity (Mann-Whitney $U = 2402.00$, $p = 0.000685$). The negative effect size (Cliff's delta = -0.310) indicates that event rates were generally but not strongly lower after 1990. Therefore, the test results suggest a reduction in slope activity after the implementation of drainage measures, which addressed the second research question.

To address the third research question, precipitation measurements from recent decades were used to test for a possible correlation between precipitation and geomorphic activity and, if so, to identify patterns that could help predict future developments. The detected events were expressed as normalized annual event rates and compared with precipitation data from a nearby measurement station in Elm. Visual inspection revealed periods of higher and lower precipitation on both monthly and annual scales. However, there was no clear relationship to the detected events in the respective years. Therefore, statistical tests were conducted to examine whether event occurrence was dependent on precipitation amounts over different time intervals. The various precipitation metrics used for this purpose (annual precipitation totals, maximum monthly sums per year, the sum of the three wettest months per year, and the highest daily maximum per year) all showed hardly any statistically significant correlation. Although some years with increased event frequency coincided with months of high precipitation, such overlaps were inconsistent across the chronology. Moreover, slope responses delayed by one year showed even weaker correlations with precipitation. The lack of correlation between detected past landslide activity and its presumed main trigger, precipitation, currently makes it difficult to predict future slope activity, which therefore requires further investigation.

These key findings make it necessary to discuss which processes and factors may have influenced these observations and trends, which aspects have not been taken into account yet, and how literature considered or neglected certain factors that may have led to different results.

6.2. Slope dynamics and geomorphic processes

The field observations of the study area in Elm are not directly comparable with other study areas, as the results of dendrogeomorphologic work depend greatly on a wide variety of local factors, such as altitude, slope gradient, substrate composition, geological layers, nutrient availability, tree species, etc. Certain similarities were identified, but also many differences, which will now be discussed in more detail.

Fabiánová et al. (2021) likewise found no evidence of recent landslide activity, such as cracks, levees, scarps, or stretched roots in their study site. They attributed the slight tilting of many trees mainly to seasonal soil creep, weathering mantle movement, or low-magnitude block displacement. Other studies, however, identified clearer geomorphic features that provide more insight into slope dynamics. Wistuba et al. (2013), for example, detected deep-seated, large-scale landslides with pronounced scarps, landslide tongues, scree slopes, secondary landslide events, and slope undermining. Such undermining and the associated sliding of lower slope sections were considered likely causes of downslope stem bending. Malik et al. (2016) found that trees on steeper slopes tilted mostly downslope. Such findings are consistent with Braam et al. (1987), who demonstrated a relationship between local hillslope features, the type of stem deformation, and tree-ring eccentricity, though inconsistent with the findings from Elm. In the present Elm study area, however, this pattern was not observed. The trees were observed to lean in diverse directions, probably linked to small-scale terrain variability with steep scarps, terraces, erosion, and deposition zones.

Much more activity was recognized in the research area of Lopez Saez et al. (2012), which was characterized by a huge landslide complex, evidence of which could be found in abundance in the form of older and recent cracks and flows. However, the authors were able to rely on technical investigations such as remote sensing technologies in combination with field observations from earlier studies, which facilitated geomorphological mapping (Lopez Saez et al., 2012). Other study areas were also too large-scale (e.g., Handwerger et al., 2013; Jones et al., 2023; Macfarlane, 2009; Oven et al., 2019), related to other processes with limited comparability (e.g., Germain et al., 2018; Strunk, 1997; Trappmann et al., 2013), or were abrupt or reactivated processes (e.g., Curioni et al., 2024; Fantucci & Sorriso-Valvo, 1999; Šilhán & Stoffel, 2015; Tichavský et al., 2019).

Classifying the type of landslide was challenging, as various forms were possible. Clearly defined sliding zones or detachment scarps were absent, and the signs of slope movement were generally subtle at the site of Elm. Based on comparisons with other landslide types, the processes present in the research area were classified as a slow-moving landslide with both rotational and translational components, following the overview by Tumajer and Treml (2013, p. 60). The strong similarities in slope morphology to the sites described by Malik et al. (2016) support the interpretation of slow movement. According to Šilhán (2021), rotational landslides typically involve slow rotating movements in weak material, often featuring steep main scarps, tension cracks, and characteristic tree responses such as reaction wood and ring eccentricity caused by stem tilting. Such indicators were observed in the study slope. In general, trees that grow on rotational landslides are tilted upslope (Šilhán, 2021). However, the direction of inclination of the trunks in the study area was not uniform, but rather oriented both uphill and downhill, as well as in some cases sideways. However, the findings by Van Den Eeckhaut et al. (2009) suggest that a bimodal distribution of inclination direction is typical for a rotational slide. In contrast, translational landslides are often associated with uniform downslope tilting (Van Den Eeckhaut et al., 2009). Translational sliding refers to the sliding of the uppermost soil layer along an existing discontinuity in the subsoil, such as the contact zone between the bedrock and surface deposits (Germain et al., 2018). Signs such as unconsolidated surface materials in the study area could indicate translational landslides (Germain et al., 2018), but it is challenging to assess this movement based on the signs found in the field. Šilhán (2021) highlights the complexity of assigning tree inclination to slope movement processes. Therefore, no clear assignment of process and tree response is possible within the study site. Instead, a combination of processes likely acts on different parts of the slope in Elm, suggesting a slow-moving landslide with mixed rotational and translational components.

It also remains uncertain whether the selected tree species, Norway spruce, responds differently to specific landslide types or depths compared to other species, as its shallow root system is less resistant to geomorphologic disturbances, reducing its stability on steep, moving slopes (Tichavský et al., 2019). Depending on the depth of the landslide, spruce trees may show stronger tilting reactions than other tree species. Unfortunately, there is no evidence regarding the depth of the sliding horizon. According to Grämiger (2024), no long-term measurements of landslide movement rates or data on the depth of the sliding surfaces in the area are available. The reported displacement rates of well over 10 cm per year and, in some cases, more than 60 cm per year are only estimates (Grämiger, 2024). Consequently, the surface mapping would need to be complemented by exploratory ground drilling or long-term monitoring to obtain more precise information on the depth, velocity, and ultimately the characteristics of the landslide.

6.3. Tree-ring signals and their interpretation

The trees in the research area showed diverse growth responses, which were easily quantifiable both visually and mathematically. However, eccentricity signals alone were insufficient to reliably confirm landslide events. Eccentricity indices were calculated after Wistuba et al. (2013), adapting their methodological approach of using the variation of the index instead of absolute values for event detection. This was also applied to the reference values for threshold calculation. For this reason, thresholds reflected the normal background noise of eccentricity in undisturbed areas. Disturbance years in research trees were identified only when their eccentricity variation exceeded these reference thresholds, indicating abrupt deviations that are more likely to be linked to slope movement.

Despite this approach, the variation of the eccentricity index resulted in an unrealistically high number of detected events, partly due to the reference signal itself, as discussed further in Chapter 6.6. *Methodological considerations and limitations*. So, additional filtering criteria were used, allowing plausible landslide events to be distinguished from recovery growth or non-geomorphic influences. Events were considered only if reaction wood was assumed additionally to eccentric growth, and only the first year of a reaction series was counted. In about ten instances, reaction wood appeared one year earlier than eccentric growth. In these and other cases, event detection became more reliable when eccentricity patterns were evaluated together with visual and microscopic evidence of reaction wood, rather than relying on eccentricity alone. One limitation remained for tilting events at the end of the growing season, when no wood could be formed in response, and the reaction wood only appeared in the following ring. Nevertheless, combining tree-ring eccentricity analysis with wood anatomical methods significantly enhances the reliability of landslide reconstruction (Heinrich et al., 2006).

Although the eccentricity index itself is independent of tree age, previous studies have shown that tree sensitivity to geomorphic disturbance signals can vary with age or diameter (Šilhán & Stoffel, 2015; Stoffel & Corona, 2014; Trappmann et al., 2013). Growth suppression is most marked in older conifers (from 70 years), while compression wood tends to occur more frequently in younger individuals (Fabiánová et al., 2021). Older trees also display eccentric growth more often than reaction wood due to their less elastic stems (Šilhán, 2017; Šilhán & Stoffel, 2015; Stoffel & Bollschweiler, 2008). With increasing size, trees react more strongly to tilting caused by mass movements (Sitko et al., 2022). Juvenile growth, however, is known for its high variability and sensitivity to geomorphic as well as non-geomorphic influences (Šilhán & Stoffel, 2015). The different reaction patterns could also be observed in the samples taken. Young trees tended to form reaction wood, whereas eccentric growth of old increments was not always accompanied by clear reaction wood.

To avoid bias from early growth patterns, Šilhán & Stoffel (2015) recommend excluding the first decades from analysis. Additionally, it is important to handle early rings with caution to avoid bias chronologies, e.g., by standardization (Esper & Gärtner, 2001). Following this in the study, the first 20 increments of each sample were neglected, and the subsequent two decades were treated with caution. This approach helped to reduce noise from early growth and improved the accuracy of event detection. Trees of all available age classes were sampled to ensure sensitivity across the full chronology. Because the use of the variation of the eccentricity index already minimized the age trend, no further age standardization was required.

Another source of uncertainty in evaluating tree-ring growth responses concerns the years 1988 and 1999, during which no clear eccentricity was observed in many rings. Instead, the cores from both sides of the trees exhibited increased ring width, often accompanied by reaction wood. Because both sides showed this simultaneous growth increase, the eccentricity index calculations did not, or only partially, indicate eccentricity. The absence of distinct eccentricity suggests that the coring direction may not have captured the axis of maximum eccentric growth. Consequently, the difference in ring width between the two sides of the stem was not fully expressed, explaining the lack of eccentricity. The concurrent presence of reaction wood, however, supported the interpretation of a geomorphic trigger. Another possible explanation was growth releases, which increased the overall ring width over several consecutive years. However, such releases are typically caused by abrupt changes in conditions, such as the loss of competition or improved light or nutrient availability. Since these factors rarely affect many trees simultaneously, it is more likely that the observations in this case resulted from imprecise sampling orientation and the absence of detectable eccentricity.

This observation demonstrates that eccentricity alone is not always sufficient for event identification, as it can depend on the orientation of sampling cores. At this point, it should be mentioned once again that whole tree discs naturally make it much easier to analyze eccentricity and reaction wood, but clearing so many trees is usually not justifiable and feasible. Therefore, the increment cores, which usually indicate growth reactions when drilled perpendicular to the point of maximum curvature, must be sufficient. At least, the simultaneous occurrence of increased ring width and reaction wood in several trees indicates that the growth anomalies are most likely linked to geomorphic disturbances, supporting the inclusion of these years in the reconstructed event chronology.

The combination of eccentricity analysis and careful filtering, such as reaction wood analysis, provides a robust basis for interpreting geomorphic activity. As every growth reaction to a mass movement event has its own limitations, their combination is recommended (Tumajer & Treml, 2013). Thereby, the continuous background signal of ongoing slope activity is most likely detected, which helps to verify unambiguously the nature of the triggering factors (Gussenstätter & Bräuning, 2003). Absolute verification is not possible due to the absence of comparable studies in the area. Therefore, the reconstructed chronology represents the best possible approximation of landslide-related disturbance events within the limitations of the dataset and methodological approaches.

6.4. Climate influences and precipitation-landslide relationship

The precipitation measurements from the Elm weather station were quite convincing, as the data appeared to be almost identical to weather data gathered from the KNMI Climate Explorer, despite different data aggregation. When visually comparing the monthly and yearly precipitation data with the event chronology, no clear trend could be observed. Furthermore, no statistical correlation was found between events and various precipitation metrics, even with a delay of one year. Only the test with yearly sums showed a statistically significant but rather low correlation, even though strong precipitation years do not consistently correspond with more intense growth reactions in trees (Schmid & Schweingruber, 1995).

The highest monthly precipitation sum per year is more likely to trigger landslides, due to increased infiltration, pore-water pressure, and reduced effective stress along basal shear zones, keeping slopes close to failure thresholds (Handwerger et al., 2013; Macfarlane, 2009; Malik et al., 2016). According to Handwerger et al. (2013), slow-moving landslides typically respond to seasonal rainfall accumulation over several weeks to months, rather than to short-term precipitation peaks. Consequently, monthly or seasonal precipitation sums are more appropriate for assessing their hydrologic triggering. However, monthly totals and the sum of the three wettest months also failed to explain event frequency in the study site. A limitation of the sum of the three wettest months was that it did not take into account that the months should follow each other. Other studies identified short, intense rainfall events as direct triggers of landslide reactivation

(Lopez Saez et al., 2012; Papciak et al., 2015; Šilhán, 2020), highlighting the possibility that short-term precipitation accumulation can contribute to higher slope activity. The daily maximum per year, however, was probably too short-term, as long-term ground saturation is decisive for slope failure (Massey et al., 2013; Papciak et al., 2015). Therefore, no single precipitation metric tested here appeared optimal for capturing the complexity of slope-precipitation interactions.

The slope in Elm is affected by slow-moving slides, but without signals for abrupt, extensive slope failures that were recorded by several trees in the same year. Precipitation sums are not expected to be a clear, direct cause of slope movement in Elm, but rather one of several factors. A general limitation of the tree-ring-based dating is the maximum precision, which is sufficient for the calculation of landslide frequency, but may be insufficient for the detailed identification of a specific triggering event (Lopez Saez et al., 2012; Šilhán, 2021). This suggests that, for the present study site, it is difficult to determine the exact triggers based on dendrogeomorphic signals, and that only the approximate frequency of the events could be determined.

The dendrogeomorphic event record is limited to annual or partly seasonal resolution. However, this study did not aim to date growth disturbances with seasonal precision, as this would have required extensive microscopic analysis to distinguish the timing of growth reactions within the annual rings. Still, other researchers could detect seasonal precipitation as a triggering factor in surface slope movements using dendrogeomorphic methods. Papciak et al. (2015) could identify significant correlations between landsliding and high winter precipitation totals. Leonelli et al. (2021) found that high precipitation sums in summer may likely trigger landslide instabilities that are recorded by trees during the year of growth or one year later. In Elm, however, where it was expected that high summer precipitation events are a key trigger for landslide activity and therefore influence tree growth responses, no such relationships could be found.

Another limitation could be the precipitation measurement itself, as the weather station is located 1.5 km further west and 300 m lower. Precipitation and temperature may differ slightly at the study site, but no significant differences are expected. Malik et al. (2016) assumed that their poor correlation of the dendrochronological record with the rainfall record could be linked to imperfections in the rainfall record itself. In the case of Elm, however, it can be assumed that the rainfall record is of sufficient quality. At most, there could have been a significant improvement in measurement accuracy since the beginning of the measurement period in 1900. However, this would not explain the lack of correlation either.

Triggers of landslides are way more complex than using just precipitation sums. Malik et al. (2016) found 1-2-year lags between high rainfall and the event recorded by tree growth, suggesting a link between long-term groundwater storage and delayed reactivation of landslides. Fantucci & Sorriso-Valvo (1999) emphasized the complexity of the rainfall-landslide relationship, as only a small fraction of extreme rainfall events triggered slope movements detectable in tree rings. In their study in southern Italy, seismic activity showed a stronger link to mass movements than meteorological factors. However, this is not transferable to a study in Switzerland due to the low seismic activity. The geological conditions can influence the rainfall-landslide relationship. Shallow rather than deep-seated movements respond more strongly to short-term intense rainfall (Fantucci, 1999; Malik & Wistuba, 2012). The landslide in the study site, which is expected to be shallow, does not show such strong responses. Given the shallow root system of spruce, stronger growth responses to short-term rainfall would have been expected for a shallow landslide, yet no such relationship could be observed. Overall, while precipitation is a necessary precondition for triggering slope movements, no direct correlation with the detected events could be observed on the slope. This highlights the complexity of the landslide system and the need to include additional hydrological or geomorphological indicators in future analyses.

6.5. Influence of drainage interventions

The installation of drainage channels starting in 1990 was certainly an efficient but costly measure, which has continued to prove effective. The channels drain surface water away from the slope into the streams, carrying larger amounts of water into the Raminbach stream in the valley. It appears that the channels were occasionally maintained, as their functioning certainly diminishes over time due to material deposits and blockages in the water channels, as described by Jones et al. (2023). Their functioning was reflected in the statistically significant decrease in geomorphic activity after 1990. The negative effect size using Cliff's delta indicates that event rates were generally but not strongly lower after 1990. The test results suggest a reduction in slope activity after the implementation of drainage measures, although other influencing factors cannot be excluded. Among these, precipitation remains a primary driver of slope instability. How variations in rainfall patterns interact with drainage channels and how drainage channels influence the frequency or magnitude of landslide activity is still insufficiently understood. This represents a key knowledge gap that would need deeper investigation. Nevertheless, the results show that since the installation of drainage channels, the event rate has decreased, even though heavy rainfall events have become more frequent and intense due to climate change. This indicates that the drainage system has effectively mitigated slope activity and suggests that, under stable climatic conditions, its impact might have been even more pronounced.

The area where most channels were dug is located about 250m higher up the slope compared to the central study area. Their installation mainly served to drain the slope for the immediate surroundings in order to build a road that continues further up the slope. Therefore, the effect of these channels is expected to be even stronger in areas further up the mountain. This assumption would imply that trees located higher up in the study area might show fewer growth responses compared to those further downslope. However, this pattern could not be observed, probably due to the great diversity of processes and movement mechanisms causing the different tree responses. Still, the dendrogeomorphic evidence indicates that the installation of drainage channels decreased the frequency of landslides on the slope to some extent, which addresses the second research question.

6.6. Methodological considerations and limitations

The applied methods were based on leading work, such as that of Gärtner et al. (2004), Wistuba et al. (2013), Malik et al. (2016), or Esper & Gärtner (2001). These methods helped to sample and evaluate the spruce trees on the slope in Elm, take the geomorphology of the slope into account, date the disturbance signals, and perform a comprehensive dendrogeomorphological analysis, including precipitation as a potential trigger and drainage channels as potential mitigation factors for landslide activity. Totally, the chosen methods proved to be very suitable for the study site, its conditions, and the purpose of the study.

6.6.1. Uncertainties in field work and sample processing

Despite broad support, some uncertainties remain in the methodological approach. Mapping geomorphic features proved to be very challenging, as it was difficult to identify and interpret the geomorphic influences in the visible patterns in the terrain and to classify them in the overall context of geomorphic activity. In particular, the slope activity was difficult to assess, as no clear signs of rapid slope movement were detected within the study area, but only in the surroundings. Additionally, it was difficult to relate the weak signs of landslides that were found to the geological processes described by Grämiger (2024) and to the results of other studies that conducted geomorphologic mapping. Furthermore, the morphology of the trees did not reveal any trends in relation to the slope's morphology. With the current, deeper understanding of slope processes and tree growth responses, a renewed investigation of the study area would be highly valuable. The patterns of slope movement could be classified more precisely, additional indicators of specific landslide types may be identified, and previously unrecognized correlations between tree morphology and slope morphology could be revealed.

The sampling and sample preparation process caused few difficulties and enabled the subsequent ring-width analysis. The cross-dating process proved particularly challenging and time-consuming due to missing or incorrect annual rings, incomplete cores, and the difficulty of aligning parallel (*gleichläufig*) or opposing (*gegenläufig*) trends of growth curves with the average reference curve. It was very helpful to exclude reference trees with weak or inconsistent correlations within the reference chronology, as well as research trees with weak correlations with the mean reference curve. These procedures were also used by Šilhán (2021) and helped to verify the consistency of cross-dating and to identify potential errors. The decision not to apply standardization to remove age trends was intentional. Instead, the first 20 years of juvenile growth containing growth reactions were excluded or treated with caution. Combined with the use of the eccentricity index and its year-to-year variation, reliable detection of disturbance events in both juvenile and adult increments was possible. This approach therefore provided a solid methodological foundation for the accurate detection and interpretation of geomorphic disturbance events.

6.6.2. Choice of tree species

According to many researchers, sampling of different tree species would be recommended. An adequate mixture of species and age classes would allow the reconstruction of well-balanced and minimally biased chronologies of past geomorphic activity (Stoffel et al., 2013; Stoffel & Corona, 2014; Trappmann et al., 2013). Besides, sampling multiple tree species also benefits the accuracy of landslide event records (Šilhán, 2019). Despite knowing these advantages, it was nevertheless decided to sample only spruce trees. The reasons for this decision were already explained in Chapter 2.6. *Vegetation and sampling species selection*. The main reasons were the availability, the ease of sampling and evaluation, and time savings. In retrospect, it would have been very interesting to study different tree species, as similarities and differences between them could have revealed certain patterns, deviations, and dependencies more clearly.

6.6.3. Limitations regarding the reference

Reference sites must be located as close as possible to the study area in order to ensure comparable conditions, while at the same time showing as few signs as possible of past or present mass movements (Tumajer & Treml, 2013). However, a major limitation in choosing reference sites is that reference trees are often situated in the same geological situation in the vicinity of the landslide, thereby partly affected by geomorphic activity, which reduces the suitability of the plot to act as a true reference (Gussenstätter & Bräuning, 2003). The reference slope in Elm appears very stable without any sign of slope movement. It can be argued that the research site does not show clear landslide signs as well. However, the site conditions (steepness, trees' inclination) as well as features such as embankments, material deposits, and bulges clearly speak for slope activity. The reference samples are also largely neutralized by disturbances caused by geomorphic events through sampling from the sides A and B. Therefore, this limitation has been overcome.

Another frequently mentioned limitation of reference samples is cores that exhibit systematic differences between two opposite cores, even though reference samples are taken in a way to receive as little eccentricity as possible. However, this remaining variation is precisely why the threshold values are derived statistically across multiple reference trees. By aggregating the distributions of positive and negative eccentricity variation values of reference samples, thresholds can be defined that represent the normal background noise of eccentricity. Disturbance years in research trees are only identified when their variation values exceed these thresholds. In the study by Wistuba et al. (2013), greater eccentricities arose in the reference samples because the samples were taken upslope (side C) and downslope (side D). However, this could be minimized in the present study by taking samples A and B instead of C and D, letting eccentricity reflect variation of local conditions rather than a systematic response to slope instability. Therefore, the reference samples were very suitable as a balancing chronology, which served as a solid basis for the eccentricity detection. The reference naturally represents a very consistent chronology with little variation, compared to which the research samples quickly appear eccentric. Nevertheless, it is argued that the reference is well chosen to filter out the natural variations in the tree rings. Further filtering steps then refine this analysis, as the next chapters show.

6.6.4. Uncertainties using eccentricity index

Applying the eccentricity index was not a straightforward process, as no single index is perfect and each involves uncertainties that must be carefully addressed. A complete microscopic analysis of increment cores to identify reaction wood would provide highly accurate results, but is far too time-consuming. Therefore, the eccentricity index was applied first, followed by a visual reaction wood analysis to refine and improve event detection.

An examination of different indices shows that authors often apply the methods most familiar to them, though these are not always easily transferable between sites. The eccentricity index proposed by Wistuba et al. (2013) proved particularly useful because reference samples can be used to establish thresholds that help separate true landslide signals from ordinary growth disturbances. Although Šilhán (2019) criticized the reliance on reference chronologies because tree eccentricity can vary individually, and reference trees may produce misleading signals, the literature also highlights their value in capturing the background noise of eccentric growth (e.g., Gärtner et al., 2004; Šilhán, 2019; Wistuba et al., 2013). This advantage was therefore prioritized in this study.

Further advantages of the eccentricity index by Wistuba et al. (2013) include a clear statistical framework for detecting abrupt eccentricity changes and the consideration of tilting direction. The limitation that the index does not account for delayed growth responses was mitigated by introducing additional filtering steps (as discussed in Chapter 6.3. *Tree-ring signals and their interpretation*) to exclude sequences of consecutive event years. As discussed in Chapter 3.5.1. *Eccentricity index*: each index has specific weaknesses, and the choice of method should match the sampling strategy. Overall, the eccentricity index of Wistuba et al. (2013) proved highly suitable for the aims and conditions of this study, but only when expanded to include additional tree growth responses to disturbances.

6.6.5. Challenges in reaction wood detection and dating accuracy

During the evaluation, several challenges arose in connection with reaction wood. One major limitation not fully addressed in this study was that reaction wood often forms only in a localized sector on the compressed side of the tree, rather than across the entire half-increment. If this specific sector containing reaction wood was narrowly missed during sampling, it may have affected the identification and interpretation of disturbance events. Complete stem discs could not be extracted, as this would not have been justifiable and feasible for spruce trees without specialized equipment, experience, and permission. This limitation was mitigated as far as possible by sampling cores in the direction of inclination and at the point of maximum stem tilt, thereby increasing the likelihood of intersecting reaction wood.

A further source of uncertainty arose from rings classified as eccentric by the eccentricity calculation but exhibiting only slightly darker wood. Distinguishing between compression wood and normal latewood was not always easy, and the samples often had to be re-examined under the microscope, sometimes after additional fine cutting. Useful indicators included darkened zones appearing already in the earlywood, which could then be identified as compression wood. Less frequently, compression wood cells could be recognized under the microscope by their rounder shape compared to the more angular latewood cells. Another difficulty concerned the precise dating of eccentricity and reaction wood formation. If a landslide event occurred in autumn, the tree's reaction might only become visible in the earlywood of the following year. Conversely, eccentric growth could already appear in the year prior to visible compression wood formation. These possibilities were carefully considered for each case before a disturbance event was recorded. These difficulties were minimized as far as possible, but certain uncertainties remained in the evaluation using reaction wood.

6.7. Implications and outlook

6.7.1. Implications for research and methodology

Dendrogeomorphic studies offer a cost-effective and efficient means of reconstructing slope processes and understanding landslide dynamics. This thesis has shown that, when carefully designed and applied, dendrogeomorphic methods provide highly informative results that hold significant relevance for natural hazard research. As Gärtner et al. (2004) concluded, combining detailed field assessment and process identification with subsequent tree sampling and tree-ring analysis enables a precise, year-by-year reconstruction of the spatial and temporal dynamics of geomorphologic processes. Tree-ring-based data can provide insights into a wide range of landslide aspects, although many open questions and challenges remain (Šilhán, 2020). Among these challenges are the definition of the optimal age structure of sampled trees, the filtering of tree-ring signals produced by different types of landslides, and the determination of the general sensitivity of trees to slope movements, all of which should be addressed in future research (Šilhán, 2021).

Some of these challenges were less critical in this study. The age structure was well-balanced through the inclusion of a wide range of tree ages, eccentricity index calculation further standardized the samples, and potential inaccuracies caused by juvenile growth were minimized by excluding the earliest rings. Likewise, filtering signals by landslide type was not necessary, as the processes at the Elm site, as in many landslide areas, did not have a uniform effect on tree growth. However, no general sensitivity of trees to landslide movement could be determined, primarily due to insufficient information about the underlying slope dynamics. Accurate knowledge of a past landslide system and its development is essential, especially for modeling future processes and conducting risk assessments, as it allows for more reliable predictions of its future behavior (Gärtner et al., 2004). This lack of detailed knowledge represents one of the main limitations of this work, as field observations and available data did not allow a comprehensive reconstruction of specific geomorphic processes.

The precipitation analysis also revealed limitations. The influence of rainfall on slope activity in the study area could not be statistically demonstrated. A fundamental limitation of tree-ring-based dating, highlighted by this part of the analysis, is its seasonal precision: while it enables the reconstruction of event frequency, it is insufficient for identifying short-term triggers such as individual rainfall events. The search for such triggers remains a knowledge gap that future studies should address, ideally by combining dendrogeomorphic approaches with complementary monitoring methods.

The drainage channels, on the other hand, showed measurable effects, as indicated by a decrease in event frequency after their installation. However, the magnitude of this effect remains uncertain, and it is still unclear how variations in rainfall patterns interact with the drainage infrastructure and how such measures influence the frequency or magnitude of landslide activity. This remains a crucial knowledge gap for future research and for improving landslide hazard mitigation strategies.

6.7.2. Outlook and future research

Future research should include a more detailed geomorphological process analysis within the research area and a deeper investigation of the underlying slope dynamics. Through more in-depth fieldwork and, ideally, the use of additional tools such as soil profile analyses or monitoring systems, a more comprehensive understanding of the disturbance processes that trigger tree growth responses could be gained. Even in the absence of an extensive research budget, further field inspections guided by the insights gained in this study could yield valuable results. However, due to the slow-moving nature of the slope, accurately identifying and classifying the triggers, types, and mechanisms of movement remains challenging. Furthermore, closing the critical knowledge gap regarding the identification of the key triggers for increased landslide activity will be an important part of future landslide analyses at such unexplored sites.

If financially and logistically feasible, instrumental landslide monitoring would be an especially useful complement, as it would allow for direct comparison with dendrogeomorphic reconstructions and help assess their accuracy and reliability (Šilhán, 2021). At the Elm site, however, where no significant acceleration of slope activity has been observed in recent decades, such measures may be disproportionate. Another interesting approach would be to include diverse tree species in the research, for example, one deciduous and one coniferous tree species, showing different patterns of growth reaction. These tree species may produce different event years, which would be interesting for recording slope dynamics. However, this would probably not result in a significant difference in the slope under investigation: The slope likely continues to move slowly, and the findings indicate no imminent activation of abrupt failure.

Large, rapid landslides triggered by climate change-induced extreme rainfall events or other found triggers cannot be completely ruled out. Such events could have severe consequences. In the worst case, there would be large-scale deposition in the valley, blockage of the Raminbach stream, and subsequent debris flow eruption posing a hazard to the nearby village of Elm. However, no evidence of large-scale or rapid landsliding was found within the study area. This allows, to a limited extent, the conclusion that future intensification of slope movement is unlikely, at least as long as the drainage channels remain functional.

Since no increase in event frequency was observed despite changing precipitation and climate patterns, a further rise in extreme weather events will not necessarily lead to an immediate increase in slope activity in this area. In this respect, the third research question can also be addressed: These findings allow for a cautious outlook on future slope movements, suggesting that under current conditions, a significant intensification of landslide activity is unlikely. However, predictions of future slope behavior based on past landslide activity cannot be made.

7. Conclusion

This study investigated slope dynamics and tree growth responses on a slow-moving landslide near Elm, using dendrogeomorphic methods in combination with geomorphic field observations and precipitation data. The thesis aimed to reconstruct the landslide activity by using tree growth responses such as eccentric growth, reaction wood, and growth changes, and date their appearance in tree increment cores from a hundred Norway spruce trees (*Picea abies* (L.) Karst). Although explicit forms of high landslide activity in the research area were rare, the slope morphology showed many signs of slope movement, such as material erosion, deposits, mounds, tilted or bent trees, as well as additional signs in the surroundings. The observed forms of geomorphic activity suggest that the slope is slowly moving and probably corresponds to a slow-moving landslide with both rotational and translational components.

These findings are in line with observed tree growth characteristics. Trees are frequently tilted, however, not in a uniform direction. In the tree's increments, clear growth reactions to geomorphic disturbances could be dated, mostly as eccentric growth and reaction wood. These dated event years were counted and normalized, resulting in higher event rates in subsequent years: 1913-1916, 1927-1929, 1935-1938, 1947-1952, 1963-1964, 1974-1977, 1979-1983, 1987-1988, 1995-2001, 2003-2005, 2011-2015, and 2017-2022. However, these phases of increased activity represented only two to three events per year, and the affected trees are spatially scattered without any recognizable pattern. Moreover, the absence of an independent event chronology prevents any direct comparison or validation of these reconstructed events. Nevertheless, the signals identified indicate sustained, slow, and small-scale slope activity over more than a century. These findings directly address the first research question [1]: *To what extent does landslide activity cause growth disturbances in Norway spruce compared to a stable reference site?* They demonstrate that landslide activity in Elm causes clearly detectable growth disturbances in Norway spruce and support the hypothesis that such disturbances are most clearly expressed through reaction wood formation and eccentric growth. However, it became evident that eccentricity alone is not always sufficient for reliable event detection. On one hand, the index tends to overestimate the number of events, while on the other, some events remain undetected when the coring direction was not optimal. This underlines the importance of visual analysis of reaction wood and demonstrates that combining multiple growth indicators offers a significant advantage for achieving accurate event dating.

In literature, precipitation is often identified as the decisive trigger of landslides. However, the analysis of different precipitation patterns and totals in this study revealed clear limitations, as no significant statistical relationship with the reconstructed event rates could be established. Therefore, it remains unclear which specific triggers had a decisive influence on slope activity. In contrast, the drainage channels, which were constructed beginning in 1990, showed a clear reducing effect on the event rate. This directly addresses research question [2]: *To what extent did the installation of drainage channels in the 1990s influence the frequency of landslides on the slope?* The results indicate that the installation of drainage channels contributed to a measurable decline in landslide frequency on the slope, thereby supporting the hypothesis.

Research question [3] asked: *To what extent can reconstructed past landslide activity be used for predictions of future slope activities?* This question was difficult to answer, as slope movement did not correlate with precipitation metrics, which could otherwise have served as a predictor of future slope dynamics. Within the study area, no evidence of large-scale or rapid landsliding was found. Despite changing climatic conditions, no rise in event frequency was observed. Since the installation of the drainage channels in 1990, a decrease in event frequency has been recorded.

This implies that future extreme weather events will not necessarily lead to an immediate rise in slope activity. The weak signs of slope movement, together with the spatially limited growth responses of trees, additionally suggest that an imminent activation of abrupt slope failure and future intensification of slope movement is unlikely. The slope is expected to continue moving slowly if the drainage channels remain functional. Nevertheless, large and rapid landslides triggered by climate change-induced extreme rainfall events cannot be entirely ruled out. Predictions of future slope behavior based on past landslide activity cannot be made. Therefore, these results do not support the hypothesis that past landslide activity reconstructed from tree-ring analyses contributes to predicting future slope activity.

Overall, this thesis effectively addressed the overarching research question: *To what extent do landslides affect the tree growth of Norway spruce, and which factors influence landslide dynamics on a slope near Elm, Switzerland?* Some uncertainties and limitations remain regarding the applied methods. In particular, a more detailed geomorphologic site characterization and process analysis would be highly valuable, as the field observations alone were insufficient to draw definitive conclusions about the slope dynamics. Long-term monitoring or independent event chronologies would provide valuable support for future studies as reference data. Including additional tree species could further broaden the scope of insights. Despite existing uncertainties, many methodological limitations were successfully mitigated. Overall, the applied approach proved suitable, and this thesis contributes to improving the understanding and detection of slow-moving slope processes in remote areas using dendrogeomorphic methods. In particular, the combined use of several different tree growth reaction signals, such as reaction wood and eccentricity, is recommended, as this allows for cross-verification and increases the precision in identifying disturbance events compared to relying on a single indicator. At the same time, further research in Elm or similar areas is needed to deepen the understanding of the interactions between slowly sliding slopes, the trees growing on them, and the processes that influence their dynamics. Such knowledge forms the basis for predicting the future activity of slopes with greater confidence.

8. Bibliography

Alestalo, J. (1971). Dendrochronological interpretation of geomorphic processes. *Fennia - International Journal of Geography*, *105*(1). https://fennia.journal.fi/article/view/40757

Astrade, L., Bravard, J. P., & Landon, N. (1998). Mouvements de masse et dynamique d'un géosystème alpestre : étude dendrogéomorphologique de deux sites de la vallée de Boulc (Diois, France). *Géographie Physique et Quaternaire*, *52*(2), 153–166. https://doi.org/10.7202/004765AR

Beniston, M. (2006). Mountain weather and climate: A general overview and a focus on climatic change in the Alps. *Hydrobiologia*, *562*, 3–16. https://doi.org/10.1007/s10750-005-1802-0

Bovi, R. C., Chartier, M. P., Roig, F. A., Filho, M. T., Castillo, V. D., & Cooper, M. (2019). Dynamics of erosion processes in the tropics: a dendrogeomorphological approach in an Ultisol of southeastern Brazil. *Plant and Soil*, *443*(1–2), 369–386. https://doi.org/10.1007/S11104-019-04227-2/FIGURES/9

Braam, R. R., Weiss, E. E. J., & Burrough, P. A. (1987). Spatial and temporal analysis of mass movement using dendrochronology. *CATENA*, *14*(6), 573–584. https://doi.org/10.1016/0341-8162(87)90007-5

Burkhalter, P., Egli, M., & Gärtner, H. (2019). Reconstruction and actual trends of landslide activities in Bruust-Haltiwald, Horw, canton of Lucerne, Switzerland. *Geographica Helvetica*, *74*(1), 93–103. https://doi.org/10.5194/GH-74-93-2019

Casteller, A., Christen, M., Villalba, R., Martínez, H., Stöckli, V., Leiva, J. C., & Bartelt, P. (2008). Validating numerical simulations of snow avalanches using dendrochronology: The Cerro Ventana event in Northern Patagonia, Argentina. *Natural Hazards and Earth System Science*, *8*(3), 433–443. https://doi.org/10.5194/NHESS-8-433-2008,

Curioni, S., Gattinoni, P., & Leonelli, G. (2024). Integrating Dendrogeomorphology into Stress–Strain Numerical Models: An Opportunity to Monitor Slope Dynamic. *Geosciences (Switzerland)*, *14*(5). https://doi.org/10.3390/geosciences14050129

Esper, J., & Gärtner, H. (2001). Interpretation of Tree-Ring Chronologies (Interpretation von Jahrringchronologien). *Erdkunde*, *55*(3), 277–288. http://www.jstor.org/stable/25647395

Fabiánová, A., Chalupa, V., & Šilhán, K. (2021). Dendrogeomorphic dating vs. low-magnitude landsliding. *Quaternary Geochronology*, *62*, 1–12. https://doi.org/10.1016/J.QUAGEO.2021.101150

Fantucci, R. (1999). Dendrogeomorphology in Landslide Analysis. In C. Riccardo & C. Margottini (Eds.), *Floods and Landslides: Integrated Risk Assessment* (pp. 69–81). Springer, Berlin, Heidelberg. https://doi.org/10.1007/978-3-642-58609-5_5

Fantucci, R., & Sorriso-Valvo, M. (1999). Dendrogeomorphological analysis of a slope near Lago, Calabria (Italy). *Geomorphology*, *30*, 165–174. https://doi.org/10.1016/S0169-555X(99)00052-5

Gärtner, H., Esper, J., & Treydte, K. (2004). Geomorphologie und Jahrringe – Feldmethoden in der Dendrogeomorphologie. *Schweizerische Zeitschrift Fur Forstwesen*, *155*(6), 198–207. https://doi.org/10.3188/SZF.2004.0198

Gärtner, H., & Nievergelt, D. (2010). The core-microtome: A new tool for surface preparation on cores and time series analysis of varying cell parameters. *Dendrochronologia*, *28*(2), 85–92. https://doi.org/10.1016/J.DENDRO.2009.09.002

Germain, D., Dagenais-Du-Fort, É., Lajeunesse, P., & Simard, M. (2018). Dendrogeomorphic reconstruction of the seasonal timing and rainfall threshold for debris slide occurrence in eastern Canada. *Dendrochronologia*, *52*, 57–66. https://doi.org/10.1016/J.DENDRO.2018.09.007

Gers, E., Florin, N., Gärtner, H., Glade, T., Dikau, R., & Schweingruber, F. H. (2001). Application of shrubs for dendrogeomorphological analysis to reconstruct spatial and temporal landslide movement patterns - A preliminary study. *Zeitschrift Fur Geomorphologie Supplementband*, *125*, 163–175. https://www.researchgate.net/profile/Holger-Gaertner-2/publication/283874899_Application_of_shrubs_for_dendrogeomorphological_analysis_to_reconstruct_spatial_and_temporal_landslide_movement_patterns_A_preliminary_study/links/564df61708ae1ef9296bdc76/Appli

Grämiger, L. (2024). *Geologische Untersuchung - Rutschung Raminer Stäfeli, 8767 Elm* (Issue 15063).

Guibal, F., & Guiot, J. (2021). Dendrochronology. In A. Ramstein, G., Landais, A., Bouttes, N., Sepulchre, P., Govin (Ed.), *Paleoclimatology. Frontiers in Earth Sciences* (pp. 117–122). Springer Science and Business Media Deutschland GmbH. https://doi.org/10.1007/978-3-030-24982-3_8/FIGURES/5

Gussenstätter, F., & Bräuning, A. (2003). Changes in growth rates and wood anatomy of broad-leaved and coniferous tree species after a landslide event in the Remstal Valley (southern Germany). In E. Jansma, A. Bräuning, H. Gärtner, & G. Schleser (Eds.), *TRACE Tree Rings in Archaeology, Climatology and Ecology - Proceedings of the DENDROSYMPOSIUM 2003* (44th ed., pp. 31–35). Forschungszentrum Jülich GmbH. https://edepot.wur.nl/578452#page=36

Handwerger, A. L., Roering, J. J., & Schmidt, D. A. (2013). Controls on the seasonal deformation of slow-moving landslides. *Earth and Planetary Science Letters*, *377–378*, 239–247. https://doi.org/10.1016/J.EPSL.2013.06.047

Heinrich, I., Gärtner, H., & Monbaron, M. (2006). Wood anatomy and Dendrogeomorphology-Reaction wood varieties caused by different experimental treatments. In *TRACE – Tree Rings in Archaeology, Climatology and Ecology* (pp. 224–232). https://www.dora.lib4ri.ch/wsl/islandora/object/wsl%3A12351/datastream/PDF/Heinrich-2007-Wood_anatomy_and_dendrogeomorphology_--%28published_version%29.pdf

Hock, R., Rasul, G., Adler, C., Cáceres, B., Gruber, S., Hirabayashi, Y., Jackson, M., Kääb, A., Kang, S., Kutuzov, S., Milner, A., Molau, U., Morin, S., Orlove, B., & Steltzer, H. (2019). SM2.1 Details of High-Mountain Regional Glacier and Permafrost Areas. In *IPCC Special Report on the Ocean and Cryosphere in a Changing Climate [H.-O. Pörtner, D.C. Roberts, V. Masson-Delmotte, P. Zhai, M. Tignor, E. Poloczanska, K. Mintenbeck, A. Alegría, M. Nicolai, A. Okem, J. Petzold, B. Rama, N.M. Weyer (eds.)]*. https://iris.unito.it/bitstream/2318/1803038/1/06_SROCC_Ch02_FINAL.pdf

IPCC. (2021). *Climate Change 2021 The Physical Science Basis Working Group I Contribution to the Sixth Assessment Report of the Intergovernmental Panel on Climate Change [Masson-Delmotte, V., P. Zhai, A. Pirani, S.L. Connors, C. Péan, S. Berger, N. Caud, Y. Chen, L. Go*. https://doi.org/10.1017/9781009157896.

IPCC. (2022). *Climate Change 2022: Impacts, Adaptation and Vulnerability | Climate Change 2022: Impacts, Adaptation and Vulnerability - y. Contribution of Working Group II to the Sixth Assessment Report of the Intergovernmental Panel on Climate Change [H.-O. Pörtner, D*. https://doi.org/10.1017/9781009325844.

Jones, T., Cartwright, T., Abed, M., Tardif, M., Robinson, L., Wurst, P., Mohney, C., Glover-Cutter, K., & Leshchinsky, B. (2023). Developing Systems-Level Criteria for Evaluating Performance of Horizontal Drains toward Landslide Mitigation: Case Study of the US20 Pioneer Mountain-Eddyville Realignment Project. *Journal of Geotechnical and Geoenvironmental Engineering*, *149*(5), 1–17. https://doi.org/10.1061/JGGEFK.GTENG-11164

Leonelli, G., Chelli, A., Consonni, M., Lorenzo, C., & Gattinoni, P. (2021). Multi-decadal dating of surface slope movements in forested DSGSD areas of the European Alps: detecting precipitation triggering factors. *Geografiska Annaler: Series A, Physical Geography*, *103*(1), 8–32. https://doi.org/10.1080/04353676.2020.1813983

Lopez Saez, J., Corona, C., Stoffel, M., Astrade, L., Berger, F., & Malet, J. P. (2012). Dendrogeomorphic reconstruction of past landslide reactivation with seasonal precision: The Bois Noir landslide, southeast French Alps. *Landslides*, *9*(2), 189–203. https://doi.org/10.1007/S10346-011-0284-6/FIGURES/10

Lundström, T., Heiz, U., Stoffel, M., & Stöckli, V. (2007). Fresh-wood bending: linking the mechanical and growth properties of a Norway spruce stem. *Tree Physiology*, *27*(9), 1229–1241. https://doi.org/10.1093/TREEPHYS/27.9.1229

Macfarlane, D. F. (2009). Observations and predictions of the behaviour of large, slow-moving landslides in schist, Clyde Dam reservoir, New Zealand. *Engineering Geology*, *109*(1–2), 5–15. https://doi.org/10.1016/J.ENGGEO.2009.02.005

Malik, I., & Wistuba, M. (2012). Dendrochronological methods for reconstructing mass movements -an example of landslide activity analysis using tree-ring eccentricity. *Geochronometria*, *39*(3), 180–196. https://doi.org/10.2478/S13386-012-0005-5/METRICS

Malik, I., Wistuba, M., Migoń, P., & Fajer, M. (2016). Activity of slow-moving Landslides recorded in eccentric tree rings of norway spruce trees (Picea Abies Karst.) - An example fromtfhe Kamienne Mts. (Sudetes Mts., Central Europe). *Geochronometria*, *43*, 24–37. https://doi.org/10.1515/geochr-2015-0028

Massey, C. I., Petley, D. N., & McSaveney, M. J. (2013). Patterns of movement in reactivated landslides. *Engineering Geology*, *159*, 1–19. https://doi.org/10.1016/J.ENGGEO.2013.03.011

MeteoSchweiz. (2024a). *Klimanormwerte Elm Normperiode 1961−1990*. https://www.meteoswiss.admin.ch/

MeteoSchweiz. (2024b). *Klimanormwerte Elm Normperiode 1991−2020*. https://www.meteoswiss.admin.ch/

NCCS. (2018). CH2018 - Climate Scenarios for Switzerland. In CH2018 (Ed.), *CH2018 – Climate Scenarios for Switzerland*. National Centre for Climate Services. www.bundespublikationen.admin.ch

Oven, D., Levanič, T., Jež, J., & Kobal, M. (2019). Reconstruction of Landslide Activity Using Dendrogeomorphological Analysis in the Karavanke Mountains in NW Slovenia. *Forests 2019, Vol. 10, Page 1009*, *10*(11), 1009. https://doi.org/10.3390/F10111009

Papciak, T., Malik, I., Krzemień, K., Wistuba, M., Gorczyca, E., Wrońska-Wałach, D., & Sobucki, M. (2015). Precipitation as a factor triggering landslide activity in the Kamień massif (Beskid Niski Mts, Western Carpathians). *Bulletin of Geography. Physical Geography Series*, *8*, 5–17. http://dx.doi.org/10.1515/bgeo-2015-0001

Razak, K. A., Straatsma, M. W., van Westen, C. J., Malet, J. P., & de Jong, S. M. (2011). Airborne laser scanning of forested landslides characterization: Terrain model quality and visualization. *Geomorphology*, *126*(1–2), 186–200. https://doi.org/10.1016/J.GEOMORPH.2010.11.003

Schmid, D., & Schweingruber, F. H. (1995). Datierung und Nachweis von Rutschungen mit Hilfe von Jahrringen. *Swiss Foresty Journal*, *146*(8), 641–659. https://doi.org/https://doi.org/10.5169/seals-766988

Schweingruber, F. H. (1996). *Tree Rings and Environment Dendroecology*. Haupt, Bern.

Shroder, J. F. (1978). Dendrogeomorphological analysis of mass movement on Table Cliffs Plateau, Utah. *Quaternary Research*, *9*(2), 168–185. https://doi.org/10.1016/0033-5894(78)90065-0

Šilhán, K. (2017). Evaluation of growth disturbances of Picea abies (L.) Karst. to disturbances caused by landslide movements. *Geomorphology*, *276*, 51–58. https://doi.org/10.1016/J.GEOMORPH.2016.10.005

Šilhán, K. (2019). Tree-ring eccentricity in the dendrogeomorphic analysis of landslides – A comparative study. *CATENA*, *174*, 1–10. https://doi.org/10.1016/J.CATENA.2018.11.002

Šilhán, K. (2020). Dendrogeomorphology of landslides: principles, results and perspectives. *Landslides*, *17*(10), 2421–2441. https://doi.org/10.1007/S10346-020-01397-4/METRICS

Šilhán, K. (2021). Dendrogeomorphology of Different Landslide Types: A Review. *Forests*, *12*(3), 1–19. https://doi.org/10.3390/F12030261

Šilhán, K., & Stoffel, M. (2015). Impacts of age-dependent tree sensitivity and dating approaches on dendrogeomorphic time series of landslides. *Geomorphology*, *236*, 34–43. https://doi.org/10.1016/J.GEOMORPH.2015.02.003

Sitko, K., Wistuba, M., Malik, I., Krąpiec, M., Yu, R., & Zhang, H. (2022). Dendrochronological record of soil creep and landslide activity – the comparison of tree-ring eccentricity and compression wood (examples from the Kamienne Mts., Poland). *Geology, Geophysics and Environment*, *Vol. 48*(2), 133–146. https://doi.org/10.7494/GEOL.2022.48.2.133

Słowik-Opoka, E. (2020). Eccentricity of current annual increments in the trunks of spruce (Picea Abies (L.) H. Karst) growing along the stream channel in a small mountainous catchment. *Acta Silvestria*, *56*, 77–89. https://doi.org/10.15576/ActaSilvestria/2019.LVI.77

Stoffel, M., & Bollschweiler, M. (2008). Tree-ring analysis in natural hazards research - An overview. *Natural Hazards and Earth System Science*, *8*(2), 187–202. https://doi.org/10.5194/NHESS-8-187-2008,

Stoffel, M., Butler, D. R., & Corona, C. (2013). Mass movements and tree rings: A guide to dendrogeomorphic field sampling and dating. *Geomorphology*, *200*, 106–120. https://doi.org/10.1016/J.GEOMORPH.2012.12.017

Stoffel, M., & Corona, C. (2014). Dendroecological dating of geomorphic disturbance in trees. *Tree-Ring Research*, *70*(1), 3–20. https://doi.org/10.3959/1536-1098-70.1.3

Stoffel, M., & Huggel, C. (2012). Effects of climate change on mass movements in mountain environments. *Progress in Physical Geography*, *36*(3), 421–439. https://doi.org/10.1177/0309133312441010

Strunk, H. (1997). Dating of geomorphological processes using dendrogeomorphological methods. *CATENA*, *31*(1–2), 137–151. https://doi.org/10.1016/S0341-8162(97)00031-3

Swisstopo. (2024a). *Geologischer Atlas der Schweiz [Online map]*. Federal Office of Topography Swisstopo, Swiss Confederation. https://map.geo.admin.ch/#/map?lang=de&center=2733703.41,1198587.97&z=7.165&topic=ech&layers=ch.swisstopo.geologie-geologischer_atlas&bgLayer=ch.swisstopo.pixelkarte-farbe&featureInfo=default

Swisstopo. (2024b). *swissALTI3D multidirektionales Relief [Online map]*. Federal Office of Topography Swisstopo, Swiss Confederation. https://map.geo.admin.ch/#/map?lang=de&center=2733856.08,1198443.57&z=9.005&topic=ech&layers=ch.bfs.gebaeude_wohnungs_register,f;ch.bav.haltestellen-oev,f;ch.swisstopo.swisstlm3d-wanderwege,f;ch.astra.wanderland-sperrungen_umleitungen,f;KML%7Chttps://publ

Swisstopo. (2025a). *Grundlagenkarte der Schweiz [Online map]*. Federal Office of Topography Swisstopo, Swiss Confederation. https://map.geo.admin.ch/#/map?lang=de&center=2733061.74,1198352.13&z=7.013&topic=ech&layers=ch.bfs.gebaeude_wohnungs_register,f;ch.bav.haltestellen-oev,f;ch.swisstopo.swisstlm3d-wanderwege,f;ch.astra.wanderland-sperrungen_umleitungen,f;ch.swisstopo.swiss

Swisstopo. (2025b). *SWISSIMAGE und Zeitreise - Luftbilder [Online map]*. Federal Office of Topography Swisstopo, Swiss Confederation. https://map.geo.admin.ch/mobile.html#/map?lang=de&center=2733424.26,1199018.07&z=7.091&topic=ech&layers=ch.bfs.gebaeude_wohnungs_register,f;ch.bav.haltestellen-oev,f;ch.swisstopo.swisstlm3d-wanderwege,f;ch.astra.wanderland-sperrungen_umleitungen,f;ch.swis

Swisstopo. (2025c). *swissTLM (farbig) [Online map]*. Federal Office of Topography Swisstopo, Swiss Confederation. https://map.geo.admin.ch/mobile.html#/map?lang=de&center=2734400.67,1198483.23&z=10.077&topic=ech&layers=ch.bfs.gebaeude_wohnungs_register,f;ch.bav.haltestellen-oev,f;ch.swisstopo.swisstlm3d-wanderwege,f;ch.astra.wanderland-sperrungen_umleitungen,f;ch.baf

Tichavský, R., Kluzová, O., & Šilhán, K. (2019). Differences between the responses of European larch (Larix decidua Mill.) and Norway spruce (Picea abies (L.) Karst) to landslide activity based on dendrogeomorphic and dendrometric data. *Geomorphology*, *330*, 57–68. https://doi.org/10.1016/J.GEOMORPH.2019.01.013

Timell, T. E. (1986). Compression Wood in Gymnosperms. In *Springer Berlin, Heidelberg*. https://link.springer.com/book/9783540157151

Trappmann, D., Corona, C., & Stoffel, M. (2013). Rolling stones and tree rings. *Progress in Physical Geography*, *37*(5), 701–716. https://doi.org/10.1177/0309133313506451

Tumajer, J., & Treml, V. (2013). Meta-analysis of dendrochronological dating of mass movements. *Geochronometria*, *40*(1), 59–76. https://doi.org/10.2478/S13386-012-0021-5/METRICS

Van Den Eeckhaut, M., Muys, B., Van Loy, K., Poesen, J., & Beeckman, H. (2009). Evidence for repeated re-activation of old landslides under forest. *Earth Surface Processes and Landforms*, *34*(3), 352–365. https://doi.org/10.1002/ESP.1727;PAGE:STRING:ARTICLE/CHAPTER

Wistuba, M., Malik, I., Gärtner, H., Kojs, P., & Owczarek, P. (2013). Application of eccentric growth of trees as a tool for landslide analyses: The example of Picea abies Karst. in the Carpathian and Sudeten Mountains (Central Europe). *CATENA*, *111*, 41–55. https://doi.org/10.1016/J.CATENA.2013.06.027

9. Appendix

Table 4: Excerpt from the Excel table showing the recorded events after the first filtering step, in which only years with a change in the eccentricity index sign were classified as potential new events. The chronology displayed here covers only the years 2000-2024 instead of the full period starting before 1800. Rings with a value of -1 (green) represent downslope events, and rings with a value of 1 (orange) indicate upslope events. Nearly 600 events were still detected in total.

	1999	2000	2001	2002	2003	2004	2005	2006	2007	2008	2009	2010	2011	2012	2013	2014	2015	2016	2017	2018	2019	2020	2021	2022	2023	2024	Total
Elm101		0	0	0	0	0	0	0	0	0	0	0	0	0	0	0	0	0	0	0	0	0	0	0	0	0	16
Elm103		0	0	0	0	0	0	0	0	0	0	0	0	0	0	0	0	0	0	0	0	0	0	0	0	0	3
Elm105		0	-1	0	0	0	0	0	-1	0	0	0	0	0	0	0	0	0	0	-1	0	0	-1	-1	0	-1	23
Elm107		0	0	0	0	0	0	0	0	0	0	0	-1	0	0	0	0	0	0	0	0	0	0	0	0	0	3
Elm108		0	0	0	0	0	0	0	0	0	0	0	0	0	0	0	0	0	0	-1	0	1	0	0	0	0	13
Elm109		0	0	0	0	0	0	0	0	0	0	0	0	0	0	0	0	0	0	0	0	0	0	0	0	0	4
Elm110		0	0	0	0	0	-1	0	0	0	0	0	0	0	0	0	0	0	0	0	0	0	0	0	0	0	4
Elm111		0	0	0	0	0	0	0	-1	0	0	0	0	0	0	0	0	0	0	0	0	0	0	0	0	-1	14
Elm112		0	0	0	0	0	0	0	0	0	0	0	0	0	0	0	0	0	0	0	0	0	0	0	0	0	12
Elm113		0	0	0	0	0	0	0	0	0	0	0	0	0	0	0	0	0	0	0	0	0	0	0	0	0	1
Elm114		0	0	0	0	0	0	0	0	0	0	0	0	0	0	0	0	0	0	0	0	0	0	0	0	0	7
Elm115		0	0	-1	0	0	0	0	0	0	0	0	0	0	0	0	0	0	0	0	0	0	0	-1	0	0	10
Elm116		0	0	0	0	0	0	0	0	0	0	0	0	0	0	0	0	0	0	0	0	0	1	0	0	0	16
Elm118		0	0	0	0	0	0	0	0	0	1	0	0	0	0	0	0	0	0	0	0	0	0	0	0	-1	17
Elm119		0	0	0	0	1	0	0	0	1	0	1	0	0	0	0	0	0	0	0	0	0	0	0	0	0	7
Elm120		0	0	0	0	0	0	0	0	0	0	0	0	0	0	0	0	0	0	0	0	0	0	0	0	0	8
Elm123		0	0	0	0	-1	0	0	-1	-1	0	0	0	0	0	0	0	0	0	0	0	1	0	0	0	-1	23
Elm124		0	0	0	0	0	0	0	0	0	0	0	0	0	0	0	0	0	0	0	0	-1	0	0	0	-1	18
Elm127		0	0	0	0	0	0	0	0	0	0	0	0	1	0	0	0	0	0	-1	1	0	0	0	0	0	18
Elm201		-1	-1	0	0	0	-1	0	0	0	0	0	0	0	0	0	0	0	0	0	0	0	0	-1	0	0	26
Elm202		0	0	0	0	0	0	0	1	1	0	0	0	0	0	0	0	0	0	0	0	-1	0	0	0	0	17
Elm203		0	0	0	0	0	0	0	0	0	0	0	0	0	0	0	0	0	0	0	0	0	0	0	0	0	0
Elm205		0	0	0	0	0	0	0	0	0	0	0	0	0	0	0	0	0	0	0	0	-1	0	0	0	0	2
Elm207		-1	0	0	0	0	0	0	0	0	0	0	0	0	-1	0	0	0	0	-1	0	0	0	0	0	0	4
Elm210		0	0	0	0	0	0	0	0	0	0	0	0	0	0	1	0	0	0	0	0	1	0	0	0	0	13
Elm211		0	0	0	0	0	0	0	0	0	0	0	0	-1	0	0	0	0	0	0	0	0	-1	0	0	-1	11
Elm212		0	1	0	0	1	0	0	0	0	0	1	1	1	0	0	0	0	1	0	0	0	1	0	1	1	38
Elm213		-1	0	-1	0	0	0	0	0	0	0	0	0	-1	0	0	0	0	-1	0	0	-1	0	0	0	0	7
Elm214		0	0	0	0	0	1	0	0	0	0	0	0	-1	0	0	0	0	0	0	0	0	0	0	0	0	24
Elm215		0	-1	0	0	0	0	0	0	0	0	0	0	-1	0	0	0	0	0	0	0	0	0	0	0	0	20
Elm216		0	0	0	0	0	0	0	0	0	0	0	0	0	0	0	0	0	0	0	0	0	0	0	0	0	9
Elm218		0	0	0	0	0	0	0	0	0	0	0	0	0	0	0	0	0	1	0	0	0	0	0	-1	0	2
Elm219		0	0	-1	0	0	0	0	0	0	0	0	0	0	0	0	0	0	0	0	0	0	0	0	0	0	2
Elm220		0	1	0	0	0	0	0	-1	-1	0	0	0	0	0	0	-1	0	0	0	-1	0	-1	0	0	-1	9
Elm221		0	0	0	0	0	0	1	0	0	0	1	0	0	0	0	0	0	0	1	0	0	0	0	0	0	9
Elm222		0	0	0	0	0	0	-1	0	0	0	0	0	0	1	0	0	0	0	0	1	1	0	-1	0	1	6
Elm226		0	0	0	1	0	0	0	1	0	0	0	0	0	0	0	0	0	0	0	0	0	0	1	1	0	12
Elm227		0	0	0	0	0	0	0	-1	0	0	0	0	0	0	0	0	0	0	0	0	-1	0	0	0	0	28
Elm228		0	0	1	0	0	0	0	-1	0	0	0	0	0	0	0	0	0	0	0	0	0	0	1	0	0	3
Elm229		0	0	0	1	0	-1	0	0	0	0	0	0	0	0	0	0	0	0	1	0	0	0	0	0	0	4
Elm230		0	0	0	0	0	0	0	0	0	0	0	0	0	0	0	-1	0	0	0	0	0	0	-1	0	-1	16
Elm231		0	1	0	-1	0	1	0	0	0	0	0	0	0	-1	0	0	0	0	0	-1	0	0	0	0	0	6
Elm232		0	0	0	0	0	0	0	0	0	0	0	0	0	0	0	0	1	-1	0	0	1	0	1	0	0	5
Elm233		0	0	0	0	0	0	0	0	0	0	0	0	0	0	0	0	0	0	0	0	0	0	0	0	0	3
Elm234		0	0	0	0	0	0	0	0	0	0	0	0	0	0	0	0	0	0	0	0	0	0	0	0	0	3
Elm235		0	0	0	0	0	0	0	0	0	0	0	0	0	0	0	0	0	0	0	0	0	0	0	0	0	0
Elm236		0	0	0	0	0	0	0	0	0	0	0	0	0	0	0	0	0	0	0	0	0	0	0	-1	0	5
Elm237		0	0	0	1	0	0	0	0	1	1	0	1	0	1	1	0	0	1	0	0	0	0	0	0	0	12
Elm238		0	0	0	0	0	0	0	0	0	0	0	0	0	0	0	0	0	0	0	0	1	0	0	0	-1	2
Elm239		0	0	0	0	0	0	0	0	0	0	0	0	0	0	0	0	0	0	0	0	0	0	0	0	0	0
Elm240		0	0	0	0	0	0	0	0	0	0	0	0	0	0	0	0	0	0	0	0	-1	-1	0	0	-1	6
Elm241		0	0	0	0	0	0	0	0	0	0	0	0	0	0	0	0	0	0	0	0	0	0	0	0	0	2
Elm242		0	0	0	0	0	-1	0	0	0	0	0	0	0	0	1	0	0	0	0	0	0	0	0	0	0	8
Elm243		0	0	0	0	0	0	0	0	0	0	0	0	-1	0	0	0	1	0	0	0	0	0	1	0	0	7
Elm244		0	0	0	0	0	0	0	0	0	0	0	0	0	0	0	0	0	0	0	0	0	0	0	0	0	2
Elm245		0	0	0	0	0	0	0	0	0	1	0	0	0	0	1	0	0	0	-1	1	0	0	1	0	0	21
Elm246		0	0	0	0	0	0	0	0	0	0	0	0	0	0	0	1	0	0	0	0	0	0	0	0	1	4
Elm247		1	0	0	0	0	0	0	0	0	0	0	0	0	0	0	0	0	0	1	0	0	0	0	0	0	2
Elm248		0	0	0	0	0	0	0	0	0	0	0	0	0	1	0	0	0	0	1	0	0	0	0	0	0	8
Total		5	6	4	5	3	6	2	8	6	3	3	3	7	6	4	3	2	5	10	5	13	6	10	4	14	599

Table 5: Excerpt from the Excel table showing the recorded events after the final filtering step based on reaction wood and the integration of samples with increased growth but without eccentricity. The chronology displayed here covers only the years 2000-2024 instead of the full period starting before 1800. Rings with a value of -2 (green) represent events in the downslope direction, while rings with a value of 2 (orange) indicate events in the upslope direction. Abbreviations: "no" = no reaction wood; "fol" = follow-up reaction; values 1 and -1 refer to samples originally classified as eccentric but, after filtering, not considered as events. Only 164 events remained.

	1999	2000	2001	2002	2003	2004	2005	2006	2007	2008	2009	2010	2011	2012	2013	2014	2015	2016	2017	2018	2019	2020	2021	2022	2023	2024	Total
Elm101		0	0	0	0	0	0	0	0	0	0	0	0	0	0	0	0	0	0	0	0	0	0	0	0	0	4
Elm103		0	0	0	0	0	0	0	0	0	0	0	0	0	0	0	0	0	0	0	0	0	0	0	0	0	2
Elm105		0	-1	0	0	0	0	0	-1	0	0	0	0	0	0	0	0	0	0	-1	0	0	0	-2	0	-1	4
Elm107		0	0	0	0	0	0	0	0	0	0	0	fol	0	0	0	0	0	0	0	0	0	0	0	0	0	1
Elm108		0	0	0	0	0	0	0	0	no	0	0	0	0	0	0	0	0	0	no	0	no	0	0	0	0	6
Elm109		0	0	0	0	0	0	0	0	0	0	0	0	0	0	0	0	0	0	0	0	0	0	0	0	0	2
Elm110		0	0	0	0	-2	fol	0	0	0	0	0	0	0	0	0	0	0	0	0	0	0	0	0	0	0	4
Elm111		0	0	0	0	0	0	0	-1	0	0	0	0	0	0	0	0	0	0	0	0	0	0	0	0	no	3
Elm112		0	0	0	0	0	0	0	0	0	0	0	0	0	0	0	0	0	0	0	0	0	0	0	0	0	3
Elm113		0	0	no	0	0	0	0	0	0	0	0	0	no	0	0	0	0	0	0	0	0	0	0	0	0	0
Elm114		0	0	0	0	0	0	0	0	0	0	0	0	0	0	no	0	0	0	0	0	0	0	0	0	0	3
Elm115		0	0	-1	0	0	0	0	0	0	0	0	0	0	0	0	0	0	0	0	0	0	0	no	0	0	3
Elm116		2	0	0	0	no	0	0	0	0	0	0	0	0	0	0	0	0	0	0	2	0	fol	0	0	0	4
Elm118		0	0	0	0	0	0	0	0	0	1	0	0	0	0	0	0	0	0	0	0	0	0	0	0	no	5
Elm119		0	0	0	0	1	0	0	2	fol	0	fol	0	0	0	0	0	0	0	0	0	0	0	0	0	0	3
Elm120		0	0	0	0	0	0	0	0	0	0	0	0	0	0	0	0	0	0	0	0	0	0	0	0	0	1
Elm123		0	0	0	0	fol	0	0	no	fol	0	0	0	0	0	0	0	0	0	0	0	no	0	0	0	no	3
Elm124		0	0	0	0	0	0	0	0	0	0	0	0	0	0	0	0	0	0	0	0	-1	0	0	0	no	2
Elm127		0	0	0	0	0	0	0	0	0	0	0	0	1	0	0	0	0	0	no	no	0	0	0	0	0	4
Elm201		no	fol	0	0	0	-1	0	0	0	0	0	0	0	0	0	0	0	0	0	0	0	no	fol	0	0	1
Elm202		0	0	0	0	0	0	0	no	fol	0	0	0	0	0	0	0	0	0	0	0	no	0	0	0	0	3
Elm203		0	0	0	0	0	0	0	0	0	0	0	0	0	0	0	0	0	0	0	0	0	0	0	0	0	0
Elm205		0	0	0	0	0	0	0	0	0	0	0	0	0	0	-2	0	0	0	0	0	-2	0	0	0	0	3
Elm207		fol	0	0	0	0	0	0	0	0	0	0	0	0	-1	0	0	0	0	-1	0	0	0	0	0	0	1
Elm210		0	0	0	0	0	0	0	0	0	no	0	no	0	0	2	0	0	0	0	0	fol	0	0	0	0	8
Elm211		0	0	0	0	0	0	0	0	0	0	0	0	-1	0	0	0	0	0	0	0	0	-2	0	0	no	2
Elm212		0	1	0	0	1	0	0	0	0	0	1	2	fol	0	0	0	0	1	0	0	0	2	0	fol	fol	13
Elm213		fol	0	fol	0	0	0	0	0	0	0	0	0	-1	0	0	0	0	-1	0	0	-1	0	0	0	0	1
Elm214		0	0	0	0	2	no	0	0	0	fol	0	fol	-1	0	0	no	0	0	0	0	0	no	0	0	0	4
Elm215		0	-1	0	0	0	0	0	0	0	0	0	0	no	0	0	0	0	0	0	0	0	0	0	0	0	5
Elm216		-2	1	0	0	0	0	0	0	2	0	0	0	0	0	0	no	0	0	0	0	0	no	0	0	0	4
Elm218		0	0	0	0	0	0	0	0	0	0	0	0	0	no	0	0	0	no	0	0	0	0	no	no	0	0
Elm219		0	0	fol	0	0	0	0	0	0	0	0	0	0	0	0	0	0	0	no	0	0	0	0	no	0	1
Elm220		0	no	0	0	0	0	0	-2	fol	0	0	0	0	0	0	-1	0	0	0	-1	0	no	0	0	no	2
Elm221		0	no	0	0	0	0	no	0	0	0	1	0	0	0	0	0	0	0	no	0	0	0	0	0	0	1
Elm222		0	0	0	0	0	no	no	0	0	0	no	no	0	no	fol	0	0	0	no	no	fol	0	no	0	no	0
Elm226		0	0	0	1	0	0	0	no	0	0	0	0	0	0	0	0	0	0	0	0	0	0	no	fol	0	2
Elm227		fol	0	0	0	0	no	fol	fol	0	0	0	0	0	0	0	0	0	no	fol	fol	fol	0	0	0	0	3
Elm228		0	0	no	0	0	0	0	no	0	0	0	0	0	no	-2	0	0	0	0	0	no	no	no	0	no	2
Elm229		no	0	0	-2	fol	fol	0	0	0	0	0	0	-2	0	0	0	0	2	no	0	0	0	0	0	0	3
Elm230		0	0	no	0	0	0	0	0	0	0	0	0	0	0	0	no	0	0	0	0	0	0	no	0	no	4
Elm231		0	no	0	no	0	-2	fol	0	0	0	0	0	0	-2	0	0	0	0	0	fol	0	0	fol	0	0	3
Elm232		0	0	0	0	0	0	0	0	0	0	0	0	0	0	0	0	no	no	no	no	fol	0	fol	0	0	0
Elm233		0	0	0	0	0	0	0	0	0	0	0	0	0	0	no	0	0	0	no	0	0	0	0	no	0	2
Elm234		no	0	0	0	0	0	0	0	0	no	0	0	0	0	no	0	0	0	0	0	0	0	0	0	0	2
Elm235		0	0	0	0	0	0	0	0	0	0	no	0	0	0	0	0	0	0	0	0	0	0	no	0	0	0
Elm236		0	0	0	0	-2	fol	0	fol	0	0	0	0	0	0	0	0	0	0	0	0	0	0	0	no	0	3
Elm237		0	fol	fol	fol	0	0	0	2	1	fol	0	fol	0	fol	fol	0	0	1	0	0	0	0	0	0	0	4
Elm238		0	0	0	0	0	0	0	0	0	0	0	no	0	0	0	-2	0	0	0	0	2	0	0	0	no	2
Elm239		0	0	0	0	no	0	0	0	0	0	0	0	0	0	0	0	0	0	0	2	fol	0	0	0	0	1
Elm240		0	0	no	0	0	0	0	0	0	0	0	0	0	no	0	0	0	0	0	0	-2	fol	0	0	fol	2
Elm241		0	0	0	0	0	0	0	0	0	0	0	0	0	0	0	0	0	0	0	0	0	0	0	0	0	2
Elm242		0	0	0	0	0	-2	0	0	0	0	0	0	0	0	2	fol	0	0	0	0	0	0	0	0	0	3
Elm243		0	0	0	no	fol	0	0	0	0	0	0	0	-2	0	0	0	no	0	2	0	0	0	fol	0	0	6
Elm244		0	0	0	0	0	0	0	0	0	0	0	0	0	0	0	0	0	0	0	0	0	0	0	no	0	0
Elm245		0	0	0	0	0	0	0	0	0	1	0	0	0	0	1	0	0	0	-1	1	0	0	no	0	0	3
Elm246		fol	0	0	0	fol	0	0	0	0	0	0	0	-2	0	0	no	0	0	0	0	no	0	no	0	no	2
Elm247		fol	0	0	0	0	0	0	0	0	0	0	0	0	0	0	0	0	0	2	0	0	no	0	0	0	2
Elm248		0	0	0	0	0	0	0	0	0	0	0	0	0	1	0	0	0	0	no	0	0	0	0	0	0	0
Total		2	0	0	1	3	2	0	3	1	0	0	1	3	1	4	1	0	1	2	2	3	2	1	0	0	**164**

Figure 43: Deforestation a few weeks before fieldwork in research area 2. Many old tree species were cut down, primarily spruce. Unfortunately, this coincidence limited the selection of trees to be sampled.

Figure 44: Extracting an increment core using the extractor of the Pressler borer set.

Table 6: Fieldwork notes (written in German) on the trees in the research area 1. Tree inclination was rated from 0 (straight trunk) to 5 (inclination greater than 10°) and the direction was indicated as "hangabwärts" = downslope, "hangaufwärts" = upslope, "rechts" = right (looking from above) and "links" = left. Notes on the immediate soil morphology were also recorded.

Index	Inclination	Ground morphology
Elm101	1 hangaufwärts	35grad, oben viel Material
Elm102	3 rechts	45grad+, wird dort steil, gegen Tal und rechts abfallend
Elm103	1 hangaufwärts	30grad, oberhalb viel Material
Elm104	1 hangaufwärts	20grad, oberhalb eher viel Material
Elm105	2 hangaufwärts	15grad, oberhalb viel Material
Elm106	0, aber Säbelwuchs	25grad, in steilem Abschnitt
Elm107	1 hangaufwärts	25grad, auf wulstigem steileren Abschnitt
Elm108	Gerade	10grad, auf Ausläufer von wulstigem Abschnitt
Elm109	Gerade	5grad, auf Ausläufer von wulstigem Abschnitt
Elm110	1 hangabwärts	30grad aufgrund trockener Bachrinne rechts unterhalb
Elm111	2 hangaufwärts	30grad, am Ende von flachem Bereich, wird wieder steil
Elm112	1 nach links	20grad, normaler Hang, aber fällt ab nach links
Elm113	Gerade	10grad, aber links nebenan ist gleich trockene Rinne
Elm114	2 nach links, 1 hangaufwärts	10grad, an Schwelle zu steilerem Hang
Elm115	1 nach links, 2 hangaufwärts	10grad, an Schwelle zu steilerem Hang
Elm116	1 hangaufwärts	20grad, gleich zu Beginn des steileren Hangs
Elm117	2 hangaufwärts	20grad, gleich zu Beginn des steileren Hangs
Elm118	1 hangaufwärts	20grad, am Ende eines kleinen Wulst
Elm119	3 hangabwärts, 3 nach rechts	35grad, am Ende eines Wulst, scheint runterzudrücken
Elm120	1 nach links, 1 hangaufwärts	10grad, anfangs flacher Bereich
Elm121	2 hangaufwärts	10grad, im flachen Bereich
Elm122	1 nach rechts	30grad, steiler flacher Hang
Elm123	1 hangabwärts	35grad, am Ende einer Wulst, scheint runterzudrücken
Elm124	1 nach rechts, 1 hangaufwärts	25grad, Kleiner Wulst oberhalb, viel Material
Elm125	1 hangabwärts unten, ab 10m wieder 0	30grad, gleich nach Schwelle zum Hang, oberhalb eher flach und viel Material
Elm126	5 hangaufwärts, 2 auf rechts	30grad, gleich an Schwelle zu steilem Gelände
Elm127	Schlange: unten: 2 rechts, oben: 1 hangabwärts	40grad, ebenfalls gleich an Schwelle zu Rinne unterhalb-rechts

Table 7: Fieldwork notes (written in German) on the trees in the research area 2. Tree inclination was rated from 0 (straight trunk) to 5 (inclination greater than 10°) and the direction was indicated as "hangabwärts" = downslope, "hangaufwärts" = upslope, "rechts" = right (looking from above) and "links" = left. Notes on the immediate soil morphology were also recorded.

Index	Inclination	Ground morphology
Elm201	4 unten, 5 oben (ab 10m) talabwärts, 2 auf rechts	30grad, mitten in gleichmässigem Hang
Elm202	5 unten, 4 oben (ab 13m) talabwärts	30grad, mitten in gleichmässigem Hang
Elm203	Unten 1 hangabwärts, leichter Säbelwuchs	30grad, Untergrund ist etwas nach unten rechts gekippt.
Elm204	Gerade	25grad, unterhalb steilerem wulstiger Abhang (2-3m) mit viel Material
Elm205	Gerade	25grad, unterhalb steilerem wulstiger Abhang (2-3m) mit viel Material
Elm206	1 hangabwärts	10grad, unterhalb steilerem wulstiger Abhang (2-3m) mit viel Material
Elm207	Gerade	15grad, schon eher im flachen Teil
Elm208	1 hangabwärts	20grad, gleich oberhalb steilerer Abhang (2-3m) mit viel Material
Elm209	Unten 5 hangabwärts, oben (10m) 2 hangabwärts, unten 2 rechts, oben 1 rechts	40grad, am Rand eines steilen "Abgrunds", oberhalb eher flach (10grad) und viel Material
Elm210	Unten 2 hangaufwärts, oben 2 hangabwärts, 1 auf rechts	15grad, mitten im flachem Hang, oberhalb türmt sich wieder Wulst auf
Elm211	Gerade	25grad, gewöhnlicher Hang
Elm212	Unten 2 hangaufwärts, oben gerade	30grad, gewöhnlicher Hang. Beginnt seitlich links abzukippen
Elm213	Ganz unten 5 hangabwärts, mitte gerade, oben (5m) 3 hangaufwärts. 1 nach rechts	40grad, Schmaler Wulst nach hangabwärts links, Baum kippt rechts
Elm214	2 hangaufwärts, 1 links	40grad, weil lokal durch Rinne sehr steil
Elm215	Gerade	30grad, links Bach, rechts Rinne, Baum selbst auf Wulst
Elm216	Unten 1 rechts, oben gerade (ab 10m)	45grad, sehr steil, auch auf Wulst, am Anfang des steilsten Teils
Elm217	Ganz unten 2 hangabwärts, dann 0, oben 2 hangaufwärts	25grad, beginnt genau dort, steil zu werden.
Elm218	Gerade	25grad, mitten im Hang
Elm219	Gerade	25grad, mitten im Hang
Elm220	Unten 2 rechts und hangabwärts, oben gerade,	55grad, bei der Wulstzunge, hält viel Material auf
Elm221	Gerade	55grad, bei der Wulstzunge, hält viel Material auf
Elm222	Gerade	30grad, auf einem breiten Wulst
Elm223	Gerade	20grad, wulst
Elm224	Unten 1 hangabwärts, oben gerade	30grad, auch auf Wulst
Elm225	Sehr krumm, unten 5 links und hangabwärts, oben 0	25grad, aber am Rand eines Wulst, daher Kippung
Elm226	Gerade	10grad
Elm227	Unten 2 hangaufwärts, oben gerade	30grad
Elm228	Unten 2 hangabwärts, oben gerade, 1 rechts	20grad, aber uneben, rechts und links Rinne, Baum auf kleinem Hügel
Elm229	1 hangaufwärts, 1 links, oben gerade	35grad, steht mitten in der Rinne,
Elm230	2 hangabwärts unten, oben (10m) gerade	15grad, regelmässig, aber unterhalb Abhang zur Strasse
Elm231	Unten 3 hangabwärts, oben gerade	20grad, am Rand des 2m Abbruchs, Fundament instabil
Elm232	Gerade	45grad, am 2m Abhang, mitten drin, weniger steil als bei der Rinne
Elm233	Unten 2 hangabwärts, oben 1 hangabwärts	40grad, am Rand eines eigenen Mini-Abgrunds
Elm234	Gerade	40grad, am Rand eines eigenen Mini-Abgrunds
Elm235	Unten 1 hangabwärts, oben gerade	55grad, Wald befindet sich auf Wulst, viel Material gestaut
Elm236	Unten 4 hangabwärts, oben 1 hangabwärts (3m)	45grad, Wald befindet sich auf Wulst
Elm237	Unten 1 hangabwärts, ab 2m gerade	55grad, Wald befindet sich auf Wulst
Elm238	Gerade	35grad, breiterer Wulst, links und (grössere) rechts Rinne
Elm239	1 hangabwärts, 1 rechts, ab 5m gerade	45grad hangabwärts und rechts (Hauptrinne) oberhalb viel Material
Elm240	1 hangabwärts, nur 1m danach steckengrade	20grad, auf Wulst neben Rinne
Elm241	Unten 2 hangabwärts, oben 1,	30grad, auf Wulst, aber durch die grossen Wurzeln stabil
Elm242	Unten 1 hangabwärts	30grad, an breiterer Front eines steileren Hangs
Elm243	Unten 2 hangabwärts, oben 1,	30grad, am Fuss einer steilen Stelle
Elm244	Unten 1 hangabwärts, oben 0	55grad, steilste Stelle im Hang
Elm245	Unten 2 hangabwärts, oben 1,	50grad, ebenfalls sehr steil
Elm246	Unten 2 hangabwärts, mitte 1, oben 0; 1 links	30grad, An Schwelle zu steiler Stelle (50m)
Elm247	Unten 1 hangabwärts, oben 0	30grad, an Schwelle zu steilerem Teil
Elm248	Überall 2 hangabwärts	20grad, wulstige Form ender hier, wird gleich steiler

Table 8: Fieldwork notes (written in German) on the trees in the reference area. Tree inclination was rated from 0 (straight trunk) to 5 (inclination greater than 10°) and the direction was indicated as "hangabwärts" = downslope, "hangaufwärts" = upslope, "rechts" = right (looking from above) and "links" = left. Notes on the immediate soil morphology were also recorded.

Index	Inclination	Ground morphology
ElmR01	1 links	15grad, oberhalb gleich der Weg
ElmR02	Gerade	25grad, Auf einer kleinen Erhöhung
ElmR03	Gerade	30grad, oberhalb mehr Material
ElmR04	1 rechts	25grad, mitten in der Schräge
ElmR05	1 rechts	25grad
ElmR06	1 hangabwärts, 2 links	20grad, in flachem Teilhang drin
ElmR07	Gerade	30grad, am Ende einer flachen Stelle, abfallend nach rechts und hangabwärts
ElmR08	1 rechts, 2 habgabwärts	35grad, Im oberen Teil des Hangs
ElmR09	Gerade	35grad, mitten im Hang, Wulst 3m oberhalb
ElmR10	2 hangabwärts, 2 links, oben 2 hangabwärts	20grad, führt in Rinne
ElmR11	2 hangabwärts, 2 links, oben 2 hangabwärts, 1 links	20grad, führt in Rinne
ElmR12	Unten 2 hangabwärts, oben 0	10grad, sehr flach
ElmR13	Unten 2 hangabwärts, oben 0	10grad, sehr flach
ElmR14	Gerade	0grad, auf Steinen, darum Säbelwuchs
ElmR15	Gerade	30grad, steiler Abhang (1m)
ElmR16	Gerade	15 grad, steiler Abhang links (1m)
ElmR17	Unten 2 hangabwärts, oben (2m) 0	10grad, ziemlich flach,
ElmR18	Unten 2 hangabwärts, oben (7m) 1,	20grad, beim Start des Hangs
ElmR19	Unten 0, oben hangaufwärts Tendenz	0grad, wobei grössere Distanz 30grad
ElmR20	Gerade	20grad
ElmR25	Gerade	35grad, scheint stabil zu sein
ElmR26	Unten 2 hangabwärts, oben 1	20 grad, regelmässig aber mitten in lichtung-Hang
ElmR27	Gerade	35grad, scheint stabil zu sein
ElmR28	Gerade	10grad, ziemlich flach,
ElmR29	Gerade	20grad, beim Start des Hangs

Personal declaration

Personal declaration: I hereby declare that the submitted thesis is the result of my own, independent work. All external sources are explicitly acknowledged in the thesis.

General Artificial Intelligence (AI) statement:

AI has been used in this text as follows:

- Translation of German sentences that I wrote or rewording and correction of English sentences that I wrote using ChatGPT (Version 5)
- Assistance with creating and debugging Python prompts for statistical analyses and plots using ChatGPT (Version 5)
- Translation and stylistic improvements using DeepL Translator

All text parts created by AI have been checked by me, the author of this text. I take full responsibility for the text.

Location, Date: Uster, 24.10.25

Signature: M. [illegible]